Uso industrial de colorantes tipo T

Termoplásticos

- El colorante debe estar monodispersado en el polímero (0.01–0.30% p/p)
- Polímeros de baja T_g (poliolefinas, polivinilos)
- Evitar temperaturas de procesado > 250 °C durante tiempos largos
- Aditivos: estabilizadores fotoquímicos y térmicos, antioxidantes, absorbedores UV
- Microencapsulantes: compatibiliza más polímeros pero requiere más colorante

@ Unión colorante-oligómero creando un microambiente favorable al fotocromismo

⇒ color más intenso manteniendo cinéticas rápidas (mutuamente excluyentes)

⇒ compatibiliza al colorante con polímeros más rígidos (poliamidas,...)

ejs: botellas de refrescos, pinzas, fundas, juguetes,
sedal invisible al pez / visible al pescador

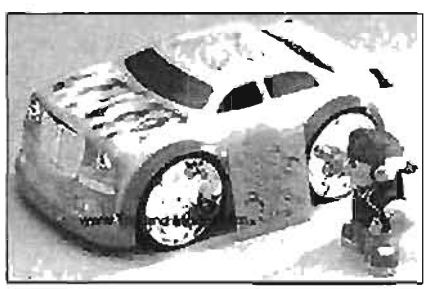

Uso industrial de colorantes tipo T

Microencapsulación en polímeros

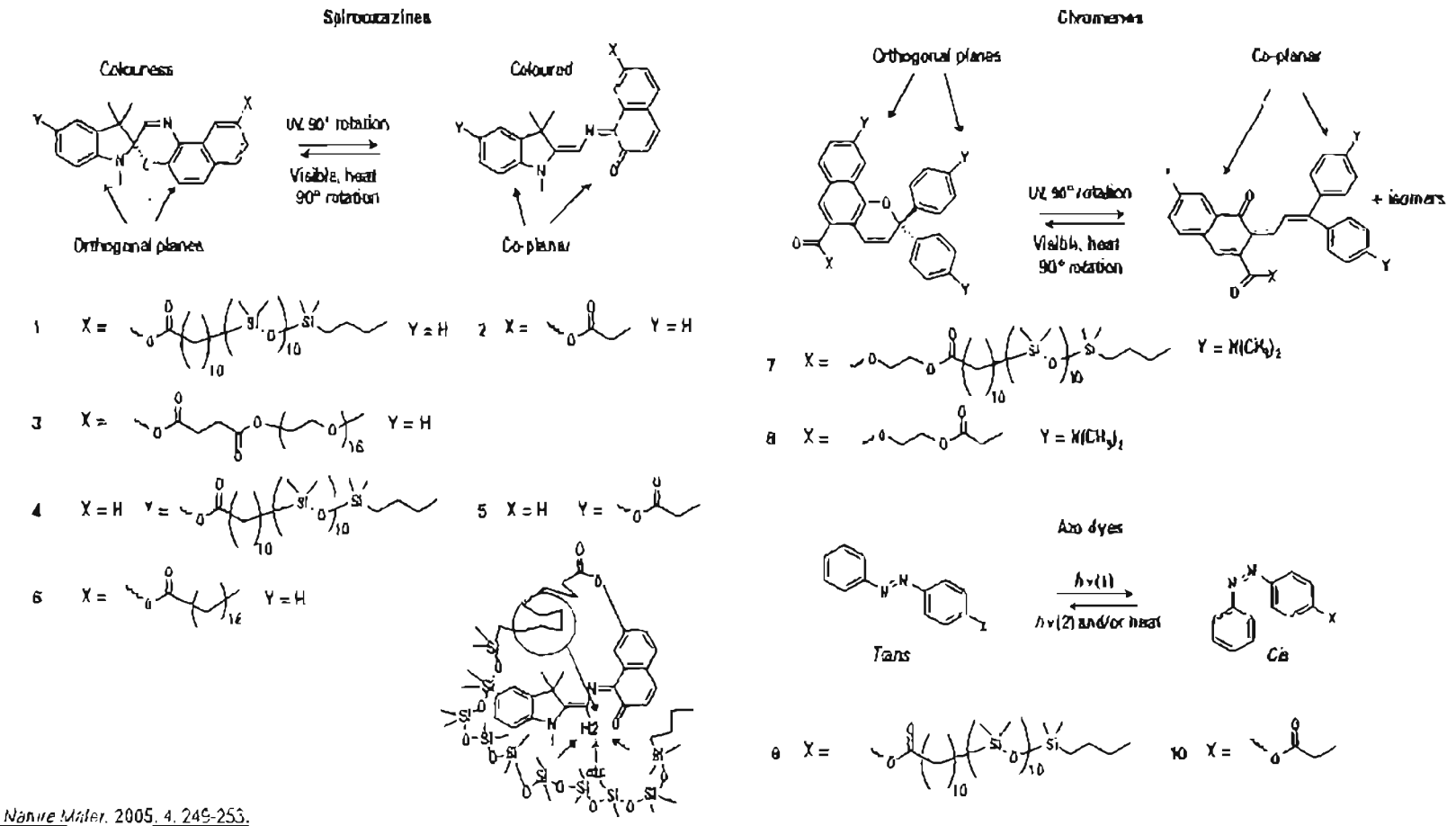

Nature Mater. 2005, 4, 249-253.

Uso industrial de colorantes tipo T

Microencapsulación en polímeros

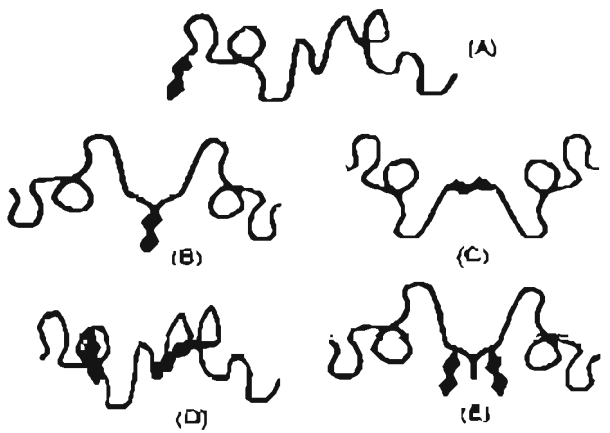

(A) (B)

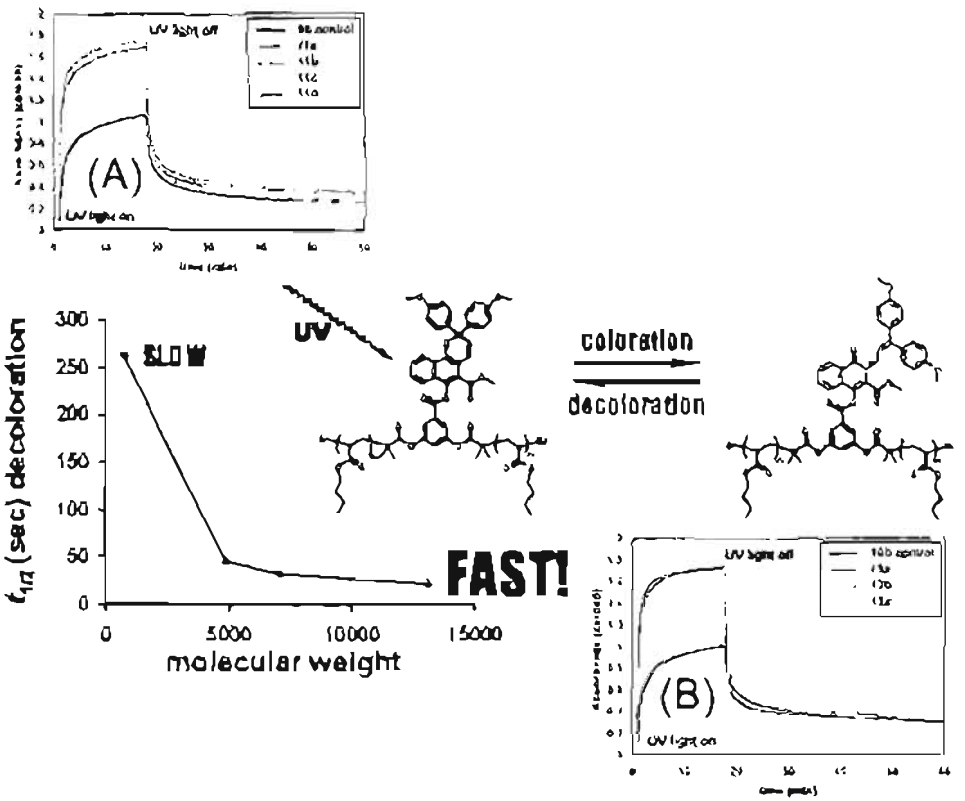

Macromol. 2008, 41, 1206-1214 Macromol. 2010, 43, 249-261

Uso industrial de colorantes tipo T

Microencapsulación en sol-gel: films porosos de ormosil

ORMOSIL (Organically Modified Silica)

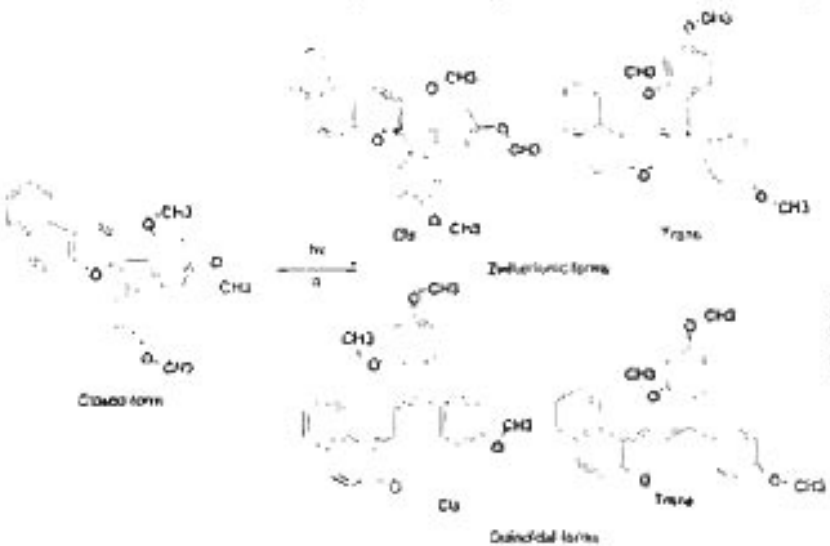

Muestras irradiadas a través de máscaras

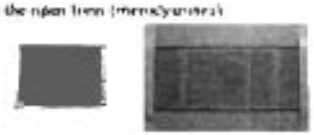

Exposición del sol-gel a luz solar

J. Sol-Gel Sci. Techn. 2006, 40, 365-370.

Cinéticas de decoloración / fotodegradación en matrices ormosil

Decoloración

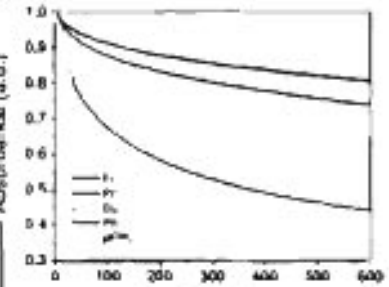

Fotodegradación

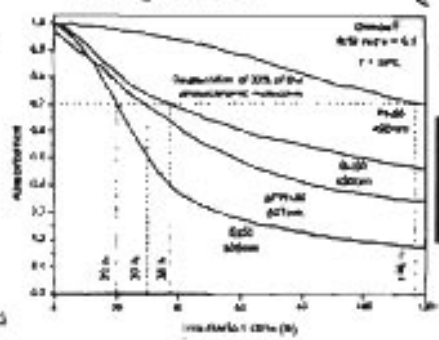

Fotodegradación en la zona ○ sin sol-gel

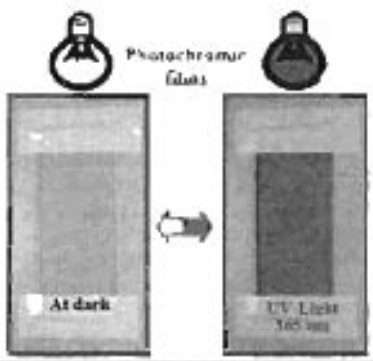

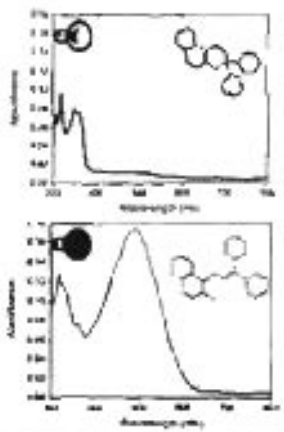

Uso industrial de colorantes tipo T

Recubrimiento de superficies / Impresión

- Tintas y barnices para uso estético o de seguridad de efectos impresos
⇒ marcas manifiestas / ocultas para evitar fraude y falsificación
- Uso de disolventes orgánicos o de microencapsulantes
- Litografía, flexografía y grabado ⇒ 1–3% p/p colorante/tinta
- Serigrafía ⇒ 0.5–1% p/p colorante/tinta
- Si la concentración de colorante es muy alta no se genera fotocromismo

Textiles

- Aún por desarrollar comercialmente de modo masivo
⇒ mejorar la coloración intensa de la fibra (poliéster / nylon) con moléc. de ↑ Vol.
⇒ mejorar la durabilidad del efecto fotocrómico

Otras aplicaciones

- Basadas en: reversibilidad, sensibilidad a la radiación UV/Vis, función concreta
- Ejs.: detección de fugas de combustible, *smart windows*, films para agricultura, cosmética (tintes, protectores solares), marcas de caducidad / seguridad

Color. Technol. **2009**, *125*, 249-261. *Chem. Brit.* **2002**, *38*, 37. Intelligent Chemical Indicators. Cap 30. En *Smart Materials*. CRC Press, Boca Ratón, FL, 2009

Colorantes comerciales de tipo P

Fulgidas y fulgimidas

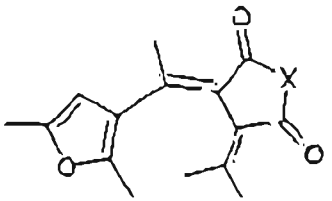

+ Efecto fotocrómico observable ya en el colorante sólido
+ Un diseño molecular adecuado permite seleccionar colores
+ Gran gama de colores (incoloro, amarillo, rojo, ... infrarrojo)
+ Las moléculas activadas no se decoloran en la oscuridad sino con luz porque ambos isómeros son térmicamente estables

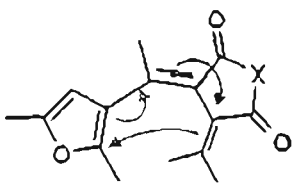

Open Form

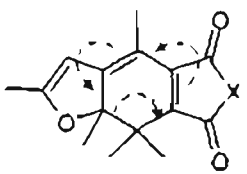

Closed Form

X = O (fulgides)

X = NR (fulgimides)

furilfulgida

Chem. Lett. 2006, 35, 1204-1209. Para conocer más moléculas que se han desarrollado recientemente.

Colorantes comerciales de tipo P

Diariletenos

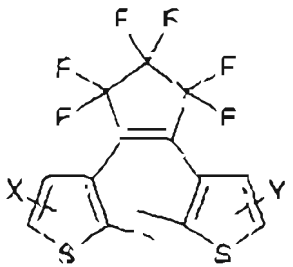

+ Fáciles de sintetizar
+ Ambos isómeros son térmicamente estables
+ Más resistentes que fulgidas
+ Pueden soportar más de 10^4 ciclos
+ Las cinéticas son muy rápidas (10 ps)
+ Sus cristales mantienen las propiedades (o las mejoran)
+ Es posible co-cristalizar diferentes moléculas de la familia

  ⇒ se pueden fotoactivar gamas de colores

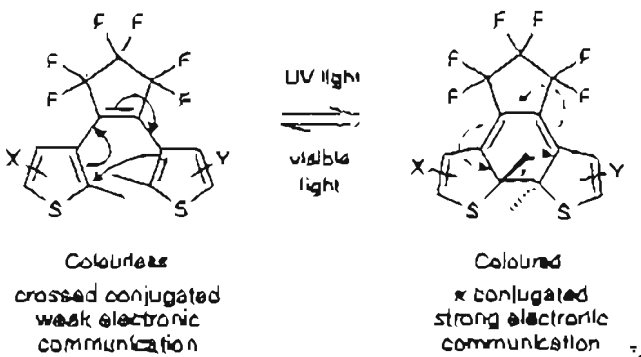

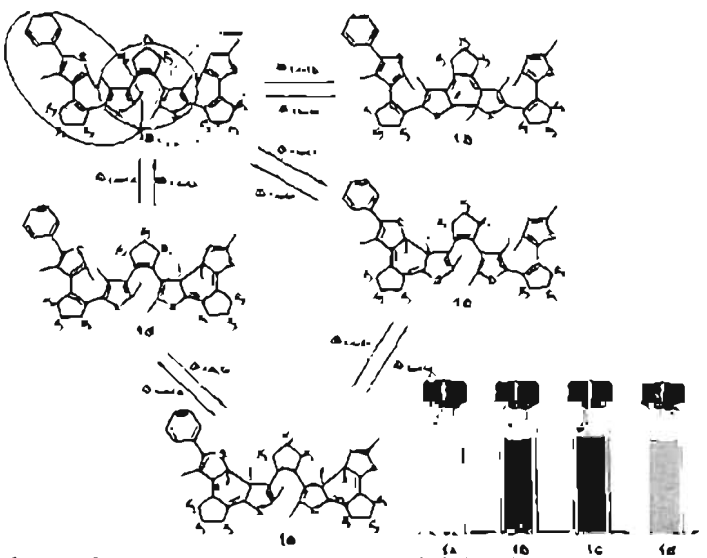

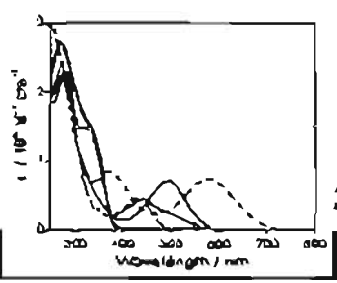

Figure 1. Photochromic reaction of diarylethenes (1). Red bar denotes the absence of the π-conjugated

* J. Am. Chem. Soc. 2005, 127, 3552-8823.

Aplicaciones de colorantes tipo P ...

Actinometría

Uso de colorantes muy resistentes térmicamente, fotoquímicamente y a la fatiga ⇒ **muy válidos para uso repetido**

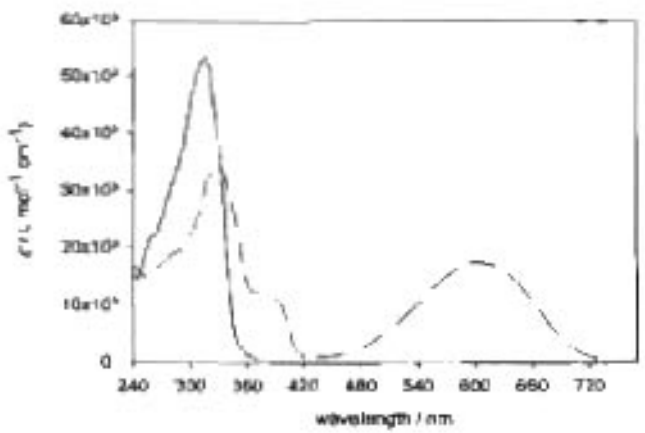

Fig. 2 Absorption spectra of the open-ring (—) and closed-ring (---) isomers of compound 1 in acetonitrile.

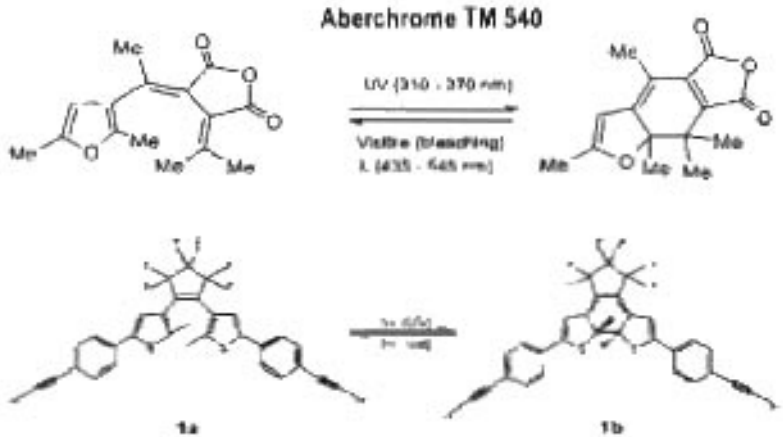

Scheme 1 Open-ring (1a) and closed-ring (1b) isomers of 1,2-bis(5-(4-ethynylphenyl)-2-methylthiophen-3-yl)perfluorocyclopentene (1).

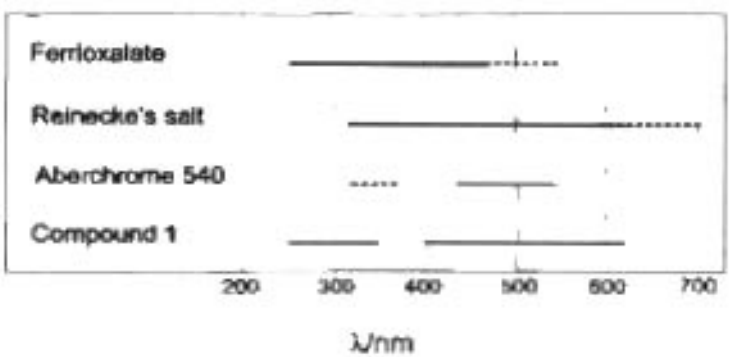

Fig. 7 Spectral range of availability of the most common actinometers in comparison with compound 1. The dashed lines indicate the range of wavelengths where the use is possible, but not recommended or simple.

☐ Pure Appl. Chem. 2001, 73, 659-666. Photochem. Photobiol. Sci. 2009, 8, 1734-1742.

Otras aplicaciones de colorantes fotocrómicos

Reversible photoinduced changes of physical and chemical properties can be transferred to the micro-environment by a photochromic molecule incorporated in the system (Fig. 2).

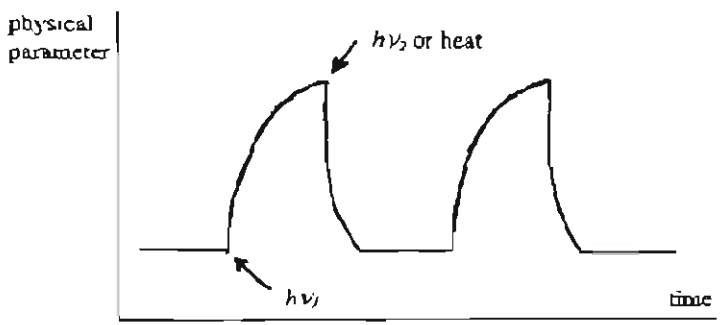

Fig. 2 Photoinduced cyclic variation of a physical property in a photoresponsive system.

Materiales fotomecánicos

- **Concepto de material fotomecánico**
- **Tipos de compuestos y materiales fotomecánicos**
  - Máquinas moleculares
  - Polímeros orgánicos
- **Aplicaciones de materiales fotomecánicos a diferentes productos / tecnologías**

This very tiny "gear-within-a-gear" can only turn in one direction.

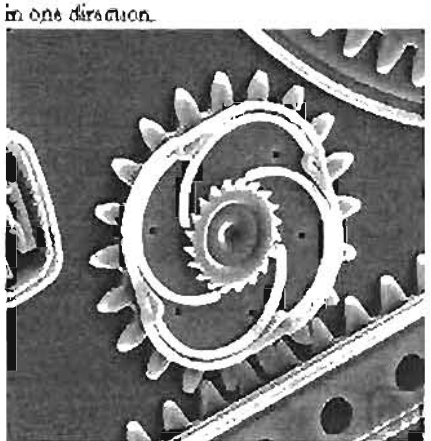

Sandia National Laboratories
http://mems.sandia.gov/scripts/images.asp

¿Se puede hacer algo más "*tiny* que *tiny*"?

top-down fabrication *vs.* ***bottom-up nanotechnologies***

auto-organización molecular

materiales / polímeros orgánicos

aparatos / interruptores moleculares

Materiales fotomecánicos

Concepto de material fotomecánico

- Sistema que, al iluminarlo, es capaz de llevar a cabo un movimiento mecánico de modo repetible, con amplitud y sentido determinados
- El *cambio de forma* en *compuestos fotocrómicos* produce un ***trabajo mecánico a nivel molecular***

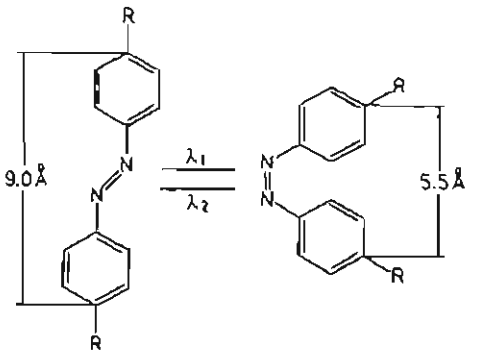

Figure 2. The geometrical structure change of an azobenzene residue along with trans–cis photoisomerization.

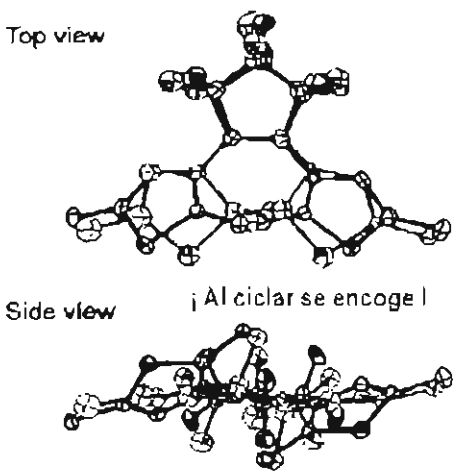

Figure 5. The molecular structure change of 1,2-bis(2,5-dimethyl-3-thienyl)perfluorocyclopentene (7) in the crystal upon irradiation with 360 nm light for 24 h. The occupancy of the closed-ring isomer was 85%.

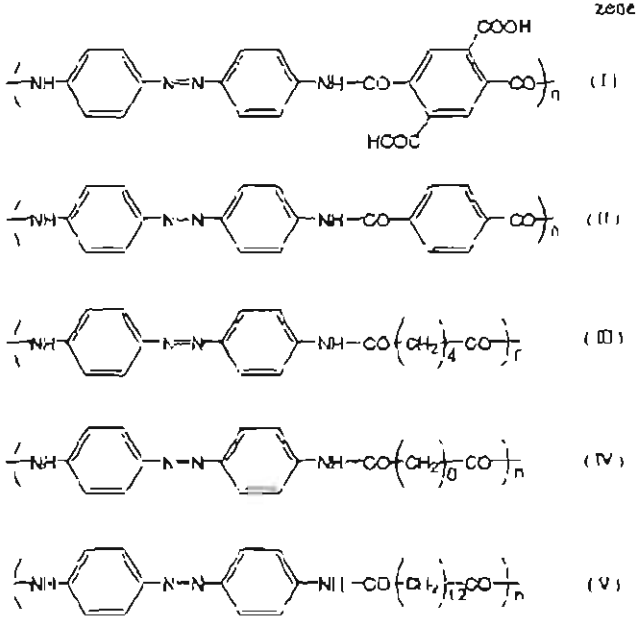

Scheme 1. Photoresponsive polyamides.

Escalas de tiempo en disoluciones de poliamidas:

Compact Conformation

10^{-7} s ↓ cis to trans photoisomerization

Compact Conformation

10^{-1} s ↓ unfolding

Extended Conformation

En polímeros, para ligar el cambio de forma molecular a un movimiento a nivel macroscópico el sistema debe estar bien organizado y densamente empaquetado

⇒ **cristalinidad...**

o directamente... **cristales**

Materiales fotomecánicos

¿Cómo "*ver*" las moléculas?...

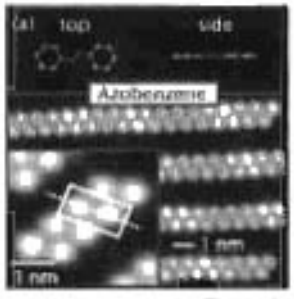

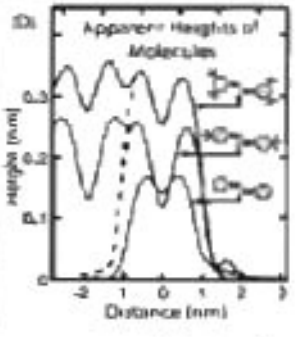

FIG. 1 (color). STM constant-current images of functionalized azobenzene molecules on Au(111) ($T = 30$ K, $V = -1$ V, $I = 25$ pA. Images are scaled identically): (a) bare azobenzene, (b) DTB-azobenzene, (c) TTB-azobenzene. Upper panels show chemical structure of the *trans* isomers of the imaged molecules. Single-molecule images are identified by white boxes in inset (dotted line in each box shows line scan trajectory for (d)). (d) Line scans across different functionalized molecules show apparent height on Au(111). DTB-azobenzene and TTB-azobenzene line scans were taken at the edge of islands. Dashed part of the line scan provides a guide to the eye for identifying single-molecule width.

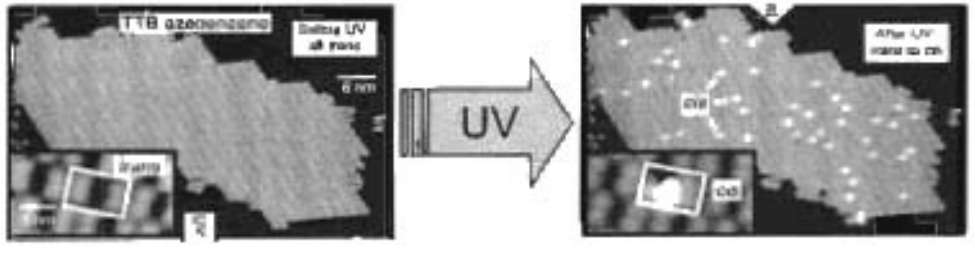

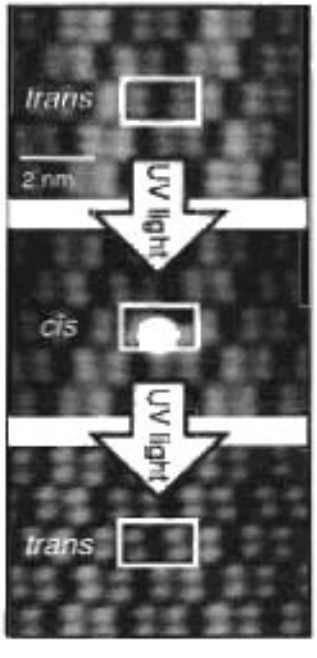

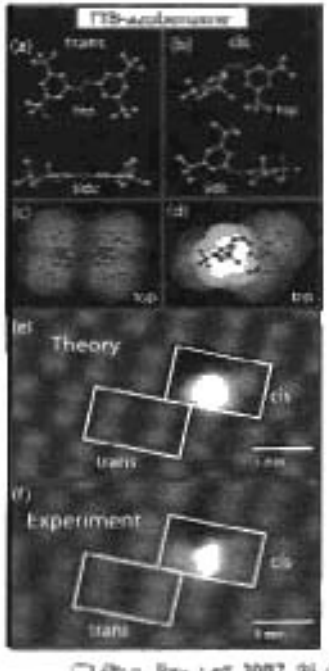

Phys. Rev. Lett. 2007, 99, 038301-1-4.

Materiales fotomecánicos

Máquinas moleculares

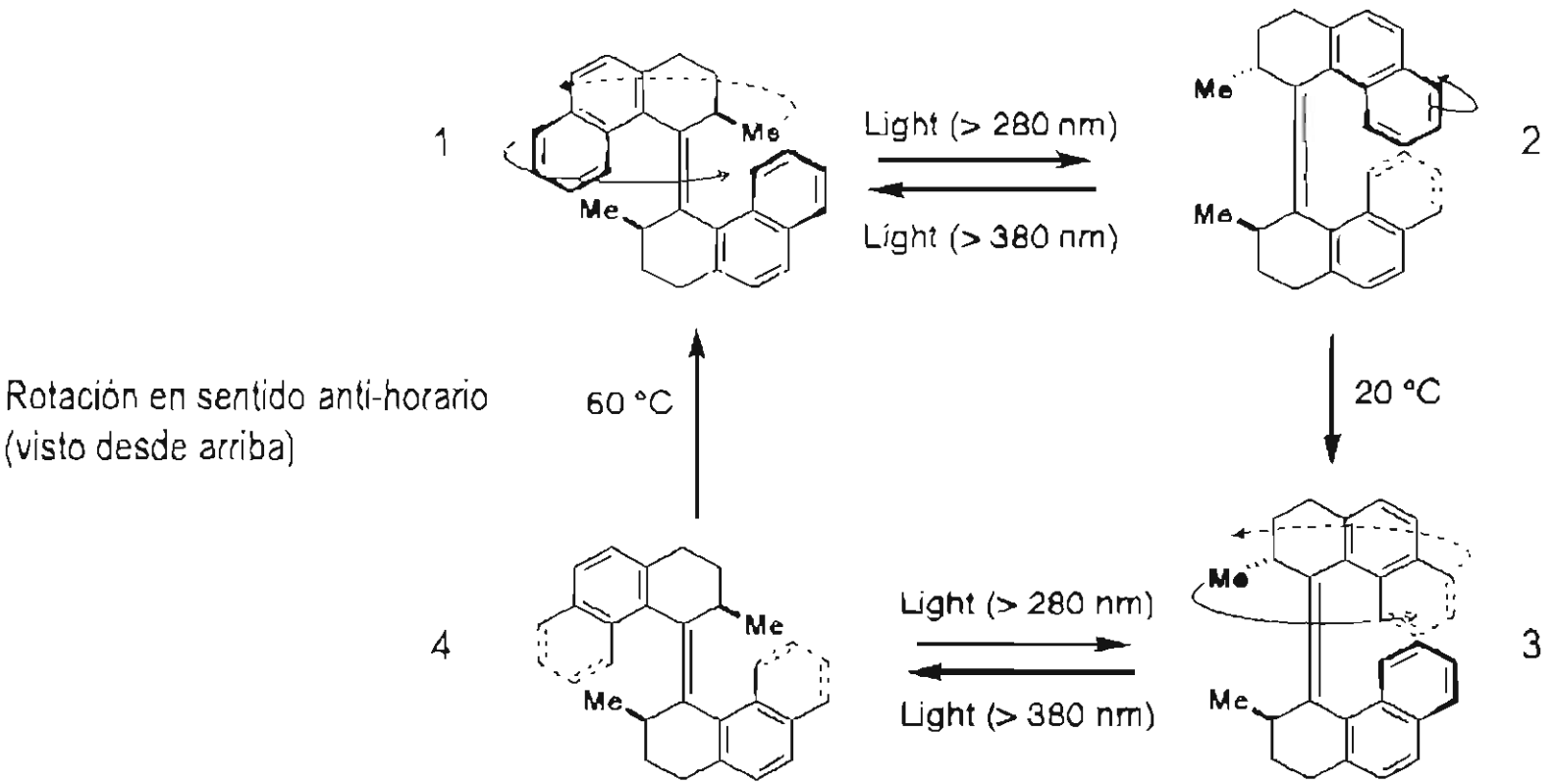

Figure 5.19. Unidirectional rotation of molecule upon irradiation with light irradiation

Applications of Supermolecules. Molecular Devices and Nanotechnology, Cap 5. En *Supramolecular Chemistry – Fundamentals and Applications*. Springer. Berlín. 2006.

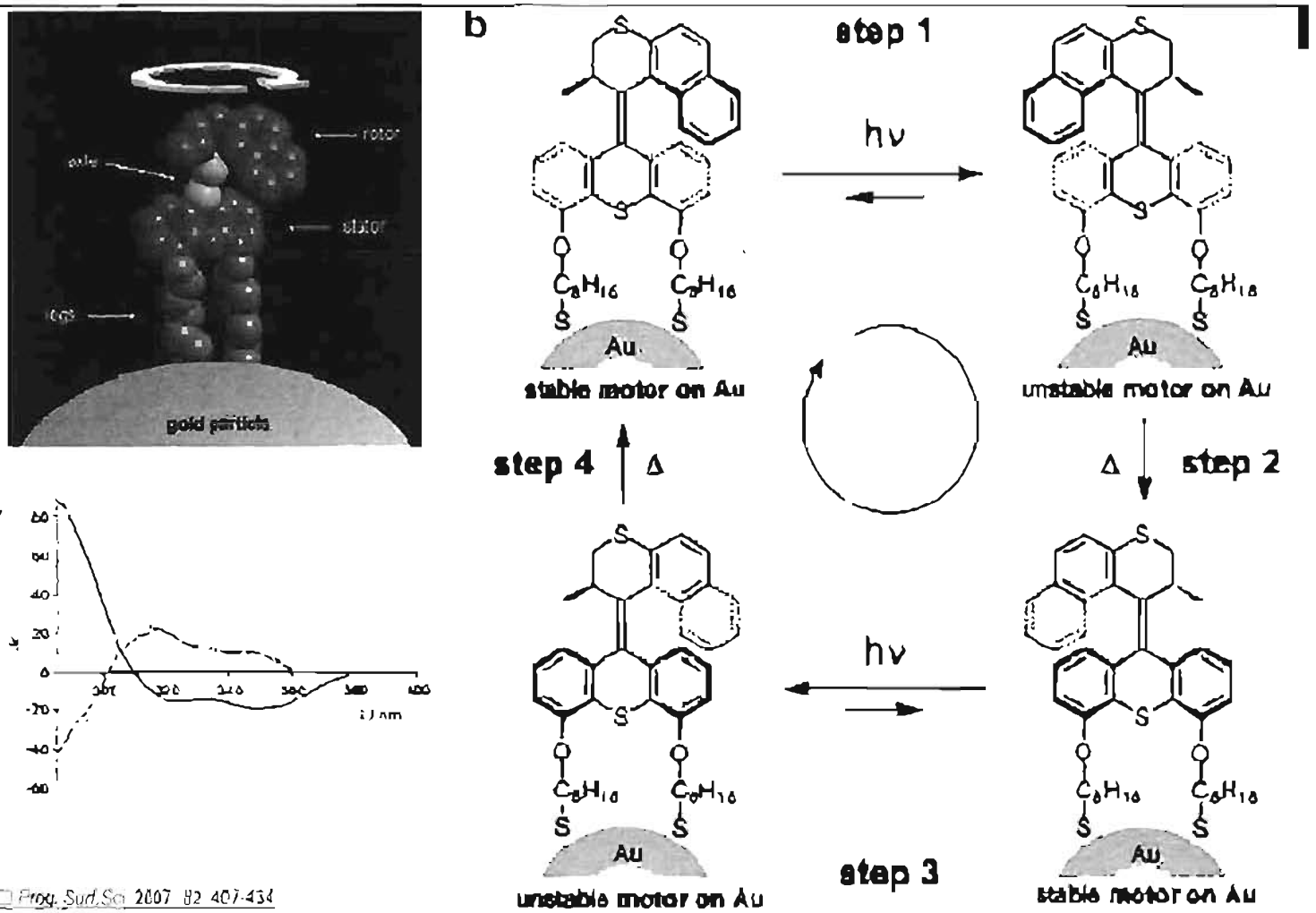

Fig. 19. (a) Schematic representation of a rotary molecular motor tethered to a gold nanoparticle through 2 legs, only one motor is shown for clarity. (b) The four-state unidirectional rotation of functionalized nanoparticle *motor on Au* is shown (*hv*: photochemical step; Δ: thermal step). (c) CD spectra of stable-*motor on Au* (solid black), photostationary state when irradiated at ⩾280 nm (dashed black), and the photostationary state when irradiated at 365 nm (dotted black) samples and after sequential photochemical and thermal isomerization steps.

Materiales fotomecánicos

Músculos moleculares poliméricos

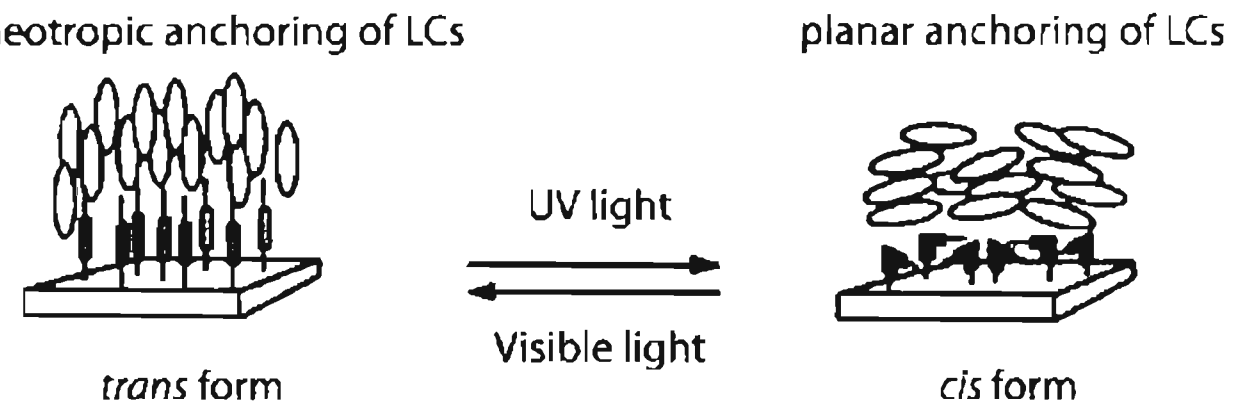

Fig. 15. Illustrative representation of the surface-assisted control of the alignment of LC molecules. The surface of which the LC molecules are deposited is functionalized by a monolayer of azobenzenes. When the azobenzene are in their *trans* form, the homeotropic anchoring of the LC molecules drives the orientation of the LCs in the whole LC mesophase. Upon irradiation with UV light, the azobenzenes undergo a *trans* → *cis* photoisomerization. Since the azobenzenes from the monolayer isomerize to form the *cis* isomer, the favoured anchoring of the LC molecules on the surface becomes the planar one and the whole alignment of the mesophase is consequently modified. This monolayer-triggerd photoalignment of LC mesophases is reversible [42].

Materiales fotomecánicos

Músculos moleculares poliméricos

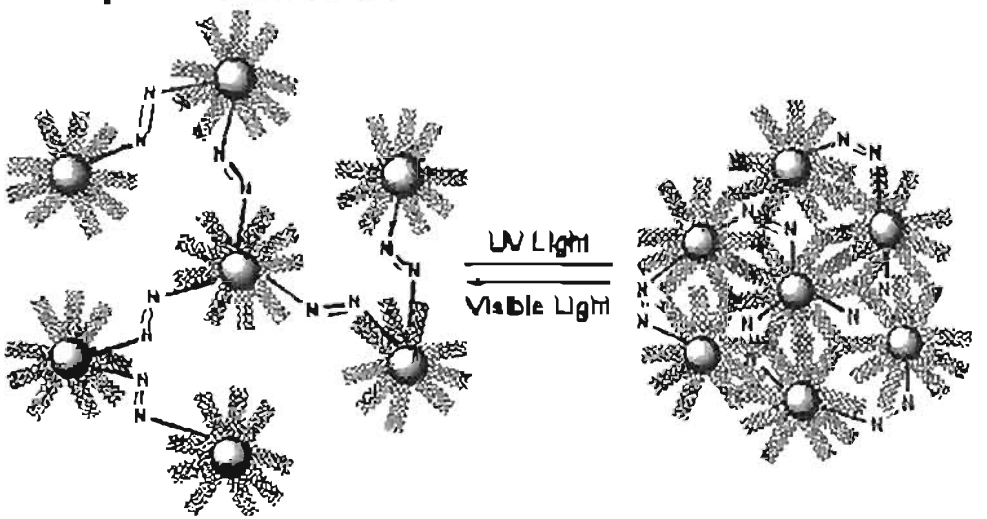

trans = breath out

cis = breath in

monolayer-protected gold nanoparticles

-N=N- azobenzene moiety

The total length of these linkers shrinks from 3 nm in the *trans* form to 2 nm in the *cis* form

Fig. 16. Schematic representation of the photocontrolled interparticle spacing in a gold nanoparticle network. This network was formed by addition of a linker molecule constituted by an azobenzene moiety suitably derivatized on either side with gold surface sensitive groups into a solution of these gold nanoparticles. The reversible *trans* – *cis* isomerization of the azobenzene moiety constituting the link in between the nanoparticles is triggering either a contraction, or reversibly an expansion of the whole network. From (89).

Materiales fotomecánicos

Músculos moleculares con geles poliméricos

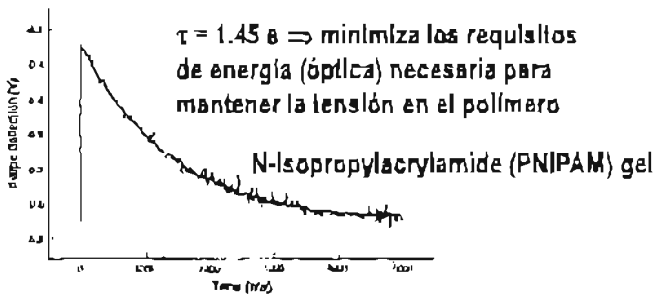

FIGURE 20: Jump Molecule Transient Absorption Decay using 455-nm radiation.

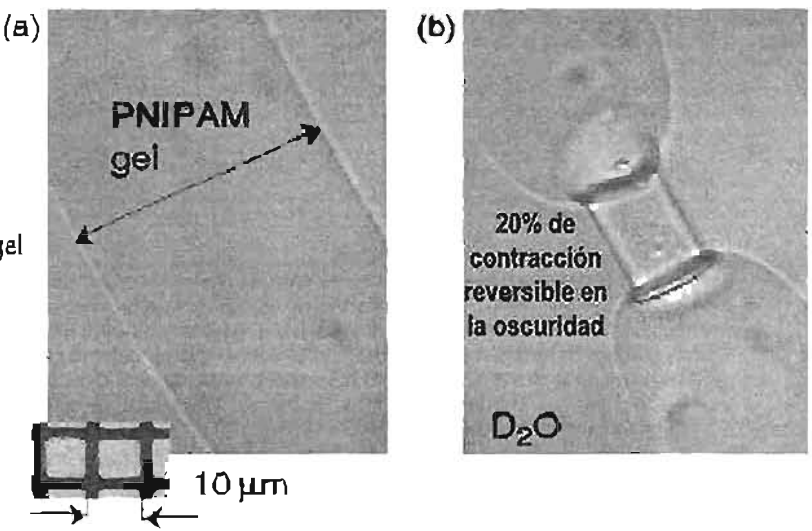

Fig. 4.31. A poly-NIPAM gel rod in D_2O before (a) and after (b) 0.75 W power laser at wavelength 1,064 nm (Becker and Glad 2000)

La irradiación del polímero con un haz de luz láser causa una interacción entre grupos funcionales de moléculas cercanas, atrayéndolas temporalmente, y originando una contracción del gel polimérico

[2] World Wide ElectroActive Polymer Newsletter 2000. 2, 11.

Materiales fotomecánicos

Músculos moleculares poliméricos

Liquid crystal nematic (left) to isotropic (right) transition

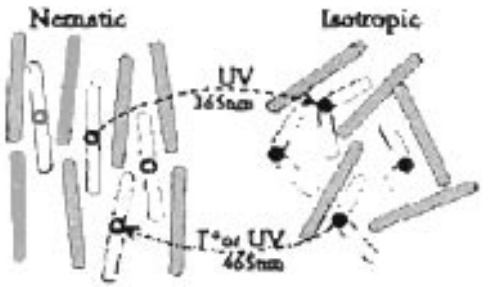

FIG. 1. Schematic depiction of nematic-isotropic phase transformation in a liquid-crystal containing photoisomerizable mesogenic molecules, which turn from a rodlike *trans* to a kinked *cis* conformation under uv irradiation.

Tiempo de respuesta tipico < 1 min

Contracción 12-18%

Proceso **reversible** térmicamente

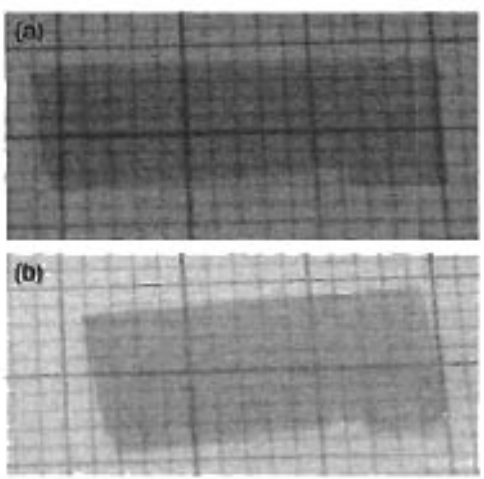

Fig. 2. Elastomer E-25 %-azo a) before UV irradiation, and b) under UV i (irradiation time: 130 s). (Background is a graphical paper).

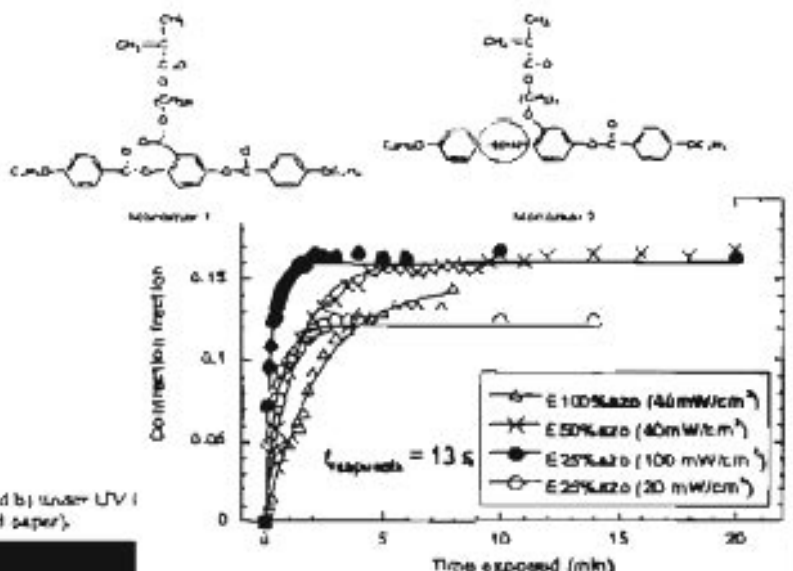

Adv. Mater. 2003, 15, 569-572.

Materiales fotomecánicos

Músculos moleculares poliméricos

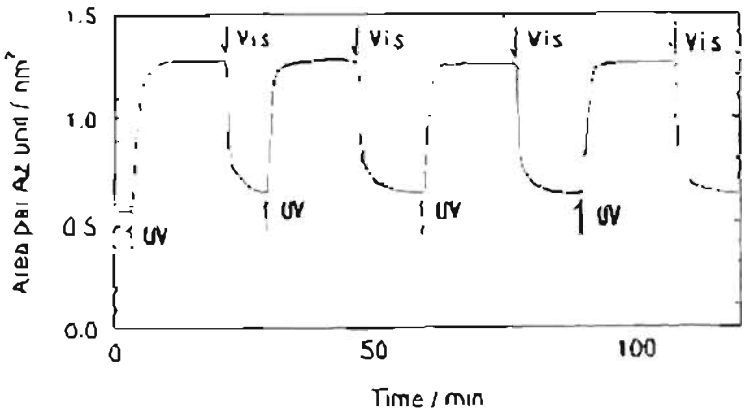

Figure 3. Time profiles of photoinduced deformation of 6AZ10-PAA monolayer on the $NaClO_4$ containing (5×10^{-4} mol dm^{-3}) subphase at 21°C. The exposure energy of the illumination was *ca.* 2 mW cm^{-2} at 365 nm (UV) and 436 nm (visible) lines.

Table 1. UV light induced expansion behavior of Az monolayers[a]

Monolayer surface pressure	6AZ10-PVA			6AZ10-PAA		
mN m^{-1}	2	5	10	2	5	10
Response time[b]/min	4	8	10	1.5	2	3.5
Factor of area expansion	3.1	2.8	1.3	1.9	2.0	1.8

[a] UV irradiation, *ca.* 2 mW cm^{-2}. [b] Response time is defined as time required for 90% change.

Polym. J. 1996, 28, 613-618

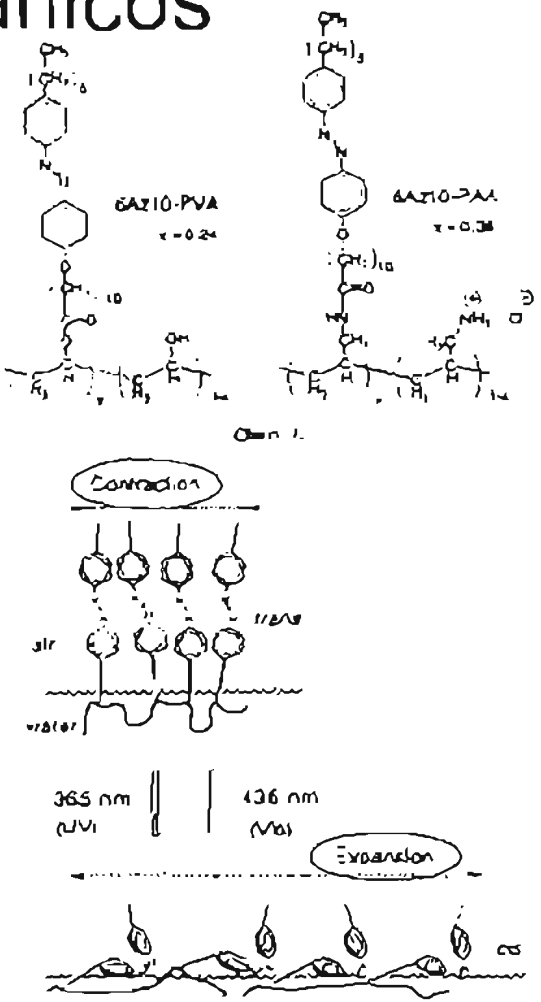

Figure 4. Schematic illustration of UV and visible light induced deformation of the polymeric Az monolayer at the air/water interface. In the process of trans to cis photoisomerization upon UV (365 nm) light illumination, the Az unit increases its polarity and experiences attraction from the water surface. This movement induces expansion of the entire monolayer. Upon visible (436 nm) light illumination the reverse process takes place, resulting in photocontraction.

Materiales fotomecánicos

Músculos moleculares cristalinos

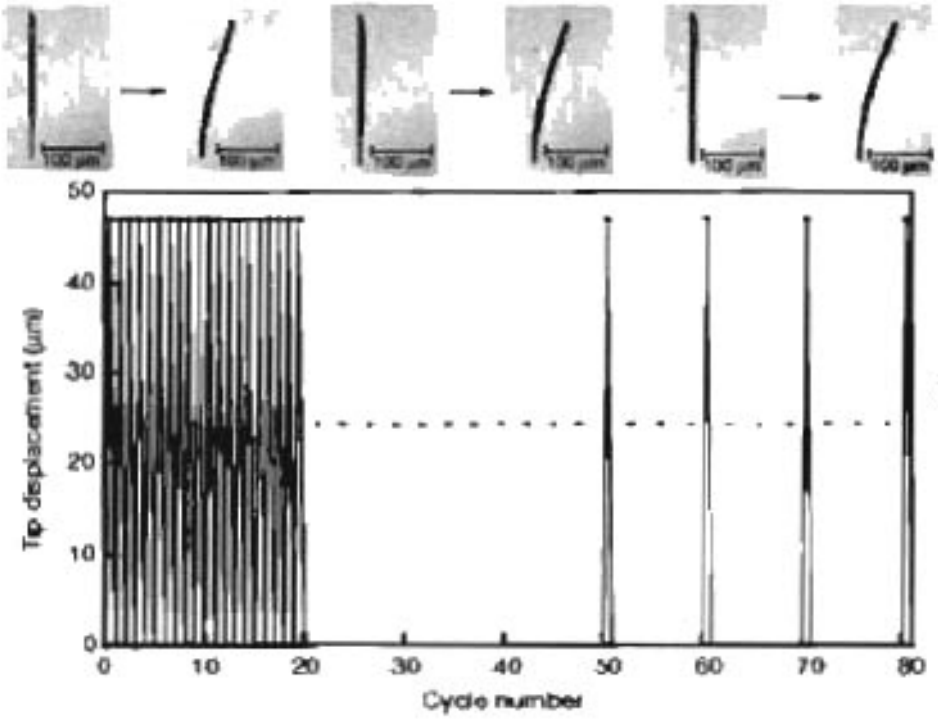

Escala de tiempos – 25 μs

Straight crystal rod

10^{5} × ⊥ photoisomerization from the open- to the closed-ring isomers

Straight crystal rod

10^{5} × ⊥ bending

Bended crystal rod

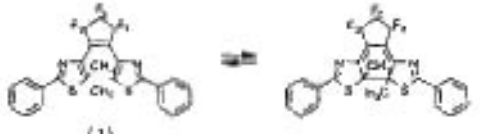

(1)

El cristal se dobla hacia la luz incidente debido al gradiente en la extensión de la isomerización, por la gran absorbancia de luz del cristal

Figure 10 Reversible bending of crystal rod **1** on alternate irradiation with ultraviolet (365 nm) light and visible (> 500 nm) light. On irradiation with ultraviolet light, the crystal rod ($225 \times 7.5 \times 5\ \mu m^3$) bent and the head moved as far as 47 μm. The bent crystal rod straightened again on irradiation with visible light. Top panel: pairs of images showing the first, fiftieth, and eightieth cycles (left to right)

sin que se rompa la microvarilla !!!

Bull. Chem. Soc. Jpn. 2008, 81, 917–926.

Materiales fotomecánicos

Músculos moleculares cristalinos

"A rod-type crystal (about 200 micrometers long and 5 micrometers Ø) was grown by sublimation on a glass plate so as to attach at one end to the glass plate. When illuminated from the side by an UV pulse light, the crystal rod bent and...

... displaced the free end by 50 micrometers. The crystal rod can launch a tiny silica-particle (80 micrometers Ø) as if it were a tennis ball, as shown in Figure 12."

Masahiro Irie

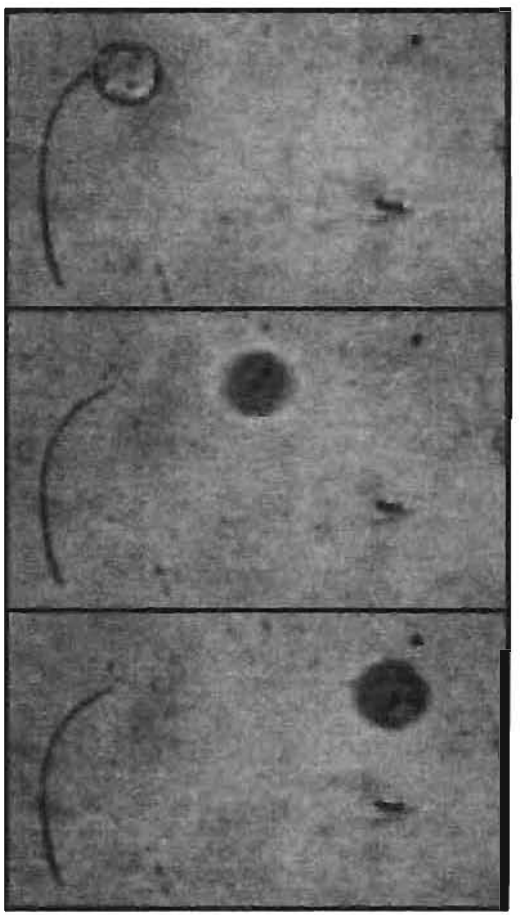

Figure 12. A shot of a silica micro-particle by crystal rod 1 upon irradiation with 365 nm light pulse.

Materiales fotomecánicos

Músculos moleculares cristalinos

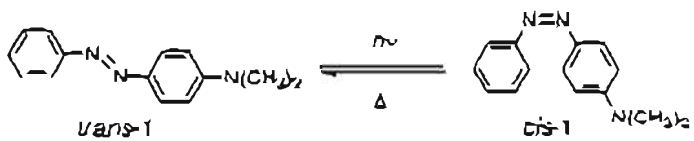

Figure 1a shows a piece of a platelike microcrystal (525 × 280 × 5 μm^3) whose lower portion was fixed to the glass surface and whose upper portion was free. The (001) surface was irradiated at 365 nm (5 mW/cm^2) from the right rear, as indicated by the arrow

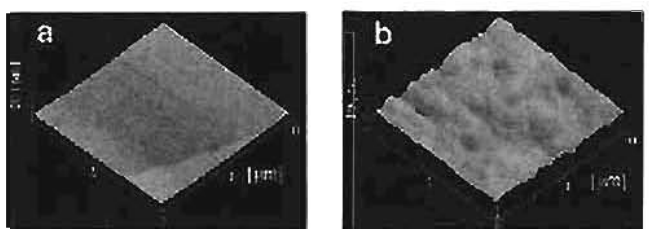

antes después

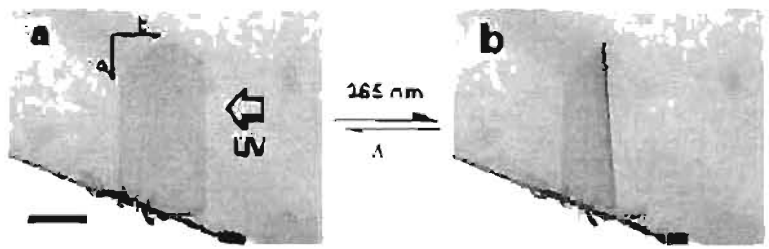

Figure 1. The (001) face of the platelike *trans*-1 microcrystal (a) before and (b) after UV irradiation from the right rear (indicated by the arrow labeled "UV"). The scale bar is 200 μm.

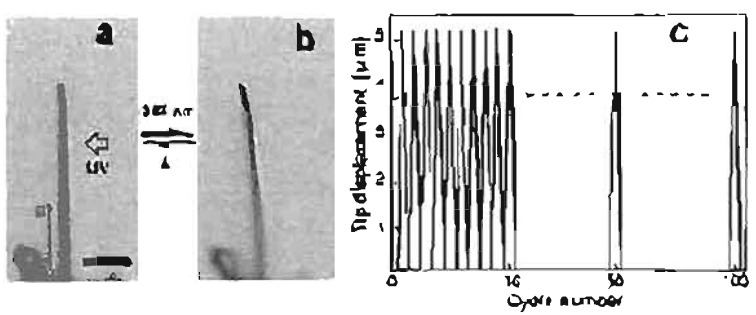

Figure 2. Bending of a narrow, platelike crystal of *trans*-1, as shown by a comparison of images acquired (a) with and (b) without UV irradiation. The scale bar is 20 μm. (c) Graph showing the repeatability of the reversible bending over as many as 100 cycles.

J. Am. Chem. Soc. 2009, 131, 6890-6891.

Materiales fotomecánicos

Objetos que se ensamblan / desensamblan

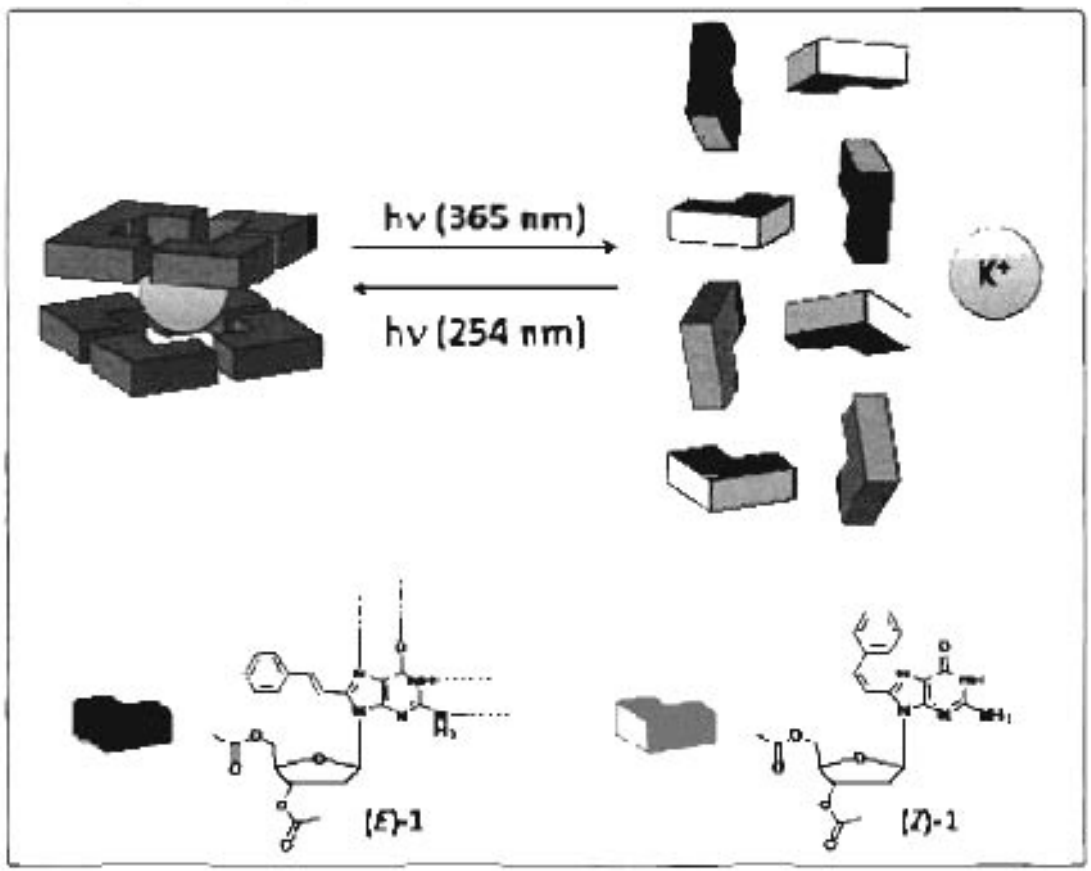

Las nucleobases de guanina se autoensamblan para formar tetrámeros que se estabilizan por parejas en presencia de K^+ (G_8K^+)

Es posible controlar con luz el autoensamblaje de los octámeros de G mediante grupos fenilvinilo unidos a G gracias a la isomerización *cis* / *trans* del C=C

El proceso es reversible

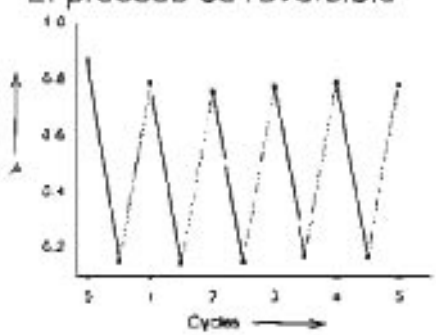

Figure 5. Switching cycles, monitored at 350 nm, between (*E*)-1/KI and (*Z*)-1 /KI by alternate irradiation with light of wavelength 365 nm (for 30 min, ——) and 254 nm (for 28 min, ····).

Angew. Chem. Int. Ed. 2010, 49, 3357-3360

Materiales fotomecánicos

Indicadores de tensión

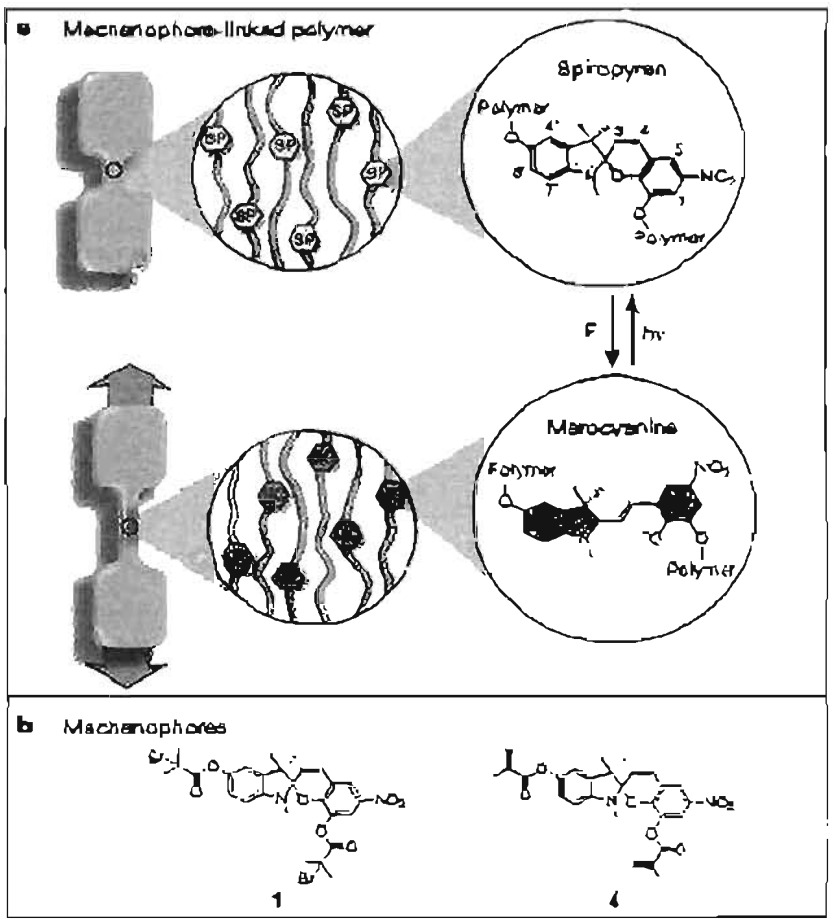

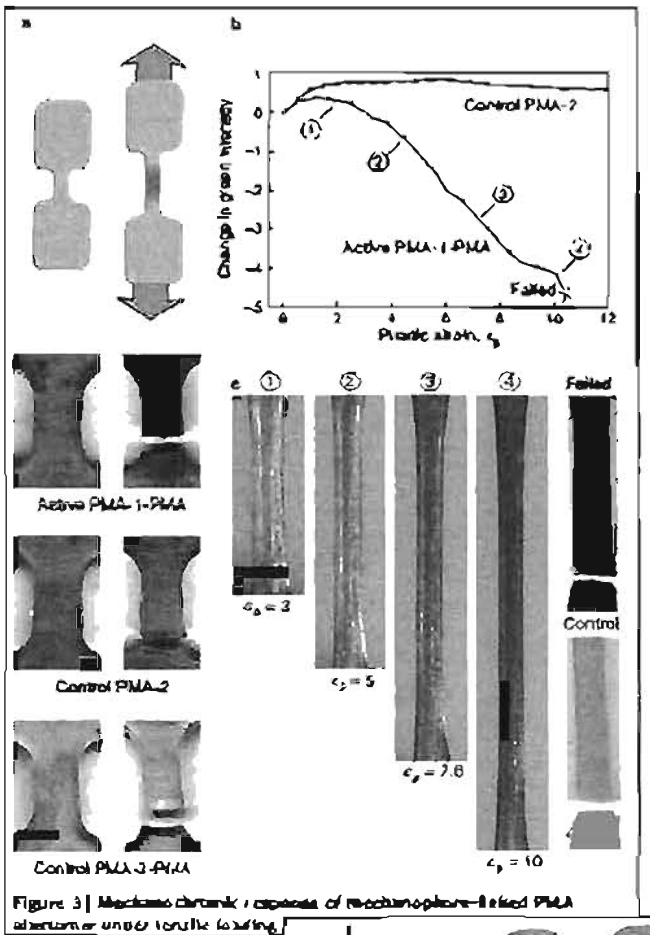

Figure 3 | Mechanochromic response of mechanophore-linked PMA elastomer under tensile loading.

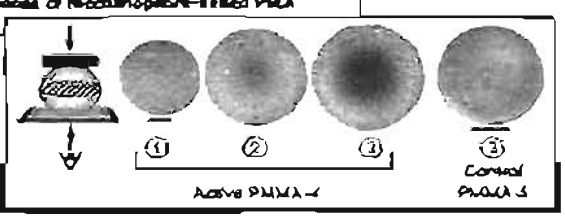

Nature 2009, 459, 68-72.

Otros materiales fotoactivos

- **Sistemas funcionales fotoactivos**
  - Funciones eléctricas
  - Funciones químicas
  - Funciones computacionales
- **Ejemplos de materiales fotoactivos y sus aplicaciones a distintos productos / tecnologías**

bottom-up nanotechnologies

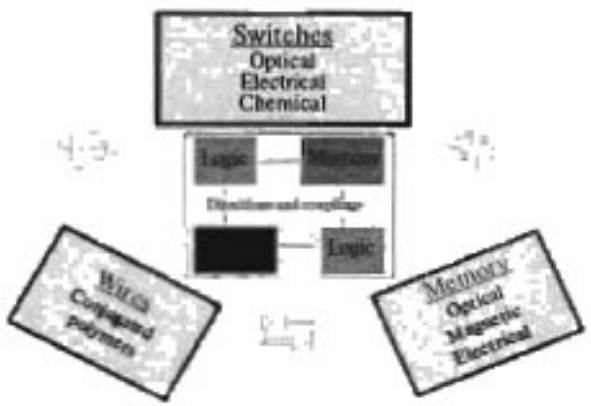

Fig. 4. Main components of molecular computers.

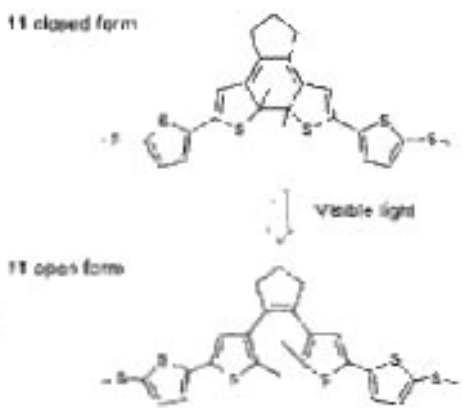

A smart fluid developed in labs at the Michigan Institute of Technology

Otros materiales fotoactivos

• Sistemas con funciones eléctricas

Molecular Electronics Roadmap

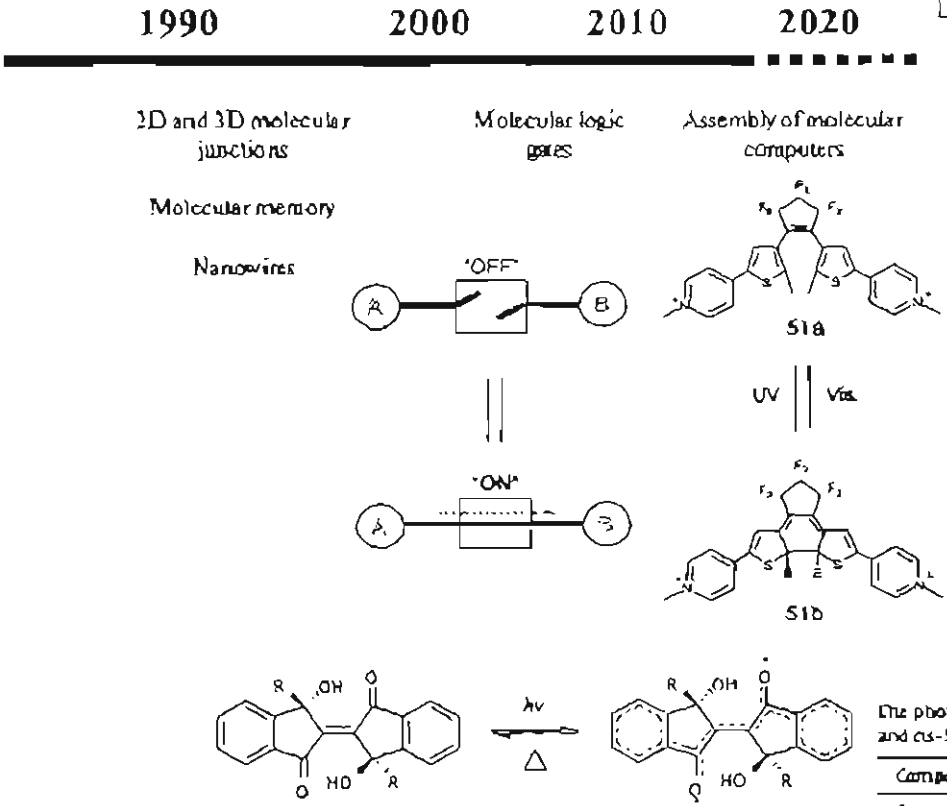

[ ] J. Photochem. Photobiol. C, 2009, 10, 141–147

The concept of controlling the interaction between terminally functionalized polyenes can also applied to magnetic interaction.[101] For this purpose, diarylethenes having two nitronyl nitroxide radicals **96** were prepared and the intramolecular magnetic interaction was compared in the open- and closed-ring forms. An appreciable difference in the interaction was observed between the open- ($2J/k_B = -2.2$ K) and the closed-ring ($2J/k_B = -11.6$ K) isomers (Scheme 32).

Scheme 32

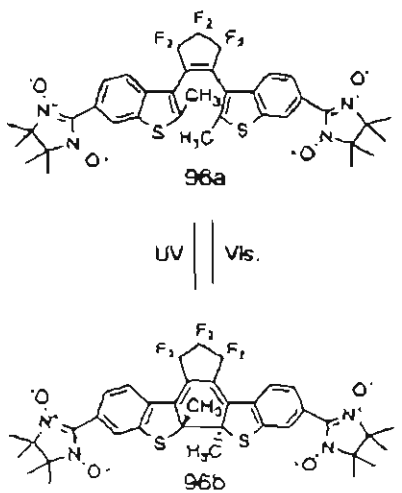

The photochromic and antiferromagnetic properties of compounds 5c, 5d, *trans*-5e and *cis*-5e.

Compound	Photochromism	ESR	Antiferromagnetism
5c	Yes	Yes	Yes
5d	Yes	Yes	No
trans-5e	Yes	Yes	No
cis-5e	No	No	No

Otros materiales fotoactivos

- **Sistemas con funciones eléctricas**

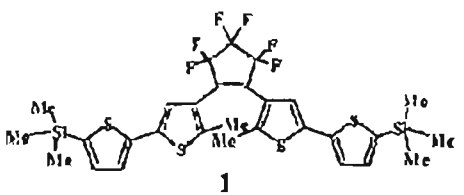

1

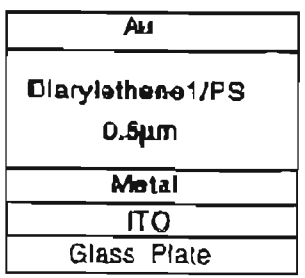

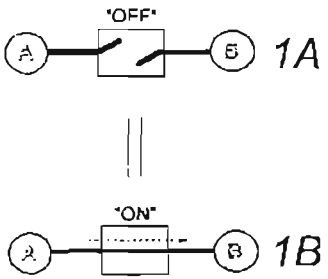

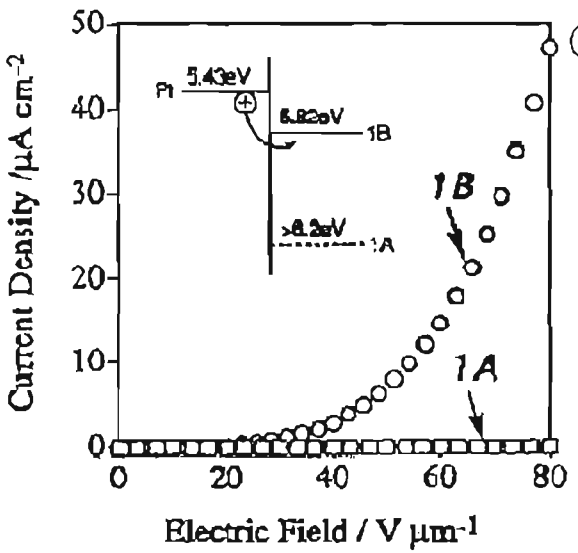

Fig. 1. Device structure and on–off characteristic in current flow based on photoisomerization of the diarylethene. 1A and 1B indicate uncolored and colored states.

[ ] J. Photochem. Photobiol. C, 2010, 11, 1-14

Otros materiales fotoactivos

- **Sistemas con funciones eléctricas**

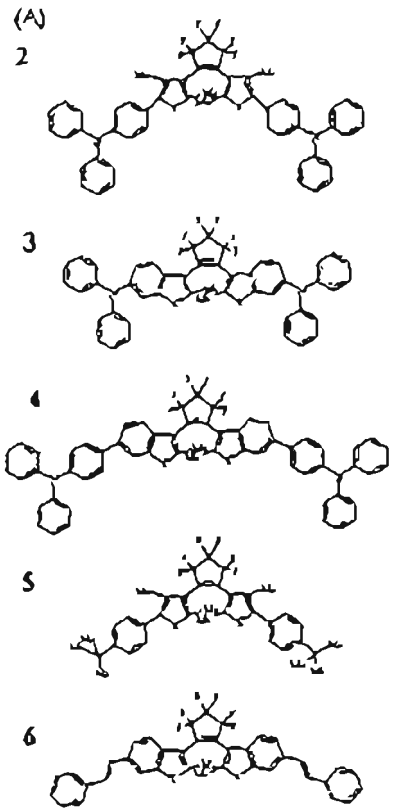

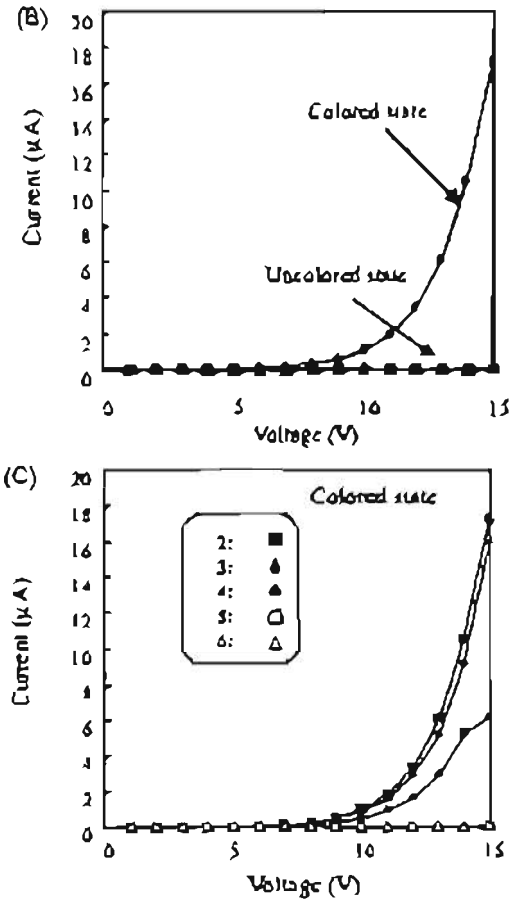

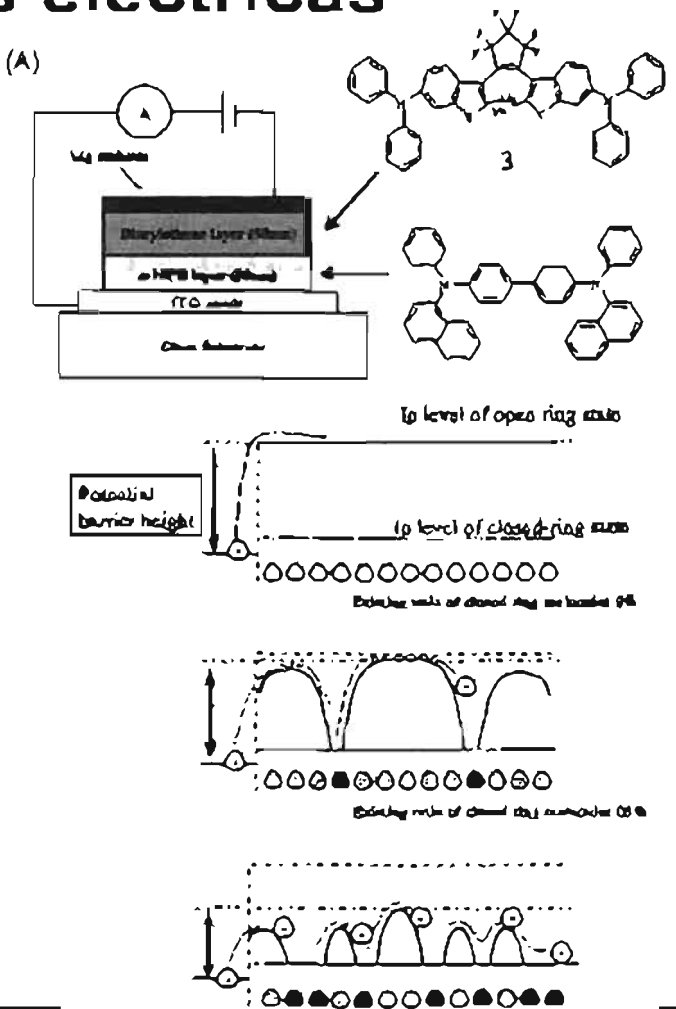

Otros materiales fotoactivos

- **Sistemas con funciones eléctricas**

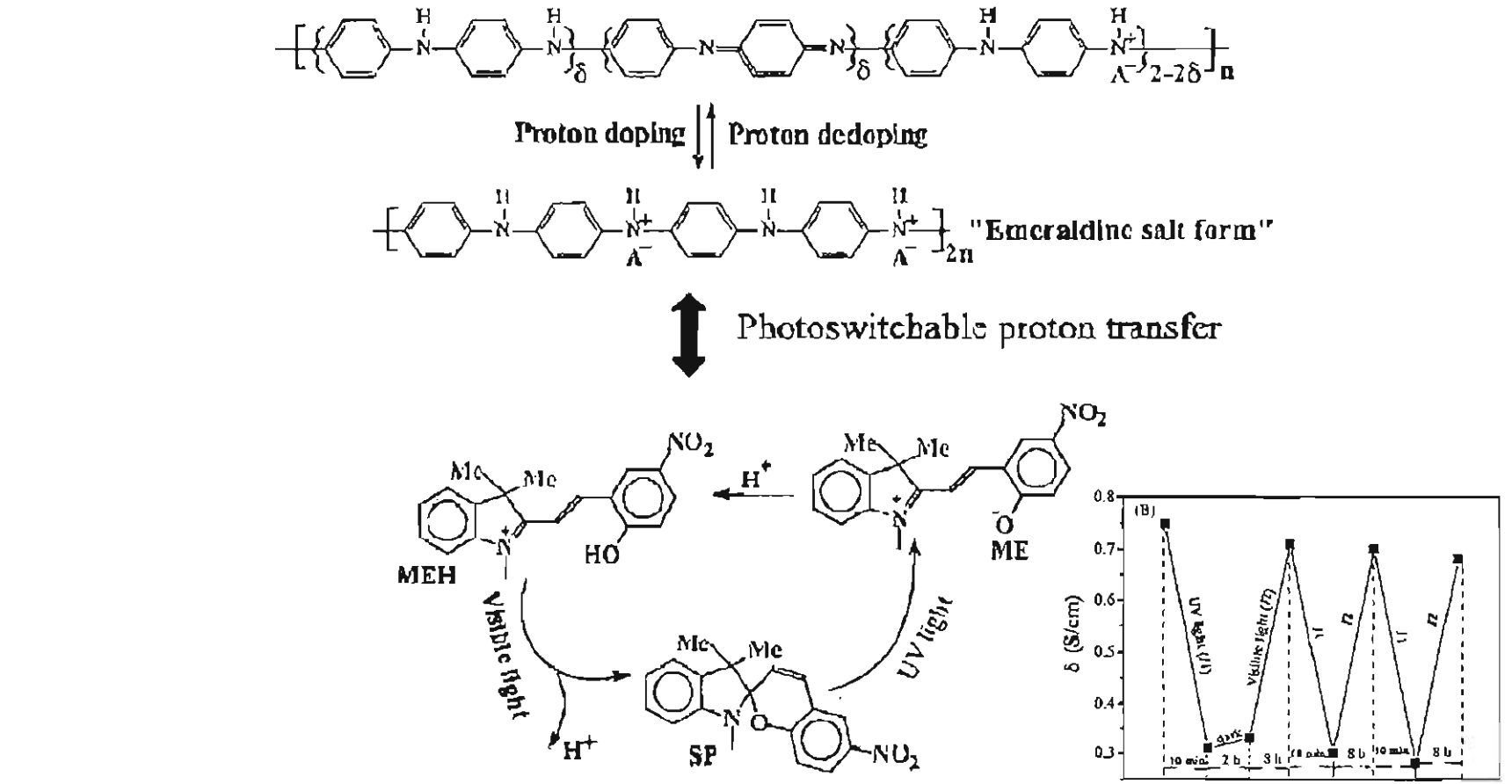

Fig 8. Mechanism of photo-induced proton transfer in a three-state molecular switch based on polyaniline containing a photochromic dye.

Otros materiales fotoactivos

- **Sistemas con funciones eléctricas**

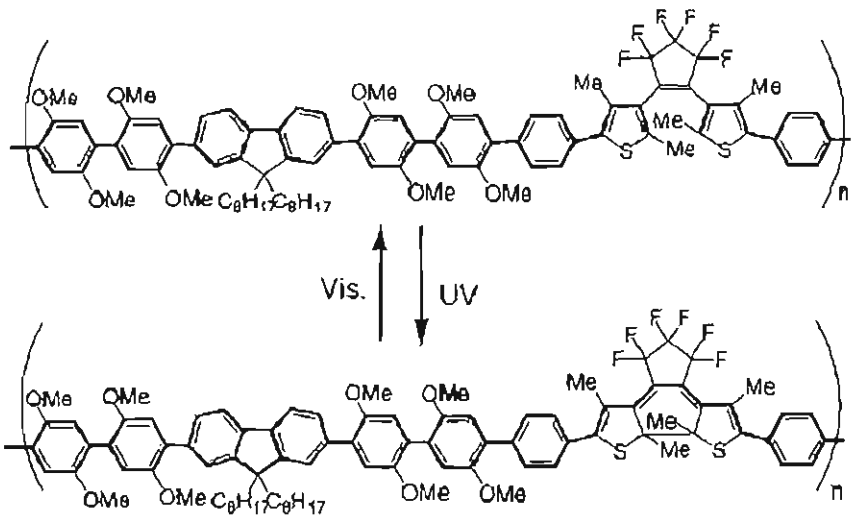

Fig. 15. Chemical structure of the polymer; the bold lines show the extension of the π-conjugated connections.

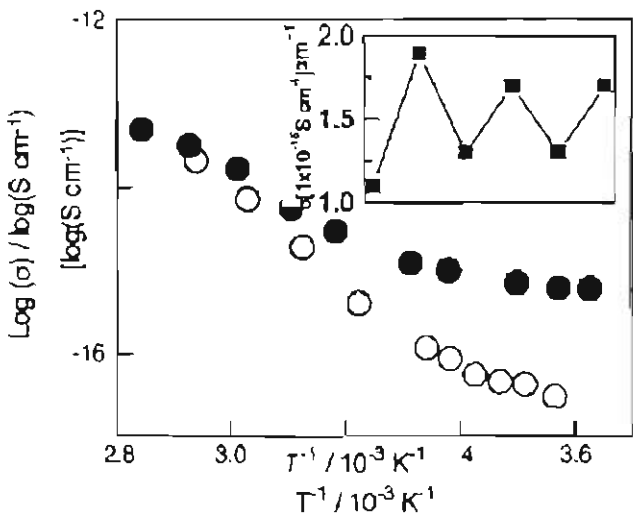

Fig. 16. Temperature dependence of the electrical conductivity of a film of the polymer: the solid circles denote the initial colored state of the polymer, and the open circles denote its state after photobleaching with visible-light irradiation. The inset shows the reversible change in electrical conductivity on alternating irradiation with UV and visible light.

Otros materiales fotoactivos

- **Sistemas con funciones eléctricas**

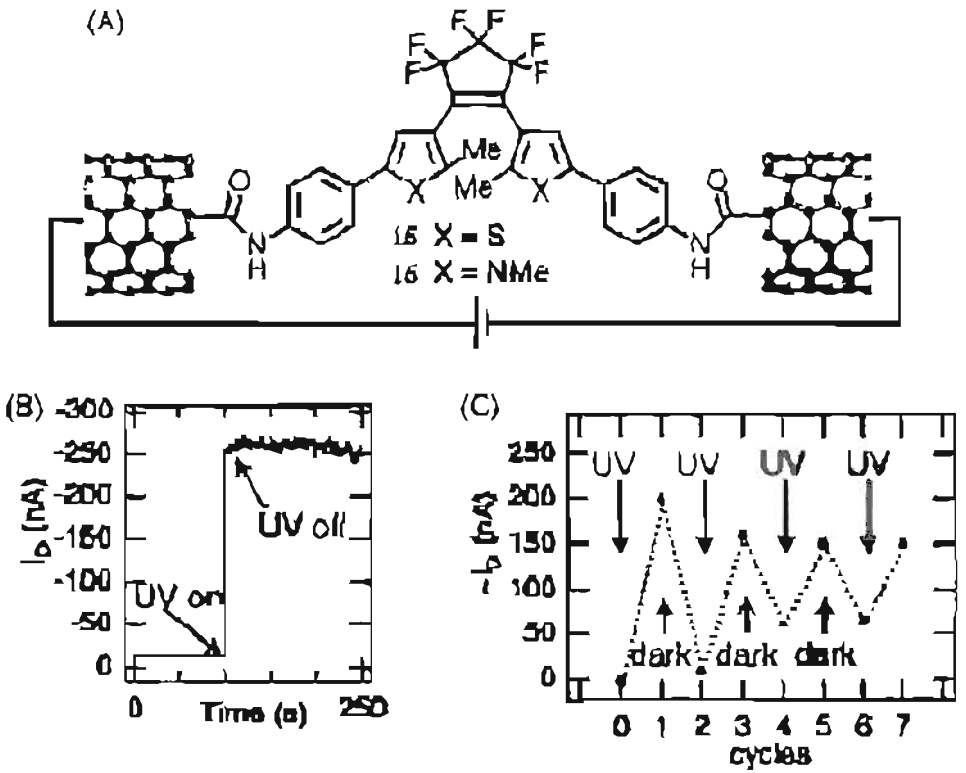

Otros materiales fotoactivos

• Sistemas con funciones eléctricas

≠ Potencial de ionización del *cis* / *trans*-azobenceno (aceptor de e^- del TCNQ)

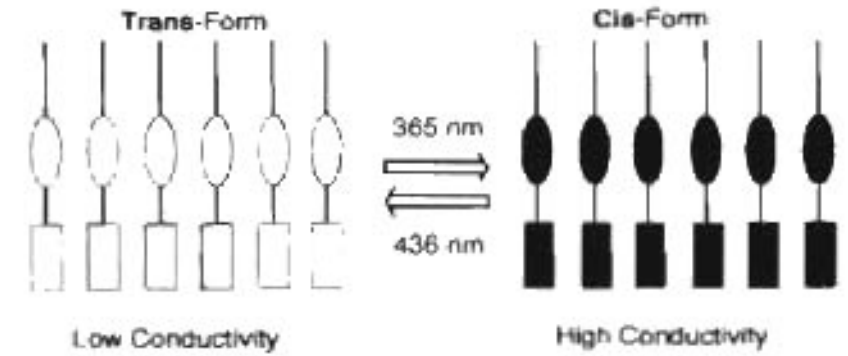

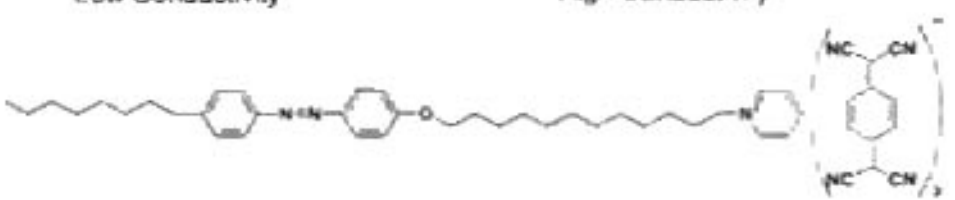

Figure 5.28. Photocontrol of conduction within a monolayer

Fotocontrol bidimensional de la conductividad eléctrica:

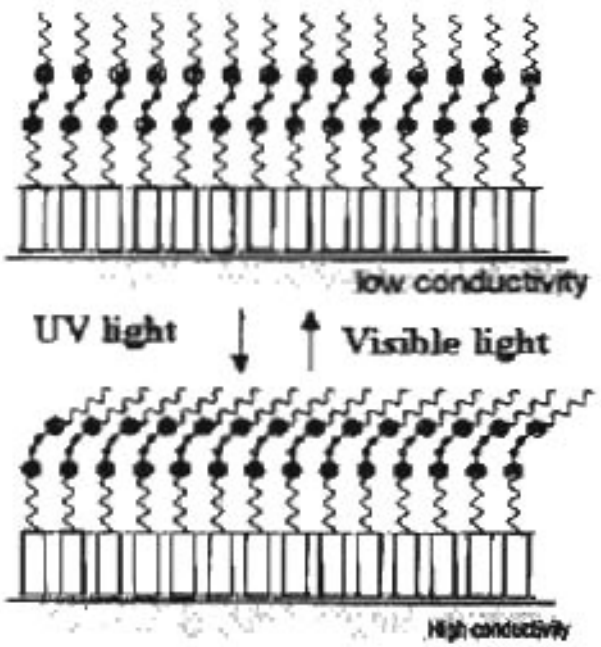

Otros materiales fotoactivos

• Sistemas con funciones eléctricas

Interruptor molecular sencillo o de una vía:

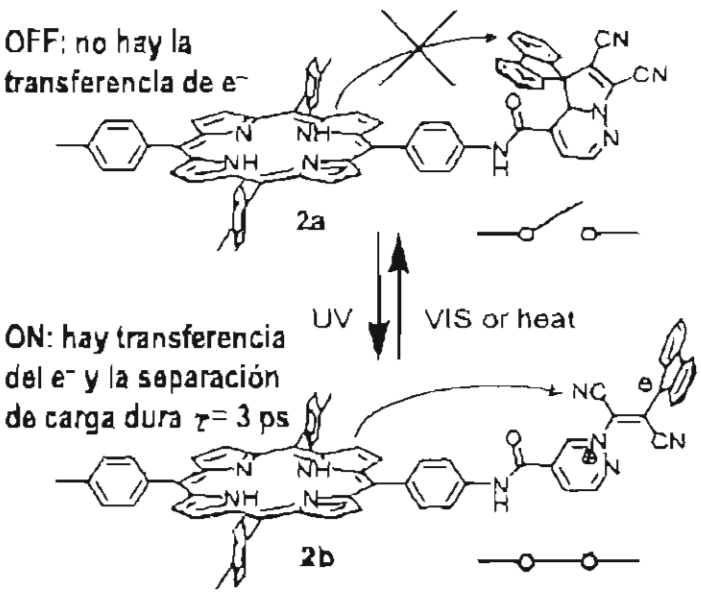

Fig. 2 A molecular single-throw switch. In 2a, photoinduced electron transfer does not occur. UV irradiation converts 2a to 2b, in which the betaine moiety can be reduced by the porphyrin first excited singlet state to yield a charge-separated state. Visible irradiation converts 2b back into the inactive form.

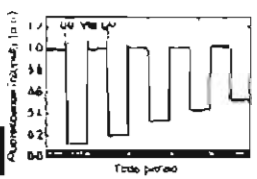

J. Chem. Commun. 2005, 1169-1173

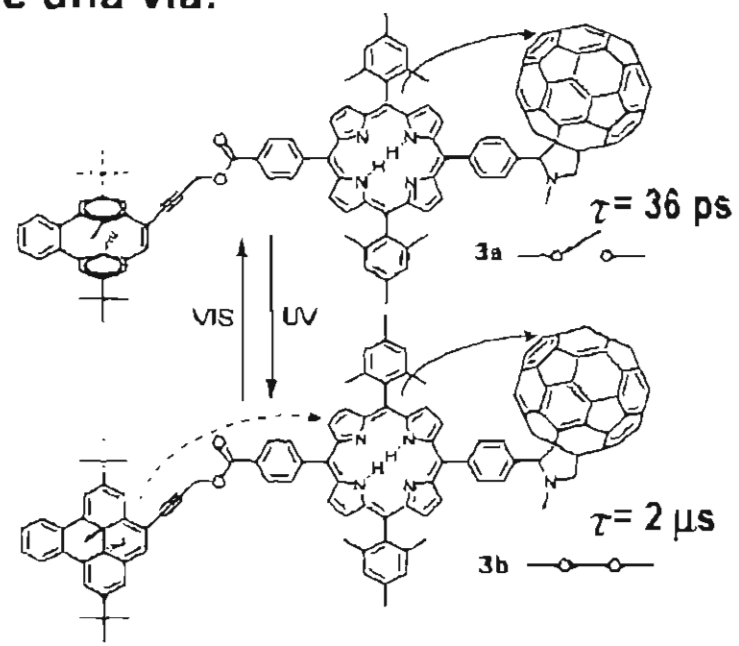

Fig. 5 CPD–P–C_{60} molecular triad 3a is converted to the dihydropyrene isomer 3b (DHP–P–C_{60}) upon irradiation with UV light, and visible irradiation regenerates 3a. The triad acts as a single-throw molecular switch based on the changes in the oxidation potential of the photochrome.

Otros materiales fotoactivos

• Sistemas con funciones eléctricas

Interruptor molecular de dos vías: *Importancia del diseño de las cadenas espaciadoras en el control de la cinética de la transferencia electrónica*

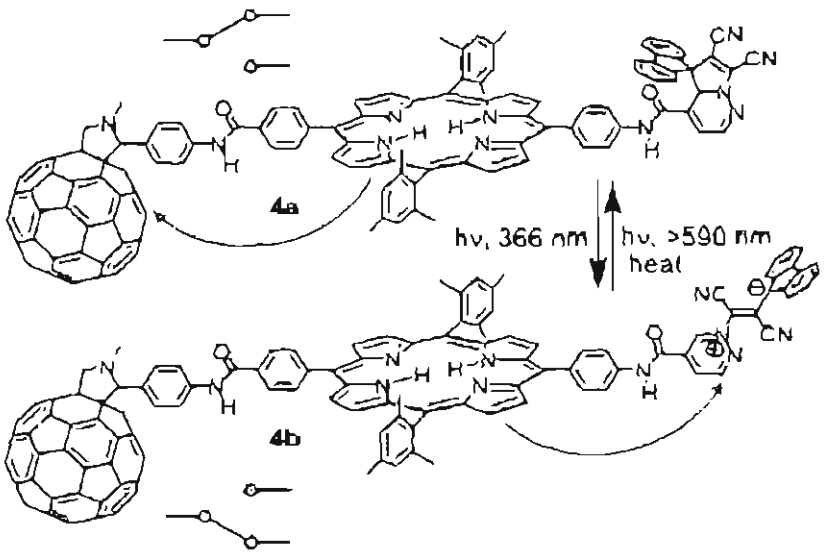

Fig. 7 Light-controlled double-throw switch. In 4a, excitation of the porphyrin leads to photoinduced electron transfer to produce DH–$P^{\bullet+}$–$C_{60}^{\bullet-}$. Photoisomerization with UV light forms 4b. Excitation of 4b results in formation of $BT^{\bullet-}$–$P^{\bullet+}$–C_{60}. Thus, photoinduced electron transfer is directed down one branch of the molecule or the other, depending upon the state of the photochromic switch.

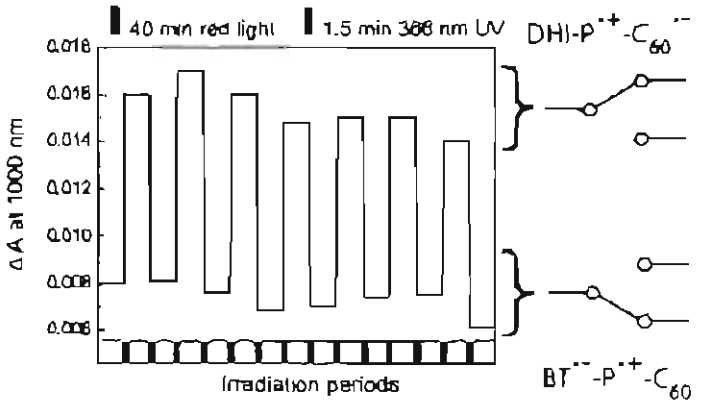

Fig. 8 Cycling of molecular double-throw switch 4. Irradiation with red light photoisomerizes the molecule to the DH-P-C_{60} form, in which photoinduced electron transfer occurs from the porphyrin to the fullerene, as indicated by the high transient absorbance values at 1000 nm. UV light converts the molecule to the BT-P-C_{60} form, wherein photoinduced electron transfer occurs preferentially to the betaine, whose radical ion lacks strong absorbance in the 1000 nm region.

Otros materiales fotoactivos

- **Sistemas con funciones químicas**

Fotocontrol del reconocimiento molecular:

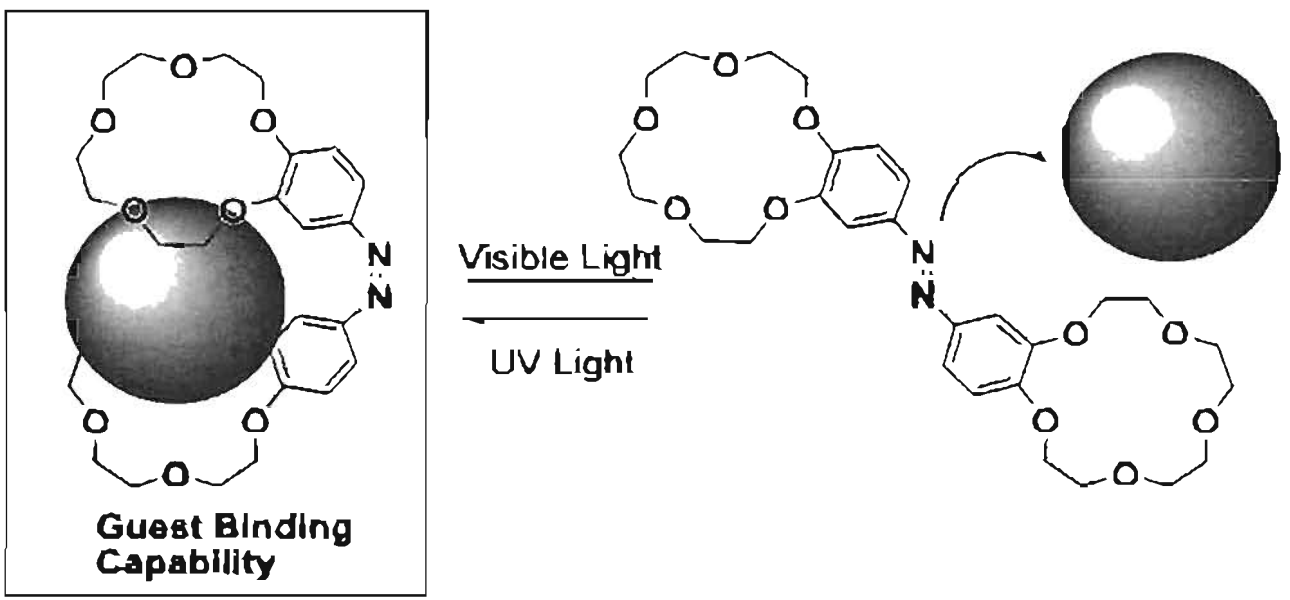

Applications of Supermolecules, Molecular Devices and Nanotechnology, Cap 5. En *Supramolecular Chemistry – Fundamentals and Applications*. Springer, Berlin. 2006.

Otros materiales fotoactivos

• Sistemas con funciones químicas

Fotocontrol del reconocimiento molecular:

Scheme 33

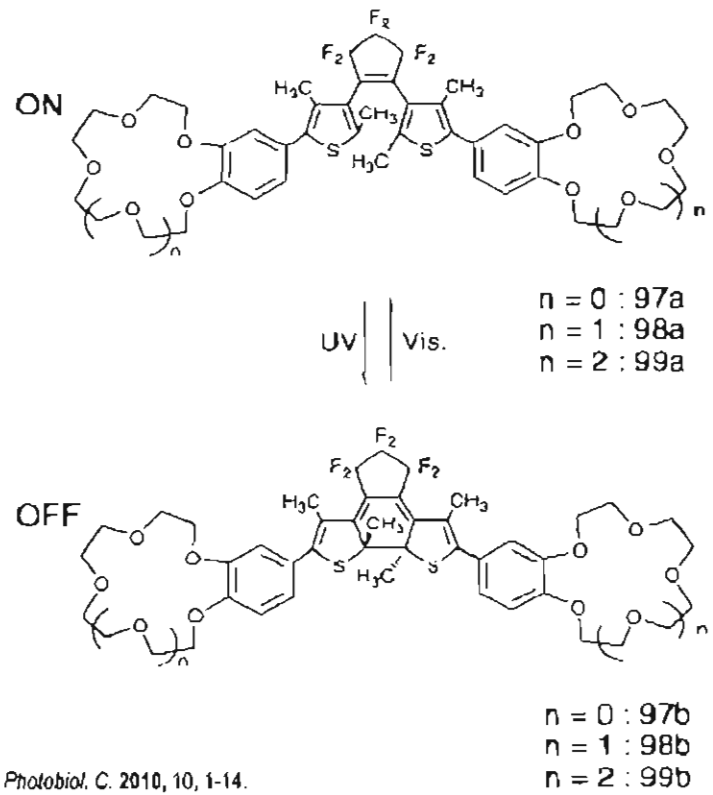

J. Photochem. Photobiol. C. 2010, 10, 1-14.

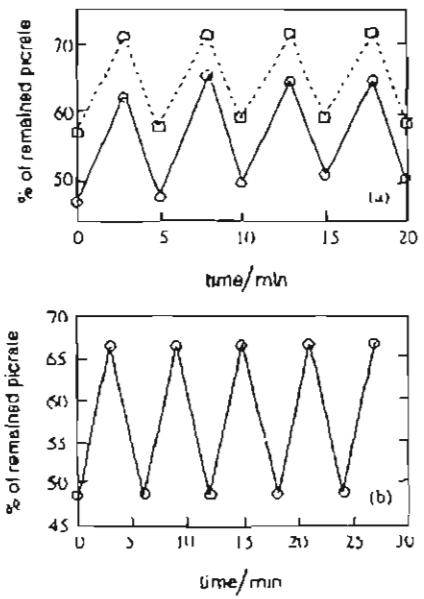

Figure 16. Control of the concentration of (a) KPic (—) and RbPic (· · ·) in the aqueous phase with **98** in CH_2Cl_2 and (b) CsPic with **99** by alternate irradiation with 330 ± 70 and >480 nm light.

Otros materiales fotoactivos

- **Sistemas con funciones químicas**

Fotocontrol del reconocimiento molecular:

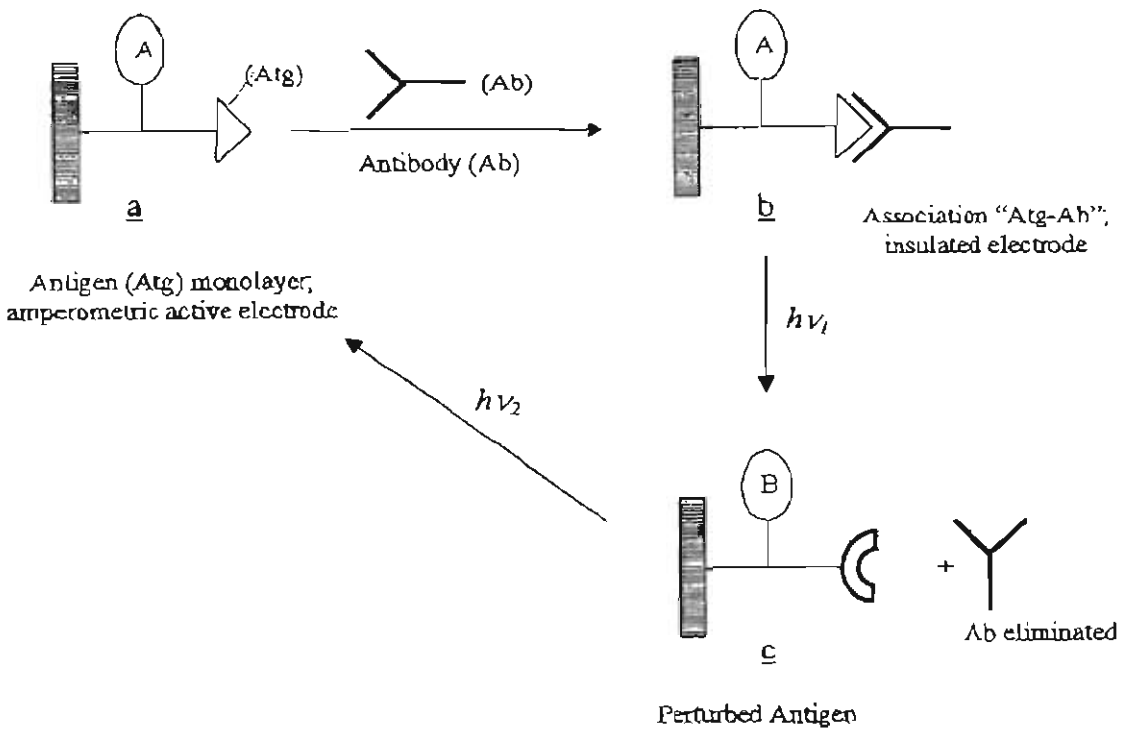

Fig. 4 Schematic assembly of a photoreversible immunosensor electrode. Reproduced from [49] with permission; copyright 1997 American Chemical Society.

Otros materiales fotoactivos

• Sistemas con funciones químicas

Fotocontrol del carácter hidrófilo / hidrófobo de una superficie:

Controlando la humectabilidad mediante la polaridad superficial del WO_3

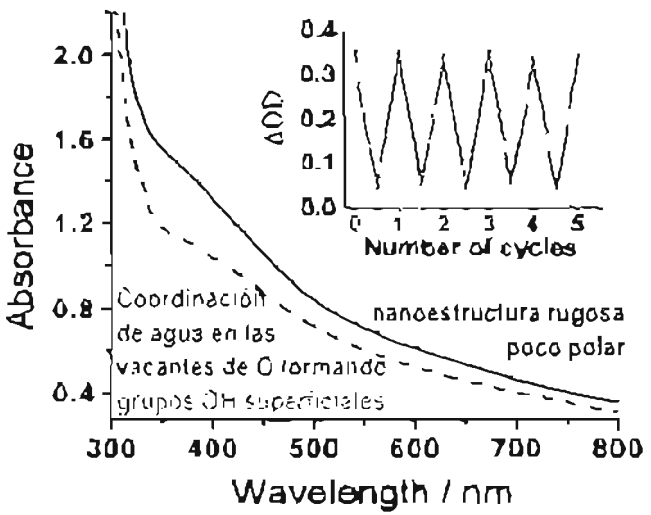

Fig. 14 Absorption spectra of an electrodeposited tungsten oxide film before (solid line) and after (dashed line) UV-light irradiation at 365 ± 10 nm. The insert shows the photochromic switching of the absorption change (monitored at 372 nm) during consecutive cycles of UV irradiation and storage in the dark.[161]

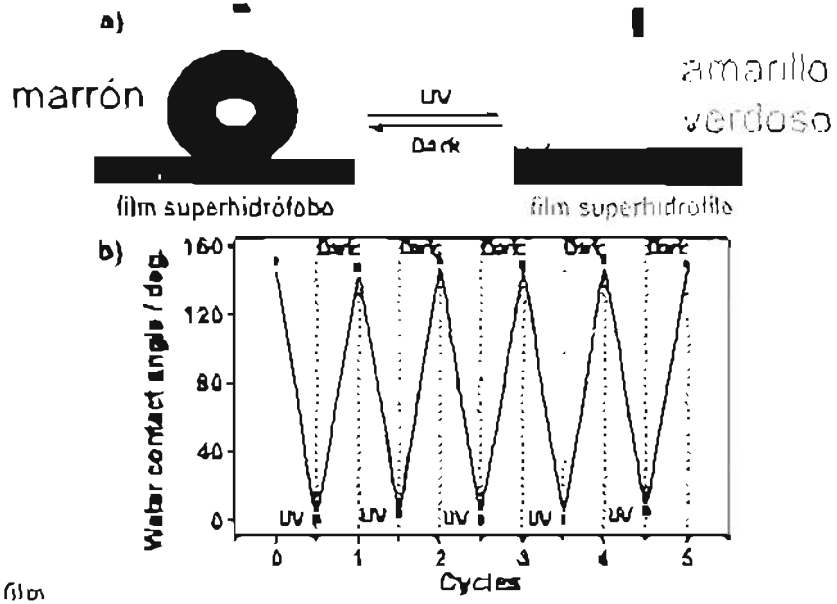

Fig. 15 (a) Water-drop profiles for the photoresponsive switch between superhydrophobicity and superhydrophilicity of a tungsten oxide film (left) before and (right) after UV irradiation. The water contact angles are 151.3 ± 2.9° and less than 5°, respectively. (b) Reversible water contact angle transition on the deposited tungsten oxide film upon alternating UV irradiation and storage in the dark.[161]

J. Mater. Chem. 2007, 17, 4547-4557.

Otros materiales fotoactivos

• Sistemas con funciones químicas

Fotocontrol del carácter hidrófilo / hidrófobo de una superficie:

a Controlando la humectabilidad mediante la polaridad de una merocianina (zwitterión)

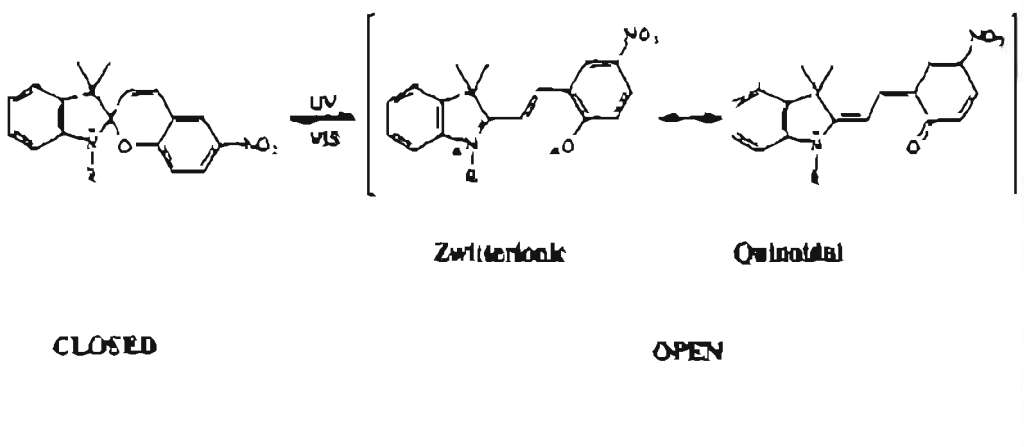

b

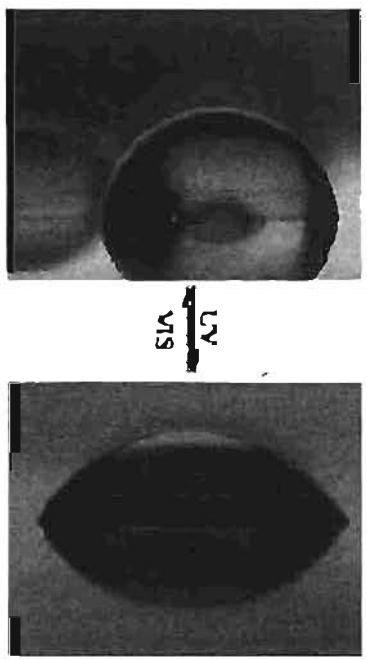

Fig. 6. (a) UV-Vis light-induced isomerization of spiropyran from closed (spirocyclic) form to open (merocyanine) form. Two resonance structures of the open form. (b) Examples of water drops deposited on spiropyran functionalized surfaces after visible and UV irradiation. From [7].

Prog. Surf. Sci. 2007, 82, 407-434.

Otros materiales fotoactivos

• Sistemas con funciones químicas

Fotocontrol del movimiento mediante la polaridad superficial:

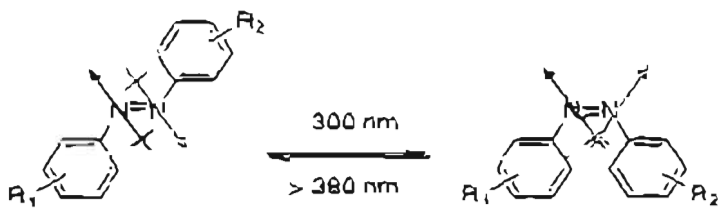

trans
apolar
o
hidrófobo
causa menor $E_{superficial}$

cis
polar
o
hidrófilo
causa mayor $E_{superficial}$
tirando de la gota
hacia su zona

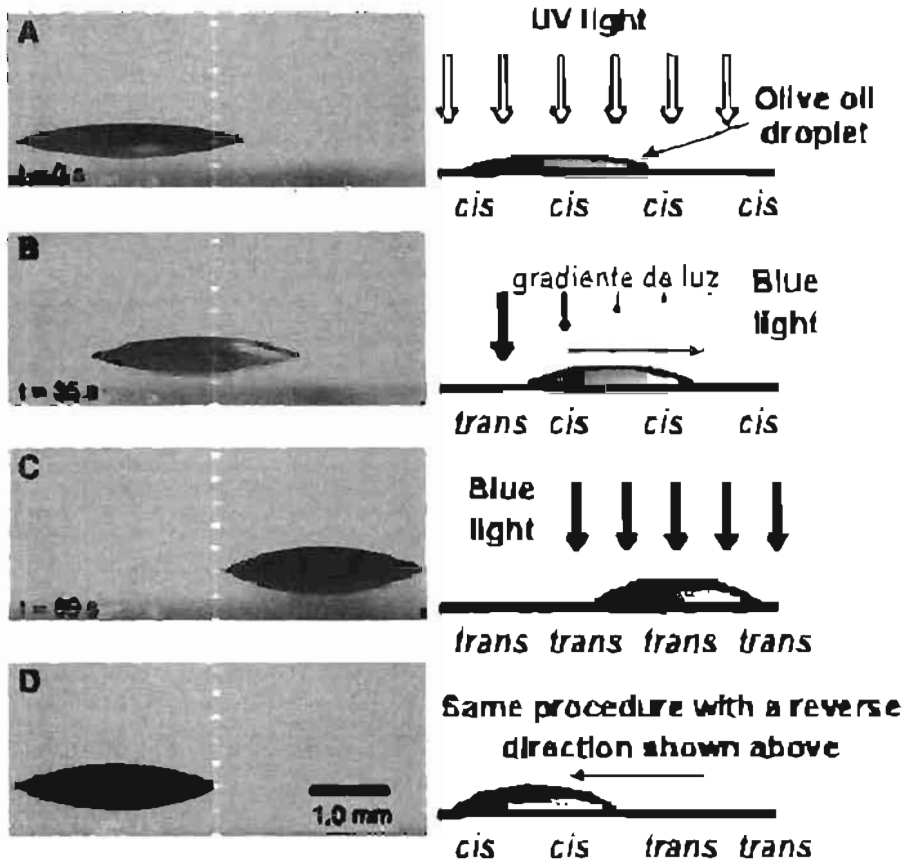

Otros materiales fotoactivos

- **Sistemas con funciones químicas**

Fotocontrol del movimiento mediante la polaridad superficial:

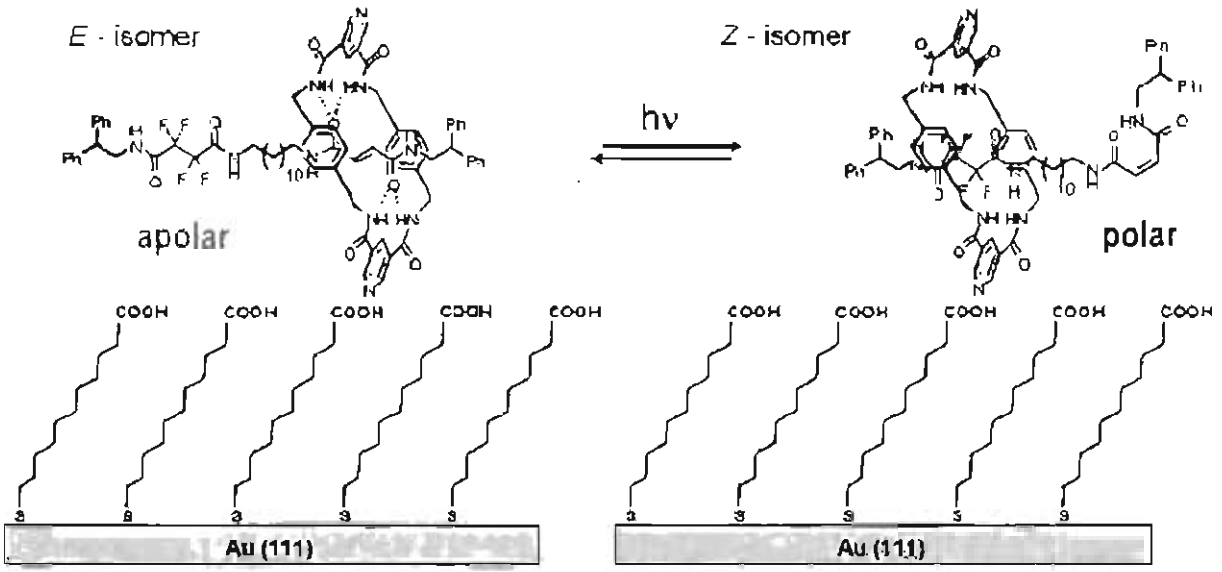

Fig. 9 Light-switchable rotaxane with the fluoroalkane station exposed (*E*-isomer) were physisorbed onto a 11-mercaptoundecanoic acid-terminated self-assembled monolayer on Au(111) (hydrophobic surface). Illumination with 240–400 nm light caused the nanometer displacement of the rotaxane thread in the shuttles to shield the fluoroalkane units (*Z*-isomer) leaving a more polarophilic surface.

Una gota de CH_2I_2 de ~ 1 μL se desplaza ~ 1 mm a 1 μm s^{-1} incluso con por una pendiente de 12º

Otros materiales fotoactivos

- **Sistemas con funciones químicas**

Fotocontrol de la rugosidad superficial:

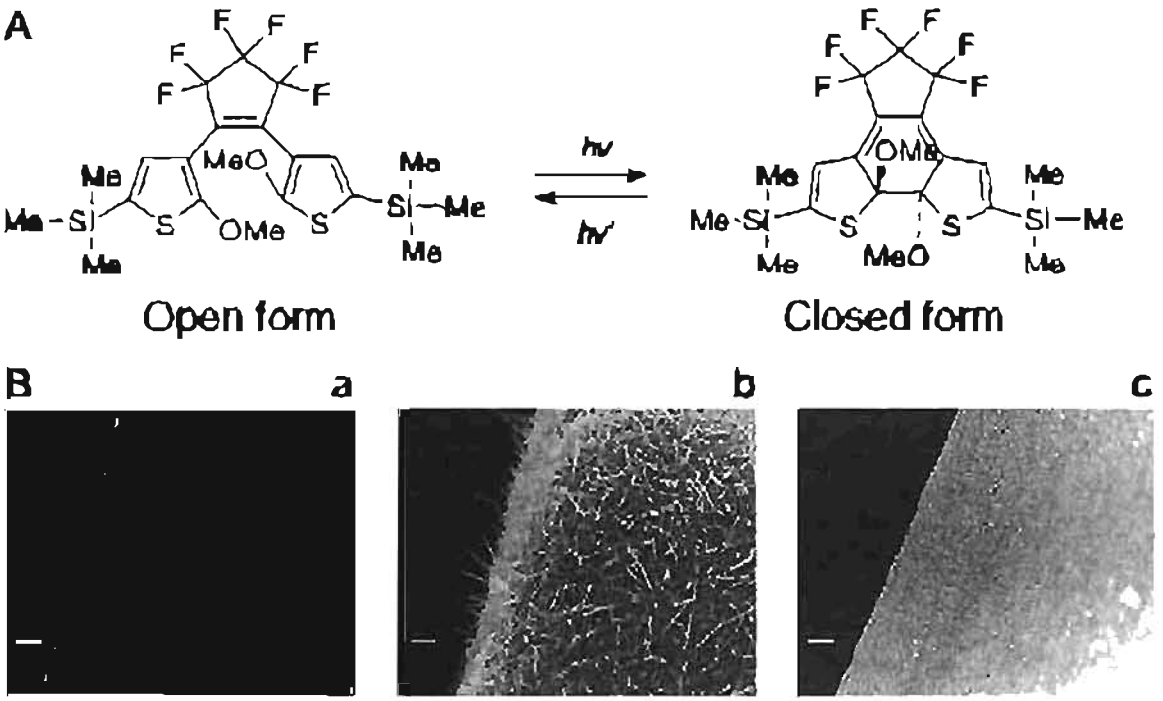

Fig. 8. (A) Reversible formation of open and closed forms. (B) Reversible changes in surface morphology of a single crystal of 1,2-dithienylethene (scale bar: 10 μm): (a) scanning electron microscope (SEM) image of the crystal surface of the open form from a side view (×1000) before UV irradiation (254 nm); (b) SEM image from a side view (×1000) of the surface after UV irradiation (254 nm, 12 W, 10 min) and storage in the dark for 24 h. (c) SEM image from a side view (×1000) of the surface after irradiation with visible light (>500 nm, 500 W, 20 min) and storage in the dark for 24 h. From [51].

Otros materiales fotoactivos

- **Sistemas con funciones químicas**

"Smart gels"

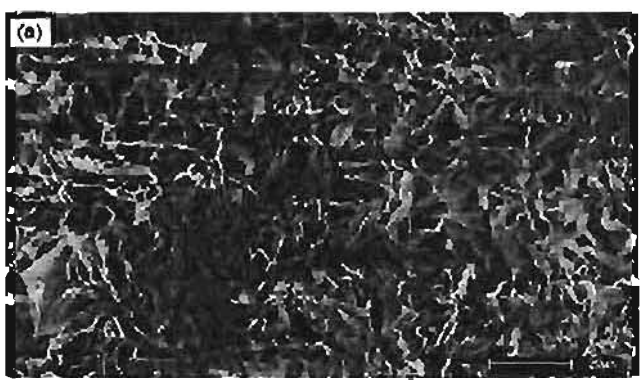

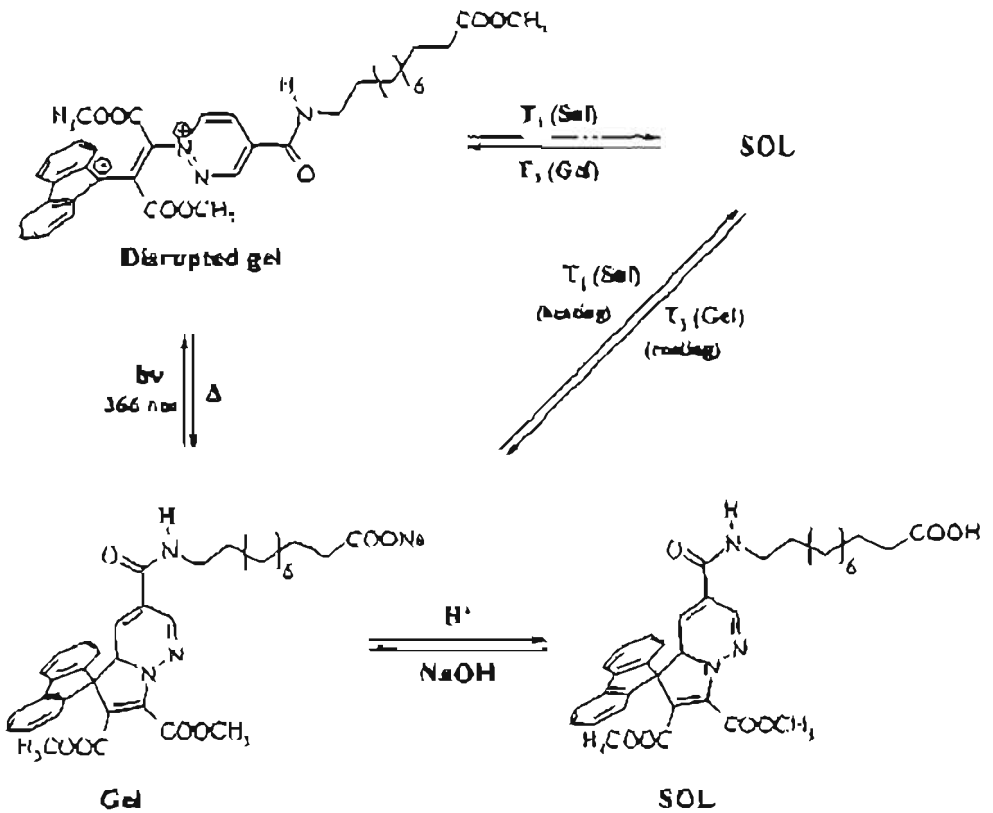

J Photochem Photobiol A Chem. 2008, 200 57-67

flash-back a ... Tipos de fotocromismo

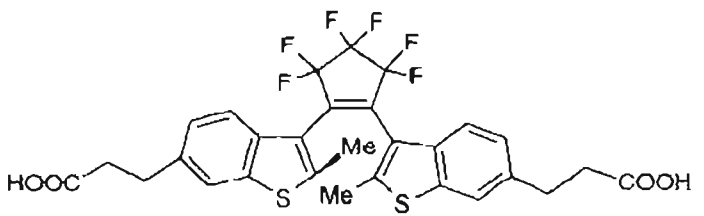

antiparallel open form

3a

cyclohexane

ethanol or heat

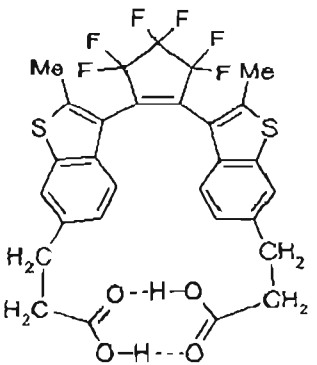

parallel open form

3b

hν' *hν*

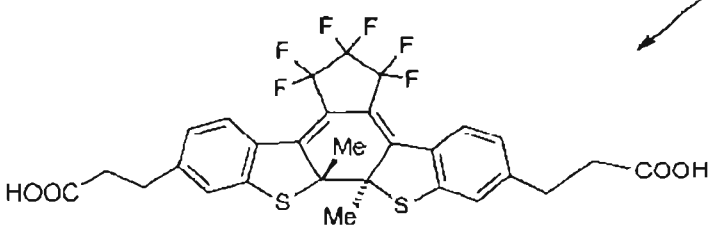

closed form (colored)

3c

Gated photochromism

Forma especial de fotocromismo en la que una **(3a)** o las dos formas del **sistema fotocrómico** (3a y 3c) se transforman reversiblemente, **química-** o electro-químicamente, en una ***forma no fotocrómica*** **(3b)**

Pure Appl. Chem. **2001**, *73*, 639-665.

flash-back a ... Tipos de fotocromismo

Acidocromismo

In acidichromism, the protonated form and the conjugate base of some compounds may have distinctly different absorption spectra. This phenomenon is well known for phenols and aromatic amines. *It can occur in addition to photochromism*, e.g., for spirooxazines (SO) which generate merocyanines (MC) [23] as illustrated in the following scheme:

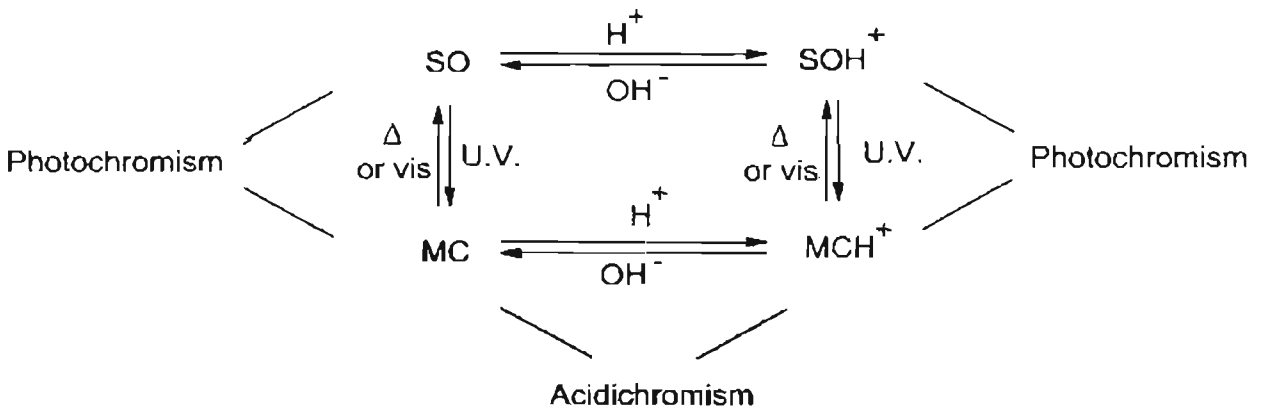

In some cases, it is possible to take advantage of acidichromism to develop nondestructive readout systems in which one of the forms can be used for readout and the others for writing and erasing

flash-back a ... Tipos de fotocromismo

Dual-mode photochromism

Fotocromismo característico de sistemas complejos que se puede activar por dos estímulos externos diferentes, como luz o corriente eléctrica. En dicho caso el fotocromismo y el "electrocromismo" se regulan mutuamente

Compound 4 may be reversibly transformed to 5 photochemically, 4 being electrically inert and 5 being active and reversibly oxidized to 6 within the −1 to +1V range.

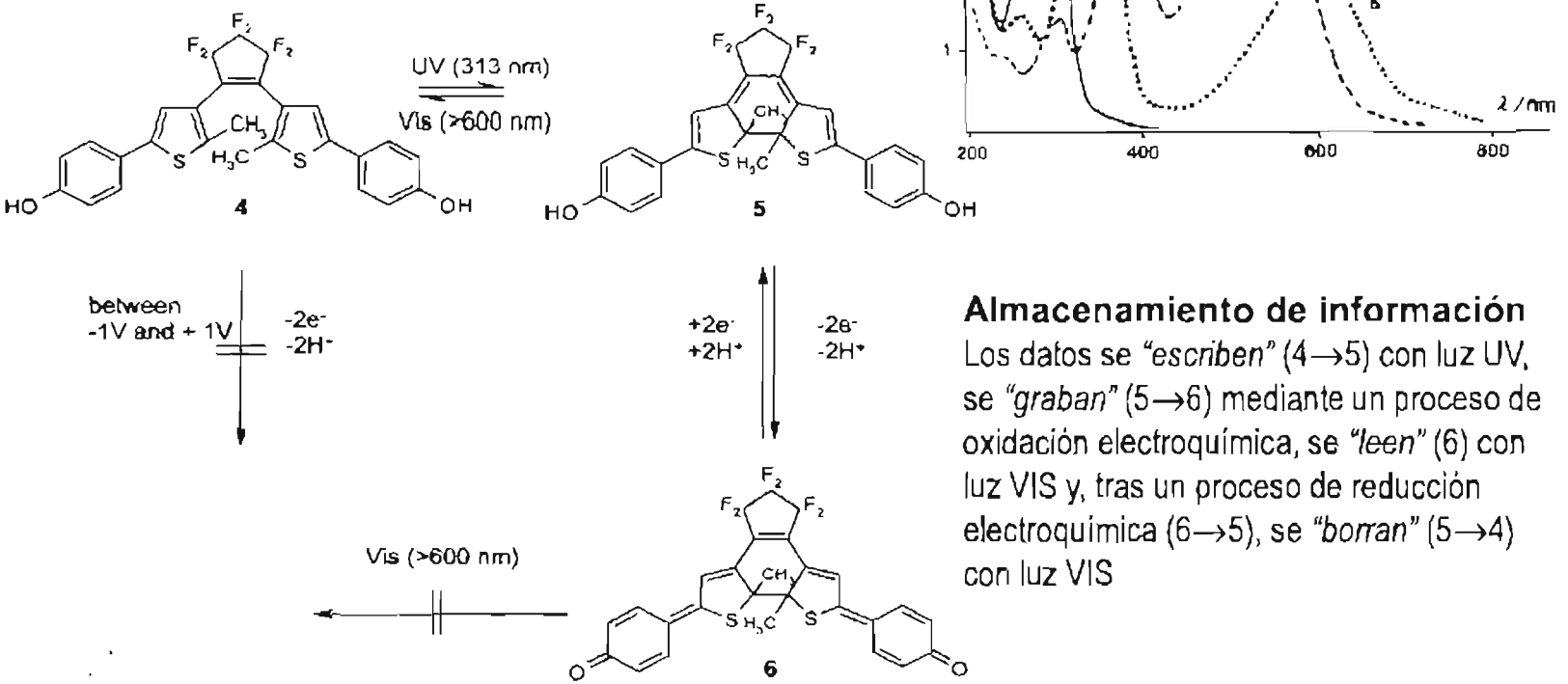

Almacenamiento de información

Los datos se *"escriben"* (4→5) con luz UV, se *"graban"* (5→6) mediante un proceso de oxidación electroquímica, se *"leen"* (6) con luz VIS y, tras un proceso de reducción electroquímica (6→5), se *"borran"* (5→4) con luz VIS

Otros materiales fotoactivos

• Sistemas con funciones computacionales

Almacenamiento de información:

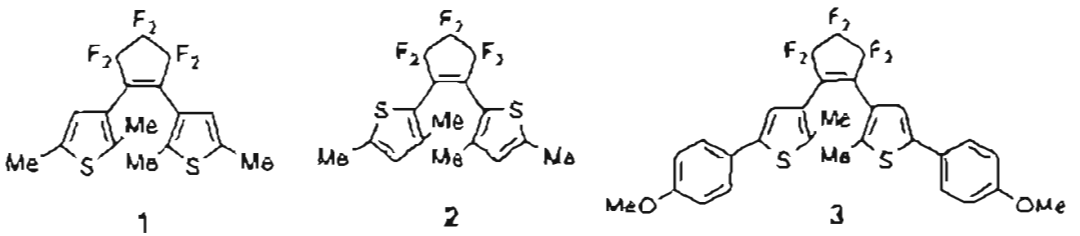

Chart 2 Diarylethenes 2 and 3.

the three colours showed that the three components are packed in a similar manner and undergo photochromic reactions in the single-crystalline phase. In addition, the combination of "ON" and "OFF" states of each primary colour gave eight colours ($2^3 = 8$), such as colourless, yellow, red, blue, orange, purple, green, and black. All the colours are thermally stable and do not fade in the dark. They are completely bleached by irradiation with visible light ($\lambda > 450$ nm). Such multi-coloured photochromic crystals have the potential for application to multi-frequency three-dimensional optical memory media and photo-switchable full-colour displays.

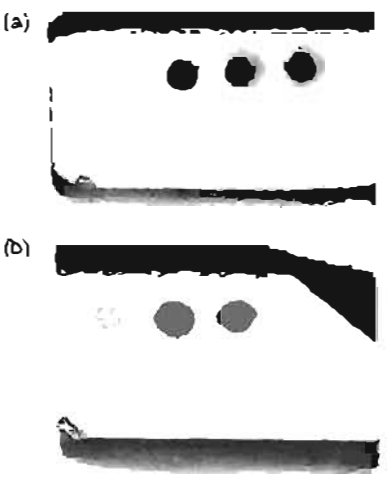

Fig. 3 Photographs of partially coloured crystals 1·3 (a) and 1·2·3

J. Chem. Commun. 2005, 3595–3605

Otros materiales fotoactivos

• Sistemas con funciones computacionales

Almacenamiento de información:

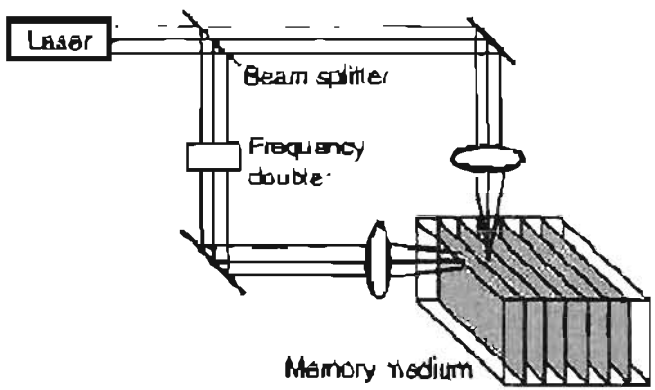

Figure 3. Principle of 3D optical memories as proposed by Rentzepis et al.[17]

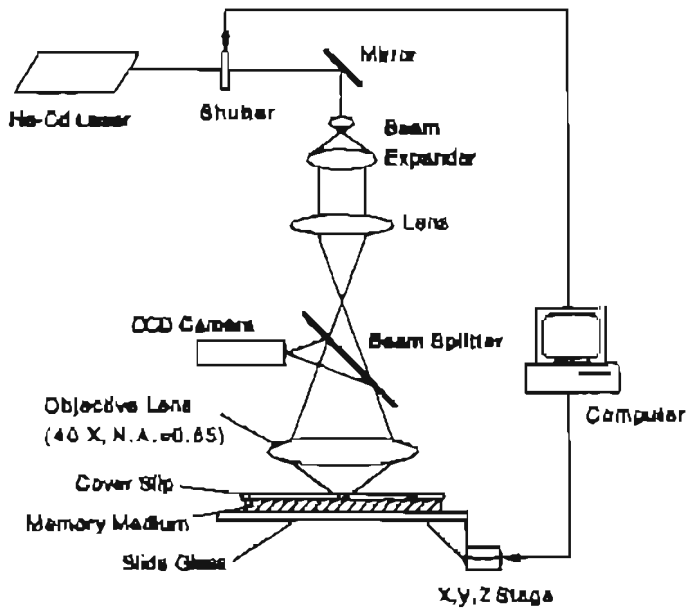

Figure 5. Optical setup for recording 3D bit information in photochromic memory.

[7] Chem. Rev. 2000, 100, 1777-1788.

Otros materiales fotoactivos

- **Sistemas con funciones computacionales**

Almacenamiento de información:

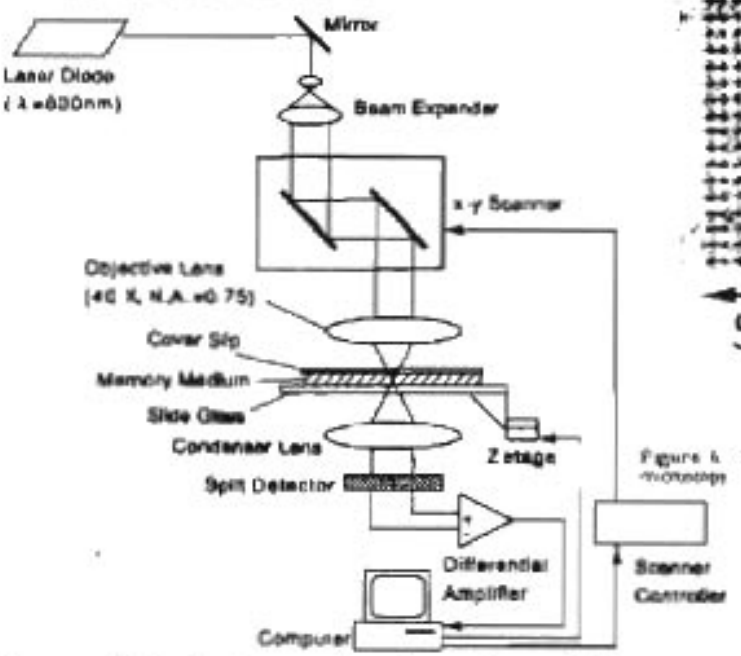

Figure 4. Optical system for the readout of 3D memory. A near-IR differential phase-contrast microscope was used for nondestructive readout.

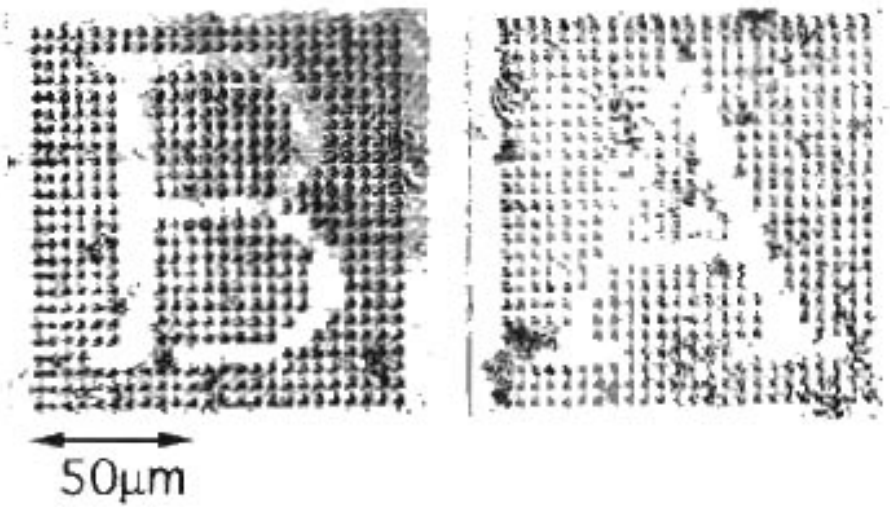

Figure 6. Bit patterns read from photochromic memory using near-IR laser-scanning differential phase-contrast microscope: (a) first layer, (b) second layer. The bit interval is 1 μm, and the layer distance is 70 μm.

Otros materiales fotoactivos

- **Sistemas con funciones computacionales**

Almacenamiento de información:

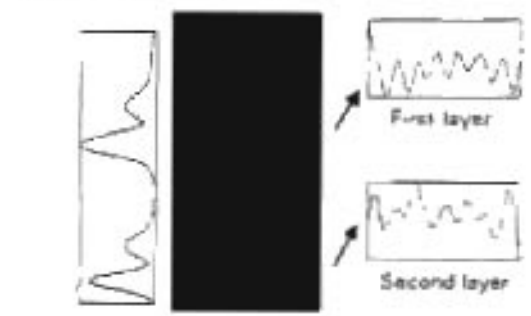

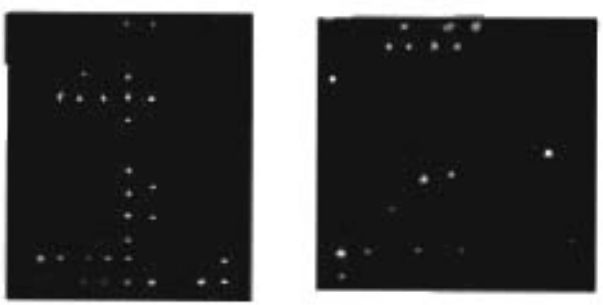

First layer Second layer

Figure 14 Data recording and reading results from the two-layer medium. The distance between neighboring bits is 3 μm, and the distance between layers is about 8 μm.

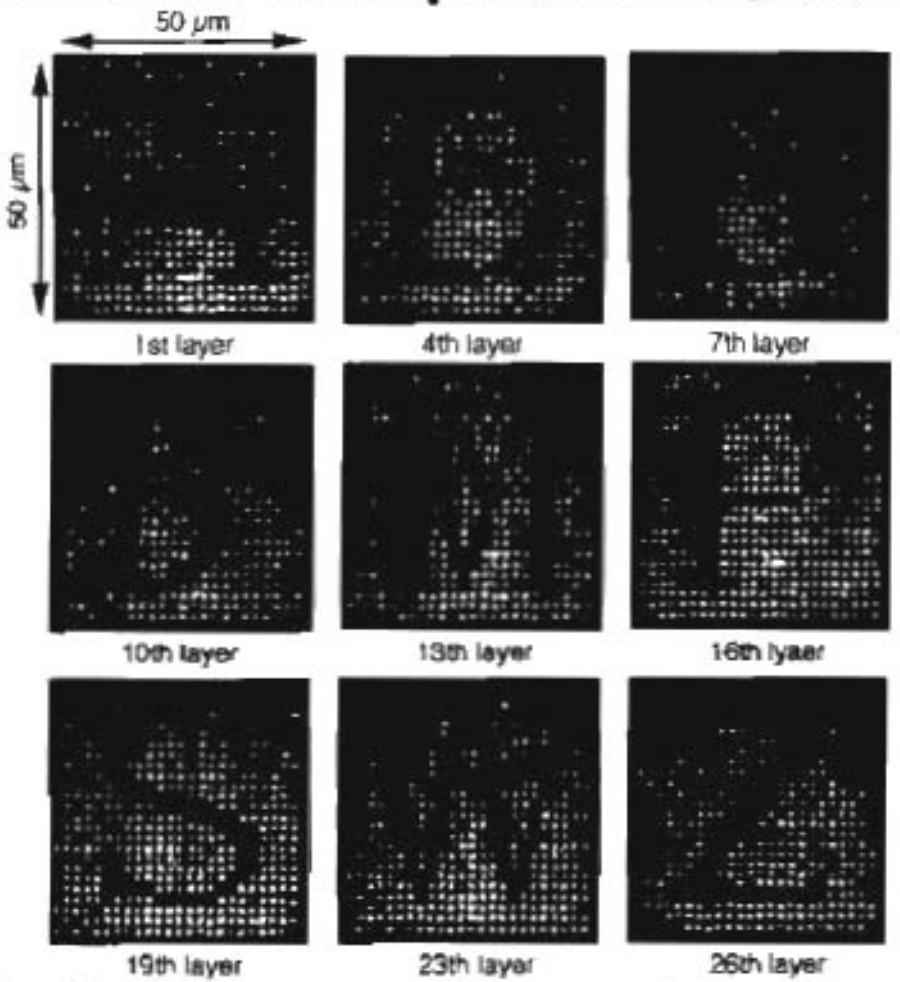

Otros materiales fotoactivos

• Sistemas con funciones computacionales

Puertas lógicas moleculares:
Se obtienen por combinación de interruptores moleculares

Chem. Commun. 2006, 1169-1171.

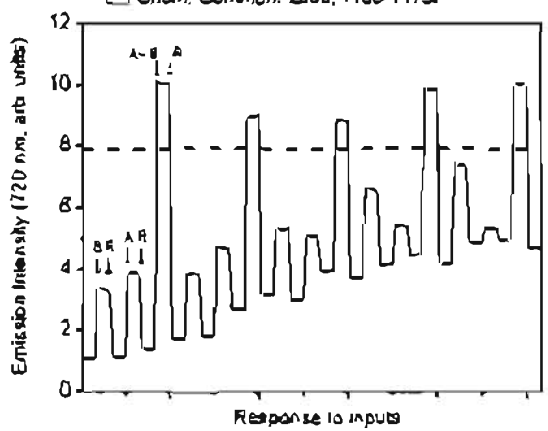

Cycling of AND gate 5. The dashed line indicates a threshold

Table 1 Truth table for AND gate

Input A (heat or IR)	Input B (red light)	Output (porphyrin fluorescence)	State of 5
0	0	0	DHP-P-BT
1	0	0	DHP-P-DHI
0	1	0	CPD-P-BT
1	1	1	CPD-P-DHI

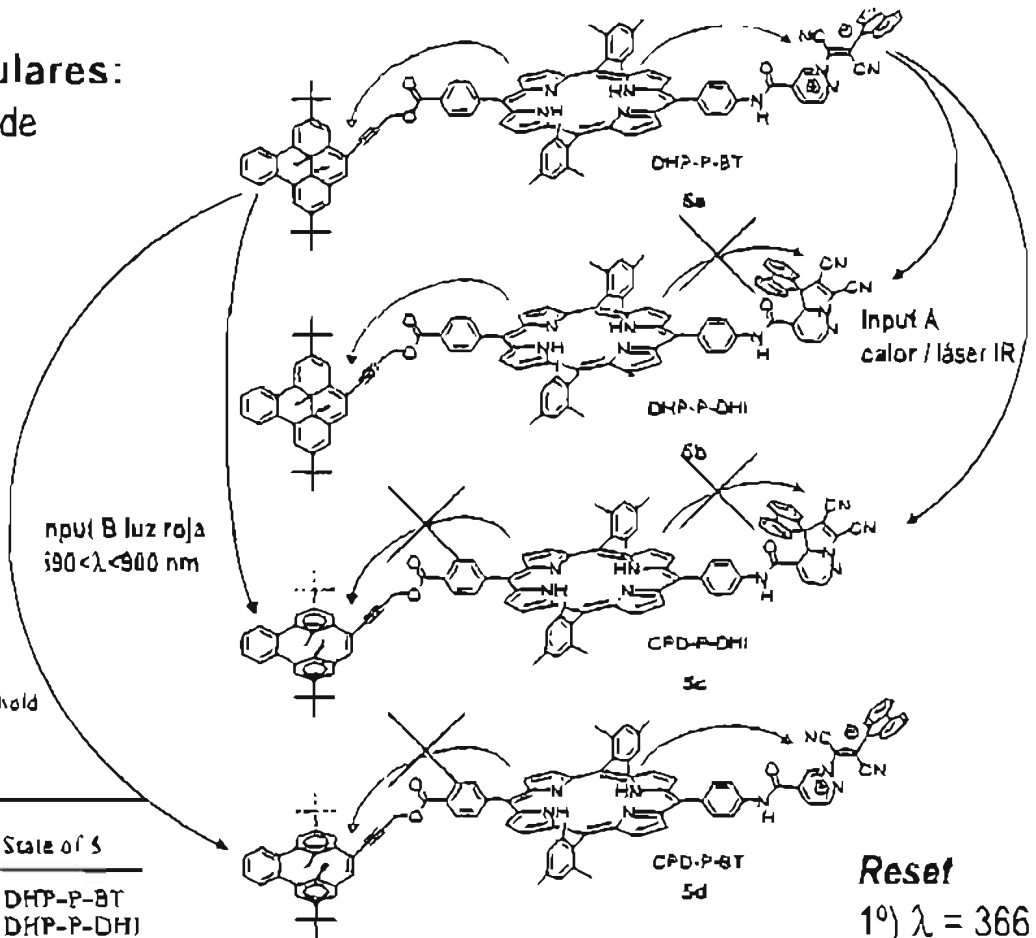

Fig. 9 Four isomeric forms of triad 5.

photonics and electronics, ranging from the relatively simple nanoscale emitter and complementary logic that can be obtained from single nanorod p–n junctions. Moreover, the direct growth of modulation-doped nanorods eliminates the lithographic steps used to create doped nanotube p–n junctions.[18,19] Therefore, we believe that controlled growth of modulation-doped nanorod p–n junctions represents an advance over previous work.[11,17,18,20]

Experimental

GaN nanorods were grown in a horizontal HVPE system. In the growth process, the Ga precursor (TN) was synthesized in the lower region of the reactor, via the reaction of HCl gas (SN) (in an N_2 diluent gas) with Ga metal (at 750 °C), to form GaCl. This precursor was then transported to the substrate area, where it was mixed with NH_3 ($GN4$) to form GaN at 475 °C (substrate temperature). After the furnace was cooled to room temperature, a dark yellow layer was found on the surface of the substrate.

Nanorods dispersed in methanol were deposited onto oxidized silicon substrates and electrical contacts were fabricated using focused ion beam (FEI company, Strata DB 235) lithography. GaN nanorod LED contacts were fabricated by a two-step process in which the n-type contact (first step) was made using Ti/Al (100 nm/200 nm) by electron-beam evaporation and then was annealed at 950 °C for 30 s to form an ohmic contact. In the second step, the p-type contact was made using Ni/Au (100 nm/200 nm) by electron-beam evaporation and then was annealed at 400 °C for 30 s to form an ohmic contact. Electrical transport measurements were made using a home-made system under computer control. In order to investigate the optical properties of GaN nanorod p–n junctions, we carried out cathodoluminescence (CL) spectroscopy and imaging. The CL spectra of the nanorods at room temperature were taken on a high-resolution scanning electron microscope (SEM, FEI company, XL 30 SFEG) combined with a CL system (Gatan, MONOCL) having a 1200 lines/mm grating blazed at 500 nm. The emission was detected using a Peltier-cooled photomultiplier. The maximum spectral resolution is 0.2 nm. The experimental conditions in CL spectroscopy were carefully established to minimize the undesired influence of electron-beam bombardment on the conditions of the specimens.

Received: October 18, 2002
Final version: December 19, 2002

[1] S. Nakamura, S. J. Pearton, G. Fasol, *The Blue Laser Diode: The Complete Story* 2nd ed., Springer, Berlin 2000.
[2] S. J. Pearton, F. Ren, *Adv. Mater.* **2000**, *12*, 1571.
[3] W. Han, S. Fan, Q. Li, Y. Hu, *Science* **1997**, *277*, 1287.
[4] W. Han, P. Redlich, F. Ernst, M. Rühle, *Appl. Phys. Lett.* **1999**, *75*, 1691.
[5] C. C. Chen, C. C. Yeh, *Adv. Mater.* **2000**, *12*, 738.
[6] J. Y. Li, X. L. Chen, Z. Y. Qiao, Y. G. Cao, Y. C. Lan, *J. Cryst. Growth* **2000**, *213*, 408.
[7] G. S. Chang, E. O. Zhang, Y. Zou, G. T. Fei, L. D. Li, *Appl. Phys. Lett.* **1999**, *75*, 2455.
[8] M. Yoshimura, A. Kitoshi, M. Mori, N. Fujita, K. Kitamura, *Jpn. J. Appl. Phys.* **1997**, *36*, L459.
[9] X. Duan, Y. Huang, Y. Cui, J. Wang, C. M. Lieber, *Nature* **2001**, *409*, 66.
[10] Y. Huang, X. Duan, Y. Cui, C. M. Lieber, *Nano Lett.* **2002**, *2*, 101.
[11] M. S. Gudiksen, L. J. Lauhon, J. Wang, D. C. Smith, C. M. Lieber, *Nature* **2002**, *415*, 617.
[12] H. M. Kim, D. S. Kim, Y. S. Park, D. Y. Kim, Y. W. Kang, K. S. Chung, *Adv. Mater.* **2002**, *14*, 991.
[13] H. M. Kim, D. S. Kim, D. Y. Kim, T. W. Kang, Y. H. Cho, K. S. Chung, *Appl. Phys. Lett.* **2002**, *81*, 2193.
[14] J. I. Pankove, T. D. Moustakas, *Gallium Nitride (GaN) I: Semiconductors and Semimetals* 50, Academic Press, San Diego, CA **1998**, p. 239.
[15] H. M. Kim, Y. H. Cho, T. W. Kang, *Adv. Mater.* **2001**, *13*, 1333.
[16] Y. Cui, X. Duan, J. Hu, C. M. Lieber, *J. Phys. Chem. B* **2000**, *104*, 5213.
[17] N. Grandjean, J. Massies, M. Leroux, P. Lorenzini, *Appl. Phys. Lett.* **1998**, *73*, 87.
[18] V. Dierolf, R. Mu, J. Appenzeller, P. Ahrens, *Nano Lett.* **2001**, *1*, 453.
[19] C. W. Zhou, J. Kong, E. Yenilmez, H. J. Dai, *Science* **2000**, *290*, 1552.
[20] J. Hu, M. Ouyang, P. Yang, C. M. Lieber, *Nature* **1999**, *399*, 48.

Light-Driven Side-On Nematic Elastomer Actuators**

By Min-Hui Li, Patrick Keller,* Bin Li, Xiangong Wang, Monique Brunet

The search for "smart materials", which respond to external stimuli (pH variation, ion concentration, temperature, electric field, etc.) by changes in shape or size, has recently attracted considerable attention from the materials research community.[1] In addition to classical approaches such as the shape memory of alloys or ferroelectric polymers (PVF_2),[1] many new materials and approaches are under active investigation, including hydrogels,[2] dielectric elastomers,[3] shape memory polymers,[4] conducting polymers,[5] carbon nanotubes,[5] and ferroelectric liquid-crystalline elastomers.[6] In addition to the obvious attractiveness of such studies in basic science, artificial muscle systems have many potential applications of great interest, including serving as the materials foundation for fabrication of sensors, micro-robots, micro-pumps, and actuators with combinations of size, weight, and performance parameters beyond those currently achievable.[1,7]

Following extensive work on thermomechanical properties of nematic liquid-crystal elastomers by Finkelmann[8] and other researchers,[9] we have recently developed a new kind of such an artificial muscle using side-on nematic liquid crystalline elastomers.[10] These systems, based on ideas proposed by de Gennes,[11] make use of a conformational change of the polymer backbone at the nematic to isotropic (N–I) phase transition as the motor for a macroscopic contraction.

Some years ago we demonstrated, using neutron scattering experiments, that the polymer backbone in side-on nematic liquid crystalline polymers is strongly extended along the nematic director, with anisotropies of the radii of gyration ($R_{\parallel}/R_{\perp}$) of around four.[12] At the N–I transition, the backbone conformation becomes isotropic, adopting a classical random coil driven by entropy. It is this conformational transition, which can be visualized as a transition from raw spaghetti to cooked spaghetti, that we have exploited in our "muscle".

[*] Dr. P. Keller, Dr. M.-H. Li
Laboratoire "Physico-Chimie Curie"
UMR 168 CNRS/Institut Curie
Institut Curie Section de Recherche
11 Rue P. et M. Curie, F-75231 Paris Cedex 05 (France)
E-mail: patrick.keller@curie.fr
Dr. B. Li, Prof. X. Wang
Department of Chemical Engineering
Material Research Center, Tsinghua University
Beijing 100084 (PR China)
Dr. M. Brunet
Groupe de Dynamique des Phases Condensé
UMR 5581, Université Montpellier II
F-34095 Montpellier Cedex 05 (France)

[**] We thank Dr. Pascal Silberzan and Prof. Qixing Zhou for many helpful discussions and Dr. Julie Plastino for her critical reading of the manuscript. This work was partly supported by "Programme Matériaux" of the CNRS (2002–04) and by "Programme de Recherches Avancées de Coopération Franco-Chinoise" (PRA MX02-06, P. Keller and X. Wang).

ADVANCED MATERIALS

As stated previously,[9] in order to visualize at a macroscopic level this conformational change occurring at a molecular level, all the macromolecules in the material have to be oriented parallel to each other in order to form a nematic liquid-crystal monodomain. This alignment is required for most applications of liquid crystals (LCs), and can be obtained in a variety of ways. The macromolecules also must be strongly associated in order to remove the possibility that individual molecules change their shapes and reorient individually by sliding. In the simplest approach, this association is obtained by covalent crosslinking.

In our previous experiments,[10] the required alignment was obtained in the nematic phase of the monomer using rubbed-polymer alignment layers. Thus, LC cells composed of two glass windows separated by spacers were fabricated, in which the windows were spin-coated with polyimide, which was then mechanically rubbed in order to induce a uniform planar orientation of the molecules in the nematic phase (molecules lay parallel to the glass windows with their long molecular axis parallel to a defined orientation direction, the rubbing direction). Such a cell was filled in the isotropic phase with a mixture composed of a nematic acrylate monomer, a diacrylate crosslinking agent, and a photoinitiator. Upon slow cooling to the nematic phase, the molecules align parallel to the surfaces, giving the desired uniform planar alignment. The sample was then irradiated with UV light in order to induce polymerization and crosslinking at the same time, "freezing" the orientation of the nematic phase in a nematic LC elastomer. In the most difficult aspect of the preparation, the cell plates were carefully pried apart, affording the free-standing elastomeric material as a thin sheet (50–100 μm) with typical lateral dimensions of 1.5 cm × 3 cm.

When this sheet was heated close to its N–I transition, it started to contract along the nematic director axis. The typical contraction was around 35–45 %, depending upon which monomers were used. Preliminary mechanical characterizations were performed that gave estimates of the generated force (around 210 kPa) and the speed of the thermo-mechanical effect (a few seconds for the contraction but a much longer time for the extension, due to the low thermal conductivity of the elastomer).[10]

Although these results are very promising since we were able to prepare artificial muscle with mechanical properties approaching those of biological muscle, the main drawback of our approach is the stimulus used, i.e., the temperature jump. It would be much more interesting from various viewpoints to use other stimuli for contraction in our side-on nematic liquid-crystalline elastomers.

The object of the present communication is to explore an approach to creation of a photochemically driven LC elastomeric muscle system.

As outlined previously, the motor for the contraction in side-on LC elastomers is the conformational change of the backbone at the N–I transition. The disorganization of the mesogenic groups in the isotropic phase results in a reduction of the orientational coupling between the mesogens and the polymer backbone, thus inducing a transition from a stretched conformation to a globular conformation for the backbone.

One can assume that upon application to the oriented nematic side-on LC elastomer of any stimulus that induces to some extent a perturbation in the orientation of the mesogenic groups, there will also be induced changes in the global organization of the backbones, mimicking the phenomenon that occurs at the N–I transition.

In the field of liquid crystals, it has been known for years that in azo-containing molecules, a liquid crystalline to isotropic phase transition can be induced upon irradiation with light of suitable wavelength. The light-induced phase transition is provoked by a *trans*- to *cis*-photoisomerization of the azo groups inducing a large change in the shape of the molecules, from a liquid crystal rod-like shape for the *trans*-isomer to a kinked non-mesogenic shape for the *cis*-isomer.

Starting from our thermally stimulated "aligned" nematic side-on elastomer artificial muscle, our natural goal was to prepare a photochemically stimulated, oriented nematic azo side-on elastomer artificial muscle. To our surprise, a careful literature search on the photochemical synthesis of pure aligned azo nematic elastomers gave no results. Obviously, there were technical difficulties to overcome in order to prepare such materials. We quickly realized that the problem was mainly related to the photopolymerization process we were planning to use in the preparation. Since the azo chromophore absorbs light strongly up to 550–600 nm, the photoinitiators used should be activated at a wavelength above 600 nm. We thus selected the near-infrared photoinitiator, 1,3,3,1′,3′,3′-hexamethyl-11-chloro-10,12-propylene-tricarbocyanine triphenylbutyl borate (CBC), first synthesized by us[13] and used in the photopolymerization in bulk of various acrylate monomers. We first tested the capacity of the photoinitiator in the preparation of a classical (i.e., non-azo) oriented side-on nematic elastomer. Upon irradiation with red light ($\lambda > 600$ nm) of a mixture of the nematic methacrylate monomer 1[14] (90 mol-%) and 1,6-hexanediol dimethacrylate (10 mol-%) containing 0.1 mol-% of the photoinitiator CBC, a nematic elastomer (E-0 %-azo) was formed, which, after removal from the cell in which the photopolymerization was performed, exhibited a contraction of around 18 % at the thermal N–I transition. See Figure 1 for monomer structures.

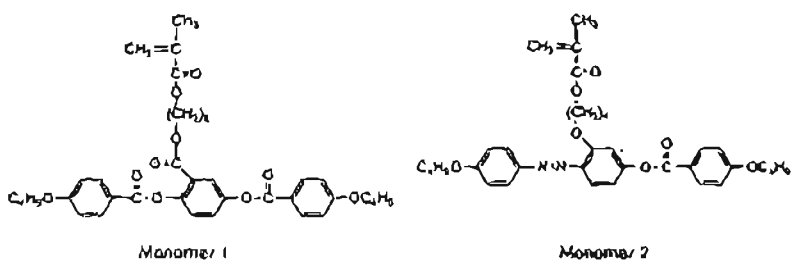

Monomer 1 Monomer 2

Fig. 1. Side-on liquid-crystalline monomer structures.

We then prepared several oriented azo-containing methacrylate elastomers, E-25 %-azo, E-50 %-azo, and E-100 %-azo, from mixtures of monomer 1 and monomer 2[13] containing 0.2–1 mol-% of photoinitiator CBC and 10 mol-% of 1,6-hexanediol dimethacrylate (for example, in E-25 %-azo, the mole ratio between monomer 2 and monomer 1 is 25:75). Upon irradiation with red light ($\lambda > 600$ nm), elastomers were formed, which, after removal from the cells, were obtained as small sheets of yellow plastic with a thickness around 20 μm, and typical lateral dimensions of 1.5 cm × 3 cm. The films were held at a temperature of 70 °C, well below their thermal N–I phase transition T_{N-I} (between 86 °C and 90 °C depending on the composition). When subjected to UV irradiation ($\lambda = 365$ nm), these films contracted quickly by up to 12–18 % (see Fig. 2 for the contraction of E-25 %-azo). Moreover, for all the elastomers, the extent of contraction triggered by the UV irradiation was essentially the same as that found in the thermally induced N–I transition (see Figs. 3,4). Also, the extent of the contraction was found to be dependent upon

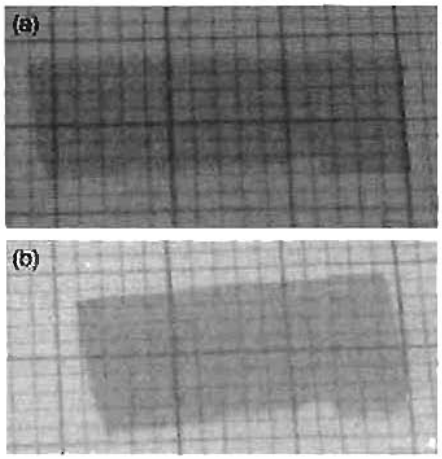

Fig. 2. Elastomer E-25 %-azo a) before UV irradiation, and b) under UV irradiation (irradiation time: 120 s). (Background is a graduated paper.)

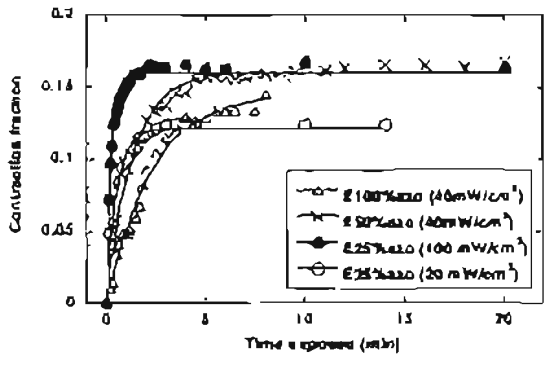

Fig. 3. Contraction fraction (F) of the azo elastomers as a function of time exposed (t) to UV light. The symbols are the experimental points. The lines are the fits with the function $F = F_{max}(1-e^{-t/\tau})$ where F_{max} is the maximal contraction and τ the characteristic time of the contraction (time to reach 63.2 % of the maximum contraction): 1 s, 13 s, 31 s, 93 s, and 135 s for E-25 %-azo (100 mW cm^{-2}), E-25 %-azo (20 mW cm^{-2}), E-50 %-azo (40 mW cm^{-2}), and E-100 %-azo (40 mW cm^{-2}), respectively. ($F = (L_0 - L)\,L_0^{-1}$).

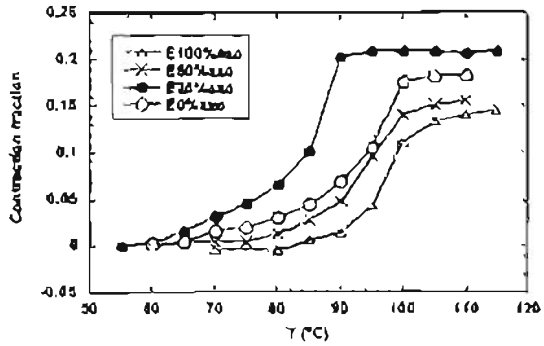

Fig. 4. Contraction fraction (F) of the elastomers as a function of temperature (lines are guides for the eye). ($F = (L_0 - L)\,L_0^{-1}$)

the intensity of the light used, as seen in Figure 3. For E-25 %-azo, the contraction fraction went from 12 % for a light intensity of 20 mW cm^{-2} to 17 % for an intensity of 100 mW cm^{-2}. As for the speed of the response as a function of the concentration of azo-monomer in the elastomers, the E-25 %-azo elastomer was the fastest, with a characteristic time τ of 13 s under UV light of 100 mW cm^{-2}.

Complete reversal of the contraction took place after the UV light was switched off because of the thermal *cis* to *trans* back reaction of the azobenzene. This process was slow for all the studied elastomers (on the order of 30 min–1 h). A reverse *cis–trans* reaction induced by irradiation at 460 nm was attempted but gave a surprising result. A halogen lamp equipped with a hot mirror and a long-pass filter was used in order to obtain light with $\lambda = 450$–700 nm. The elastomer sheet E-100 %-azo which had been contracted by exposure to UV light, was then illuminated with this visible light. The expected expansion was not observed and, more surprisingly, the thermal expansion was even blocked by the exposure to visible light. We then directly illuminated the original elastomer sheet with visible light without previous UV irradiation. A photo-contraction triggered by the visible light was observed. The reasons for this are not totally clear at this point but might be due to the broadening and red-shifting of the absorption bands of the azo groups in liquid crystalline polymers that was reported previously.[16] Another explanation might be that, under visible light, the *trans–cis* isomerization via the n–π^* mode is predominant compared to the *cis–trans* isomerization in our particular azo system.

Photo-mechanical effects using the photoisomerization of a chromophore as the active phenomenon have already been observed in various systems.[11–14] Agolini and Gay[11] reported a small stress increase in a film of semi-crystalline poly-4,4′-diphenylazopyromellitimide at constant length under UV illumination. Smets and Blauwe[19] studied rubbery poly(ethyl acrylate) crosslinked with a dimethacrylate containing two spiropyrane groups, and observed a 2–3 % shrinkage upon irradiation of stretched samples at constant temperature. Eisenbach[18] used an azobenzene-containing crosslinker to make the rubbery poly(ethyl acrylate), and obtained around 0.25 % contraction on loaded film under UV illumination. In the last

ADVANCED MATERIALS

two examples the chromophore orientation was achieved by a mechanical stretching force. The conformational change in the chromophore upon irradiation caused a change in the conformation of the adjacent chain segments, which was considered to be the main cause for the small contraction. Recently, Finkelmann[22] and Hogan[23] used azobenzene-containing crosslinkers and/or monomers to prepare monodomain side-on nematic elastomers by a two stage crosslinking technique, the second stage being performed under imposed extension. In these cases the *trans–cis* photoisomerization of the azo chromophores induced a lowering or suppression of the nematic order. The contraction of these elastomers along the nematic director reached 20 % after hours of UV irradiation. In our system, the light-induced *trans–cis* isomerization of the azo chromophores that are an integral part of the side groups induced a complete loss of the nematic order, as can be seen from the equal extent of the contractions observed both thermally and photochemically in all elastomers.

In this communication, we have reported for the first time the synthesis of aligned nematic azo side-on elastomers by photopolymerization using a near-infrared photoinitiator. The photopolymerization/photocrosslinking reaction was performed on aligned nematic azo monomer in conventional liquid-crystal cells. Thin films of these elastomers showed fast (less than 1 min) photochemical contraction up to 18 % triggered by UV light, the slow thermal back reaction being observed in the dark.

Actuators which can be activated by remote stimuli might have interesting applications in various fields, for example, micro-pumps and gates in microfluidics. The nematic azo elastomers reported here could be good candidates for these actuators. Moreover, the use of efficient near infrared photoinitiators in preparing aligned elastomers might be applied to other cases where the monomers to be polymerized have strong absorption bands in the UV and visible range. For example, these near-infrared photoinitiators could be used to prepare new ferroelectric liquid-crystal elastomers with interesting piezoelectric and NLO properties.

Received: October 28, 2002
Final version: December 20, 2002

[1] *Electroactive Polymer (EAP) Actuators as Artificial Muscles – Reality, Potential and Challenges* (Ed: Y. Bar-Cohen), Vol. PM98, SPIE–Society of Photo-optical Instrumentation Engineers, Bellingham, WA 2001.
[2] Z. S. Liu, P. Calvert, *Adv. Mater.* **2000**, *12*, 288.
[3] R. Pelrine, R. Kornbluh, Q. Pei, J. Joseph, *Science* **2000**, *287*, 836.
[4] A. Lendlein, A. M. Schmidt, R. Langer, *Proc. Natl. Acad. Sci. USA* **2001**, *98*, 842.
[5] R. H. Baughman, C. Cui, A. A. Zakhidov, Z. Iqbal, J. N. Barisci, G. M. Spinks, G. G. Wallace, A. Mazzoldi, D. De Rossi, A. G. Rinzler, O. Jaschinski, S. Roth, M. Kertesz, *Science* **1999**, *284*, 1340.
[6] W. Lehmann, H. Skupin, C. Tolksdorf, E. Gebhard, R. Zentel, P. Krüger, M. Lösche, F. Kremer, *Nature* **2001**, *410*, 447.
[7] T. Ikeda, J. U. Mamiya, R. Kikuchi, G. Sasaki, *Macromol. Mater. Eng.* **2000**, *10*, 333.
[8] a) J. Küpfer, H. Finkelmann, *Makromol. Chem., Rapid Commun.* **1991**, *12*, 717. b) H. Wermter, H. Finkelmann, *e-Polym.* **2001**, 013.
[9] S. M. Clarke, A. Hotta, A. R. Tajbakhsh, E. M. Terentjev, *Phys. Rev. E* **2001**, *64*, 061702.
[10] D. L. Thomsen, P. Keller, J. Naciri, R. Pink, H. Jeon, D. Shenoy, B. R. Ratna, *Macromolecules* **2001**, *34*, 5868.
[11] a) P.-G. de Gennes, *C. R. Acad. Sci. Paris Ser. B* **1975**, *281*, 101. b) P.-G. de Gennes, *Phys. Lett.* **1969**, *28A*, 725. c) P.-G. de Gennes, *C. R. Acad. Sci. Paris Ser. II* **1997**, *321*, 343.
[12] a) M. Lebreux, P. Keller, M. F. Achard, L. Noirez, F. Hardouin, *J. Phys. II* **1993**, *3*, 1289. b) M. Lebreux, M. F. Achard, P. Keller, F. Hardouin, *Liq. Cryst.* **1994**, *16*, 1077.
[13] S. Zhang, B. Li, L. Tang, X. Wang, D. Liu, Q. Zhou, *Polymer* **2001**, *42*, 7535.
[14] This monomer was prepared using a synthetic scheme similar to the one described in P. Keller, D. L. Thomsen, M.-H. Li, *Macromolecules* **2002**, *35*, 581.
[15] M.-H. Li, P. Auroy, P. Keller, *Liq. Cryst.* **2000**, *27*, 1497.
[16] D. Creed, in *Organic and Inorganic Photochemistry* (Eds: V. Ramamurthy, K. S. Schanze), Marcel Dekker, New York **1998**, p. 119.
[17] P. Agolini, F. P. Gay, *Macromolecules* **1970**, *3*, 349.
[18] O. Van der Veen, W. Prins, *Nature, Phys. Sci.* **1971**, *230*, 70.
[19] G. Smets, F. de Blauwe, *Pure Appl. Chem.* **1974**, *38*, 225.
[20] C. D. Eisenbach, *Polymer* **1980**, *21*, 1175.
[21] H. S. Blair, H. I. Pogue, J. E. Riordan, *Polymer* **1988**, *29*, 1195.
[22] H. Finkelmann, E. Nishikawa, G. G. Pereira, M. Warner, *Phys. Rev. Lett.* **2001**, *87*, 015501.
[23] P. M. Hogan, A. R. Tajbakhsh, E. M. Terentjev, *Phys. Rev. E* **2002**, *65*, 041720.
[24] T. Ikeda, M. Tsuda, S. Shimada, H. Miyasaka, *Synth. Metals A* **2002**, *96*, 139.

Spin-on Nanostructured Silicon–Silica Film Displaying Room-Temperature Nanosecond Lifetime Photoluminescence**

By *Yair Cohen, Benjamin Hatton, Hernán Míguez, Neil Coombs, Sébastien Fournier-Bidoz, John K. Grey, Rémi Beaulac, Christian Reber, and Geoffrey A. Ozin**

The search for a silicon-based light-emitting diode (LED) that easily integrates with silicon microelectronics and has utility in optoelectronics or photonics has inspired materials research for more than a decade.[1] In 1990 Canham discovered photoluminescence from porous silicon made by electrochemical anodic oxidation of p-doped silicon wafers.[2] This breakthrough initiated intense research activity in microfabrication and self-assembly approaches to different kinds of luminescent silicon nanostructures suitable for LEDs.[3–8] However, this has not proven to be an easy task because a practical silicon-based LED must satisfy numerous stringent criteria that include high quantum efficiency emission at room temperature (RT) with nanosecond radiative lifetimes, long-term chemical, thermal, and mechanical stability, as well as a

[*] Prof. G. A. Ozin, Dr. Y. Cohen, B. Hatton, Dr. H. Míguez [+], Dr. N. Coombs, S. Fournier-Bidoz
Materials Chemistry Research Group
Department of Chemistry, Lash Miller Chemical Laboratories
University of Toronto
80 St. George Street, Toronto, Ontario, M5S 3H6 (Canada)
E-mail: gozin@chem.utoronto.ca
J. K. Grey, R. Beaulac, Prof. C. Reber
Department of Chemistry, University of Montreal
Montreal, Quebec H3C 3J7 (Canada)
[+] Present address: Fibre Radio Group, IFACA Research Institute, Edificio Inst. Camino de Vera s/n, Universidad Politécnica de Valencia, E-46022, Valencia, Spain.
[**] GAO is Government of Canada Research Chair in Materials Chemistry. We are deeply indebted to Primaxis Technology Ventures Incorporated for generous financial support of this work.

DOI: 10.1002/anie.201000305

Supramolecular Chemistry

Triggering of Guanosine Self-Assembly by Light**

*Stefano Lena, Paolo Neviani, Stefano Masiero, Silvia Pieraccini, and Gian Piero Spada**

Controlling a function at the molecular level by means of external stimuli is one of the key requirements in the development of "smart" materials and light is a very appealing trigger because of its ready availability, easy manipulation, and noninvasive character.[1] In particular, self-assembly processes that can be controlled by photochemical stimuli are an actively pursued research field and one ultimate goal in supramolecular chemistry.[2]

In recent years lipophilic guanine derivatives (lipoGs) have received increasing attention because of their rich supramolecular behavior.[3–11] Most of the supramolecular architectures obtained from lipoGs and so far reported in the literature require the presence of a cation (usually an alkali-metal cation, but also an alkaline-earth or lanthanide cation) that stabilizes the G-quartet-based assemblies through dipole–ion interactions (Figure 1a). However, even in the absence of metal cations suitable lipoGs are able to undergo extensive self-assembly mediated by H-bonding between guanine bases, thus leading to the formation of ribbonlike architectures (e.g., Figure 1b).

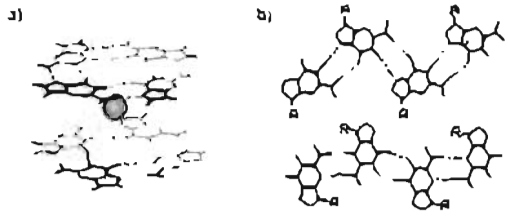

Figure 1. a) D_4-symmetric octamer and b) ribbonlike architectures.

We have already demonstrated the chemically driven switching between different supramolecular motifs for lipoGs both in solution[3a] and at the solid/liquid interface.[5a] Herein, we report the photocontrolled self-assembly of a modified guanosine nucleobase. Compound (*E*)-**1** (Scheme 1) in the presence of a measured amount of K$^+$ self-assembles into a D_4-symmetric complex consisting of two stacked G-quartets. Photoisomerization to the *Z* isomer determines the decomposition of the octameric complex, which is re-formed when the molecule is reverted to the *E* isomer by either thermal or photochemical back isomerization.

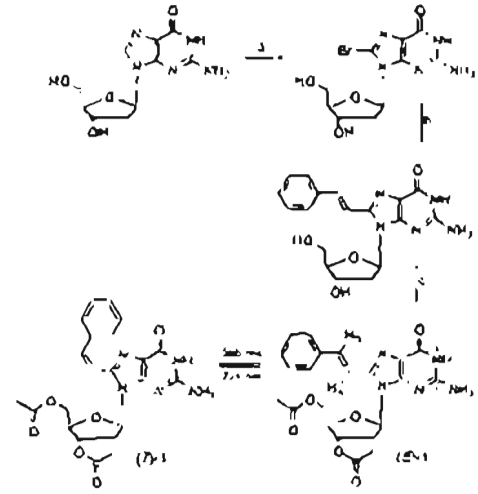

Scheme 1. Synthesis of (*E*)-**1**. a) NBS, b) *trans*-2-phenylvinylboronic acid, Na_2CO_3, TPPTS, $Pd(OAc)_2$; c) acetic anhydride, DMAP. NBS = *N*-bromosuccinimide, TPPTS = tris(3-sulfophenyl)phosphine trisodium salt, DMAP = 4-dimethylaminopyridine.

Following our experience with photoswitchable systems[3c,4] for the introduction of photochemical control over guanosine self-assembly our first approach was to introduce an azobenzene moiety in the 8-position of the guanine base. We expected that, if the photoactive moiety were placed close to the sites of base recognition, the geometrical changes associated with photoisomerization of the azo chromophore would have resulted in strong effects over guanine self-assembly. Unfortunately, the compounds obtained did not show the desired supramolecular behavior. While this work was in progress, interesting results were reported by Ogasawara and Maeda[12] for oligonucleotides containing a modified guanosine, in which an arylvinyl moiety had been introduced at the 8-position. We therefore turned our attention to the 8-styrylguanine moiety as the photoswitching unit.

Derivative (*E*)-**1** was obtained in three steps from natural guanosine (Scheme 1). Bromination at the 8-position with NBS followed by Suzuki coupling with 2-phenylvinylboronic acid and esterification of the hydroxy functions with acetic anhydride afforded (*E*)-**1** in a 48% overall yield as the pure isomer.

Compound (*E*)-**1** dissolves readily in MeCN. The ^{1}H NMR spectrum of (*E*)-**1** (Figure 2a) in CD_3CN (5 mM) shows sharp signals which suggests that extensive self-assembly to form ribbonlike aggregates does not occur under these conditions.[13] This finding is supported by

[*] Dr. S. Lena, P. Neviani, Prof. S. Masiero, Dr. S. Pieraccini, Prof. G. P. Spada
Dipartimento di Chimica Organica "A. Mangini", Alma Mater Studiorum – Università di Bologna
Via San Giacomo 11, 40126 Bologna (Italy)
E-mail: gianpiero.spada@unibo.it

[**] This work was supported by the University of Bologna.

Supporting information for this article is available on the WWW under http://dx.doi.org/10.1002/anie.201000305.

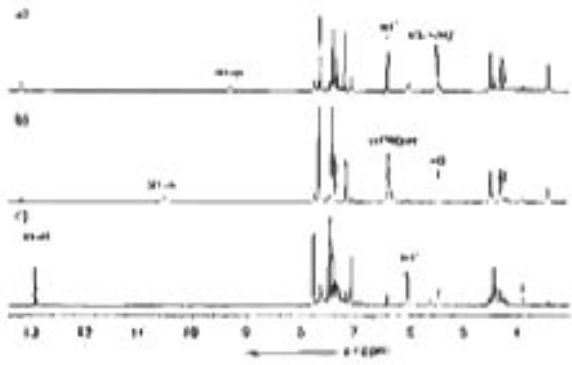

Figure 2. ^{1}H NMR spectra for a) a 5 mM solution of (*E*)-1 in CD_3CN, b) a 30 mM solution of (*E*)-1 in CD_3CN, and c) a 5 mM solution of (*E*)-1/KI in CD_3CN.

NOESY spectra, which show no cross peak attributable to intermolecular correlations. Extensive self-assembly takes place upon increasing the concentration above 20 mM: the imino N1-H and amino N2-H protons, which resonate at δ = 9.30 and 5.50 ppm, respectively, in 5 mM solution, shift downfield to δ = 10.47 and 6.22 ppm in a 30 mM solution (Figure 2b). This indicates progressive involvement of these groups in H-bonding. Accordingly, the NOESY spectrum now clearly shows an intermolecular correlation between the N2-H and H1′ of adjacent guanosine moieties. Interestingly, these spectra (see the Supporting Information) indicate a conformational change around the glycosidic bond as a function of concentration. In diluted samples (below 5 mM), a cross peak correlating H1′ and H_A suggests a *syn* conformation around the glycosidic bond, but at higher concentrations (20 mM and above) this cross peak is no longer apparent. The presence of an intermolecular peak relating the N2-H and H1′ of adjacent guanosine units indicates that a ribbonlike architecture is present and the *anti* conformation is now predominant.

The CD spectrum of (*E*)-1 in MeCN at 5 mM concentration (see the Supporting Information) shows only a weak (negative) signal. The profile is almost superimposable on the CD spectrum of (*E*)-1 in MeOH, a competing solvent for hydrogen bonding, thus suggesting the presence of a disaggregate form of (*E*)-1. Upon irradiation of this MeCN solution at 365 nm, (*E*)-1 isomerizes to the *Z* form and a *Z* photostationary state (*Z*-PSS, *Z* = 85%) is reached in 28 min, as estimated from UV/Vis spectroscopy by spectral subtraction[6a] (Figure 3). The process is perfectly reversible: the *Z* isomer reverts back to the *E* form either by irradiation at 254 nm (30 min) or thermally in the dark (150 min).

When a weighed amount of KI (0.125 mol per mol of guanine, that is, 1/8) is added to a MeCN solution of (*E*)-1, the ^{1}H NMR and CD spectra change dramatically, as expected when the formation of stacked G-quartets templated by the cation occurs. In particular, in the ^{1}H NMR spectrum (Figure 2c) the imino proton shifts downfield more than δ = 1 ppm while the H1′ signal moves upfield by δ = 0.4 ppm and the amino signal becomes unobservably broad at room temperature. No doubling of signals appears in the ^{1}H NMR

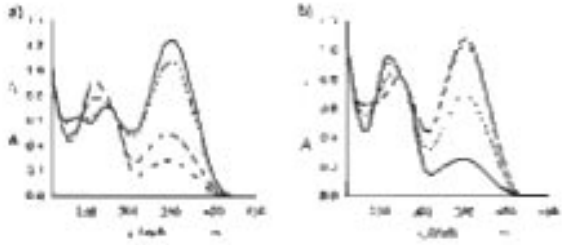

Figure 3. a) Absorption spectra for photoisomerization of (*E*)-1 (5 mM in MeCN) upon irradiation at 365 nm; initial spectrum (——) and spectra recorded after 2 (– – –), 6 (–·–·–), 22 (– – –), and 28 min (——). b) Absorption spectra for photoisomerization of (*Z*)-1 upon irradiation at 254 nm; initial spectrum (——) and spectra recorded after 3 (——), 7 (– – –), 20 (– – –), and 30 min (–·–·–).

spectrum: this suggests the formation of an octameric species composed of two stacked G-quartets arranged in a D_4 symmetry. NOESY spectra show a correlation between H1′ and H_A for both diluted and concentrated samples, which implies that in the octameric supramolecular complex all of the guanosine units adopt a *syn* conformation around the glycosidic bond, regardless of concentration.

In the CD spectrum (Figure 4a) of the (*E*)-1/K1 octameric complex, a positive band at 255 nm and a very strong, positive band at 350 nm can be observed. Although no detailed

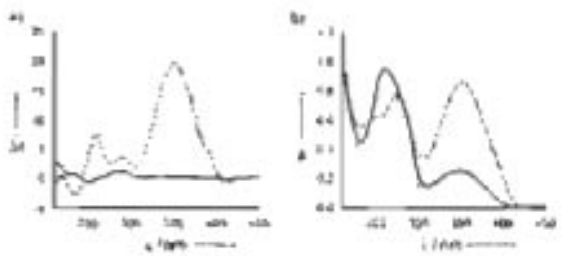

Figure 4. a) CD and b) UV/Vis spectra of a 5 mM solution of (*E*)-1/KI (– – –), of 1/KI at the *Z*-PSS (·–·–·), and of 1 at the *Z*-PSS (——) in MeCN.

information on the electronic transitions are available so far for the 5-styrylguanine chromophore, the spectral changes observed upon addition of potassium ion closely resemble those reported for other unmodified lipophilic guanosines.[5b,6d] The strong increase of the CD signal associated with the formation of the (*E*)-1/K$^+$ aggregate can analogously be attributed to interchromophore couplings taking place in the stacked complex. When samples of the (*E*)-1/K$^+$ octameric complex are irradiated at 365 nm, photoconversion to the *Z* isomer takes place and the *Z*-PSS is reached in 30 min for a 5 mM sample. The photoisomerization has a dramatic effect on the assembled species. The CD spectrum of the solution of 1/KI recorded at the *Z*-PSS shows very weak signals: this spectrum is practically superimposable on the CD spectrum of (*Z*)-1 prior to KI addition and it is similar to that of uncomplexed (*E*)-1.

A comparison of the CD and UV spectra for (*E*)-**1** before and after K^+ extraction points to the conclusion that the intensity of the CD signal is mainly attributable to interchromophore interactions. In particular, the *E* form before K^+ complexation shows a weak CD spectrum, in spite of the strong absorbance in the corresponding UV spectrum. Accordingly, the weak CD signal shown by the system at the *Z*-PSS results from the disaggregation of the stacked supramolecular complex and is not directly related to the lower molar absorptivity of the *Z* isomer. The disappearance of the strong CD bands at 255 and 350 nm is evidence of decomposition of the complex: stacked G-quartets no longer exist in solution.

The observation that (*Z*)-**1** does not form (stacked) G-quartets is most likely because in the *Z* form the phenyl group of the styryl unit is twisted[11] with respect to the G-quartet plane. The consequent steric hindrance could force quartets away from van der Waals contact or it could produce a conformational change around the glycosidic bond, which, in turn, would hamper the stacking. Additionally, in the *Z* form the N7 atom is probably shielded by the styryl unit and is no longer available for H-bonding.

Unfortunately, no NMR studies could be carried out on the *Z*-PSS solution photoisomerization with standard Hg lamps of samples large enough to be suitable for NMR analysis produced substantial amounts of photocycloaddition products, in the time required to attain the *Z*-PSS under these conditions (see the Supporting Information). Hence, direct detailed information on the type and extent of self-assembly undergone by **1** when in the *Z* form in the presence of K^+ could not be obtained. Although the disappearance of the stacked octameric structure is evident from the CD spectrum, the organization of (*Z*)-**1** into other self-assembled species cannot be ruled out.

As stated above, the *Z* form can be converted back to the *E* form either photochemically, by irradiation at 254 nm, or thermally. Reisomerization to the *E* isomer determines, at the supramolecular level, the re-creation of the octameric complex: the CD spectrum of the solution at this point perfectly overlaps the starting [(*E*)-**1**]$_8$K$^+$ trace.

Thus, the G-quartet-based complex can be cyclically assembled and disassembled by light. As shown in Figure 5, the process is perfectly reversible: no change in molar absorptivity was observed for both the *E* and *Z* states after five cycles.

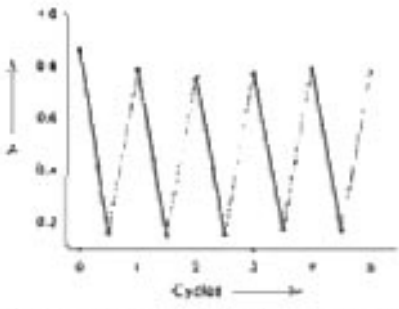

Figure 5. Switching cycles, monitored at 350 nm, between (*E*)-**1**/K$^+$ and (*Z*)-**1**/K$^+$ by alternate irradiation with light of wavelength 365 nm (for 30 min, —) and 254 nm (for 28 min, - -).

In conclusion, by the introduction of a photoactive moiety at C8 in a lipophilic guanosine derivative it is possible to operate photocontrol over the self-assembly of the molecule, such that the existence of G-quartets can be alternately switched on and off (Figure 6).

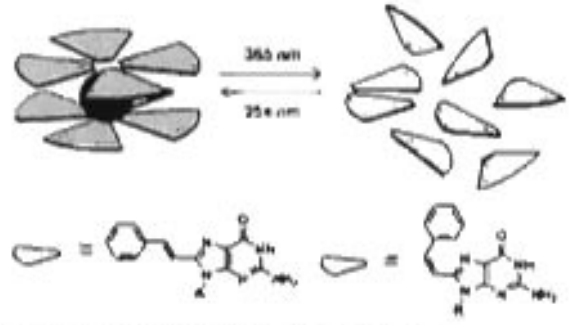

Figure 6. Phototriggering of guanosine self-assembly.

Experimental Section

The photoisomerization of (*E*)-**1** in spectrophotometric-grade acetonitrile was performed at room temperature by irradiating the samples, contained in 0.01 cm quartz cells, with the 150 W xenon lamp of the dichrograph (JASCO J-710). The monochromator of the instrument (slit width 3 mm) was employed to select the UV irradiation wavelengths (365 and 254 nm).

Received: February 9, 2010
Published online: April 9, 2010

Keywords: G-quartet · guanine · photoisomerization · self-assembly · supramolecular chemistry

[1] a) S. Saha, J. F. Stoddart, *Chem. Soc. Rev.* **2007**, *36*, 77; b) N. Katsonis, M. Lubomska, M. M. Pollard, B. L. Feringa, P. Rudolf, *Prog. Surf. Sci.* **2007**, *82*, 407; c) M. Yoshida, J. Lahann, *ACS Nano* **2008**, *2*, 1101; d) *Photochromism. Molecules and Systems* (Eds.: H. Dürr, H. Bouas-Laurent), Elsevier, Amsterdam, **2003**; e) *Molecular Switches* (Ed.: B. L. Feringa), Wiley-VCH, Weinheim, **2001**; f) Special Issue "Photochromism" (Ed.: M. Irie), *Chem. Rev.* **2000**, *100*, 1683.

[2] a) S. Yagai, A. Kitamura, *Chem. Soc. Rev.* **2008**, *37*, 1520; b) T. Ishi-i, S. Shinkai, *Top. Curr. Chem.* **2005**, *258*, 119; c) N. M. Sangeetha, U. Maitra, *Chem. Soc. Rev.* **2005**, *34*, 821; d) S. Hecht, *Small* **2005**, *1*, 26; e) F. L. Calzia, S. Soman, *Chem. Commun.* **2008**, 6179; f) S. Masiero, S. Lena, S. Pieraccini, G. P. Spada, *Angew. Chem.* **2008**, *120*, 3228; *Angew. Chem. Int. Ed.* **2008**, *47*, 3184.

[3] For review articles, see: a) J. T. Davis, *Angew. Chem.* **2004**, *116*, 684; *Angew. Chem. Int. Ed.* **2004**, *43*, 668; b) J. T. Davis, G. P. Spada, *Chem. Soc. Rev.* **2007**, *36*, 296; c) M. S. Kaucher, W. A. Harrell, Jr., J. T. Davis in *Supramolecular Nucleic Acids* (Eds.: S. Nicolis, S. Balasubramanian), RSC Publishing, Cambridge, **2006**, pp. 253 – 290; d) S. Lena, S. Masiero, S. Pieraccini, G. P. Spada, *Chem. Eur. J.* **2009**, *15*, 7792; e) S. Sivakova, S. J. Rowan, *Chem. Soc. Rev.* **2005**, *34*, 9.

[4] A few selected recent papers on the self-assembly and applications of lipoGs: a) M. del C. Rivera-Sánchez, F. Arteaga-de-

De Sanctis, M. García-Arriaga, V. Gubala, G. Hobley, J. M. Rivera, *J. Am. Chem. Soc.* **2009**, *131*, 10403; b) D. González-Rodríguez, J. L. J. van Dongen, M. Lutz, A. L. Spek, A. P. H. J. Schenning, E. W. Meijer, *Nat. Chem.* **2009**, *1*, 151; c) A. Likhitsup, S. Yu, Y.-H. Ng, C. L. L. Chai, E. K. W. Tam, *Chem. Commun.* **2009**, 4070; d) A. M. S. Kumar, J. D. Fox, L. E. Buerkle, R. E. Marchant, S. I. Rowan, *Langmuir* **2009**, *25*, 651; e) S. Mihai, A. Cazacu, C. Arnal-Hecault, G. Nasr, A. Meffre, A. van der Lee, M. Barboiu, *New J. Chem.* **2009**, *33*, 2335; f) M. Nikan, J. C. Sherman, *Angew. Chem.* **2008**, *120*, 4978; *Angew. Chem. Int. Ed.* **2008**, *47*, 4900; g) L. Ma, M. Melegari, M. Colombini, J. T. Davis, *J. Am. Chem. Soc.* **2008**, *130*, 2938; h) S. Martić, X. Liu, S. Wadg, G. Wu, *Chem. Eur. J.* **2008**, *14*, 1196; i) H. Liddar, J. Li, A. Neogi, P. B. Neogi, A. Sarkar, S. Cho, H. Morkoç, *Appl. Phys. Lett.* **2008**, *92*, 013309; j) I. Yoshikawa, S. Yanagi, Y. Yamaji, K. Araki, *Tetrahedron* **2007**, *63*, 7474; k) S. Lena, G. Brancolini, G. Gottarelli, P. Mariani, S. Masiero, A. Venturini, V. Palermo, O. Pandoli, S. Pieraccini, P. Samorì, G. P. Spada, *Chem. Eur. J.* **2007**, *13*, 3757.

[3] a) S. Pieraccini, S. Masiero, O. Pandoli, P. Samorì, G. P. Spada, *Org. Lett.* **2006**, *8*, 3123; b) P. Nevinni, E. Milco, S. Masiero, S. Pieraccini, M. Lucarini, G. P. Spada, *Org. Lett.* **2009**, *11*, 3004; c) G. P. Spada, S. Lena, S. Masiero, S. Pieraccini, M. Surin, P. Samorì, *Adv. Mater.* **2008**, *20*, 2433.

[6] A. Ciesielski, S. Lena, S. Masiero, G. P. Spada, P. Samorì, *Angew. Chem.* **2010**, *122*, 2007; *Angew. Chem. Int. Ed.* **2010**, *49*, 1963.

[7] a) S. Pieraccini, G. Gottarelli, R. Labruto, S. Masiero, O. Pandoli, G. P. Spada, *Chem. Eur. J.* **2004**, *10*, 5632; b) F. Cianetti, R. Ballardini, A. Credi, M. T. Gandolfi, S. Masiero, F. Negri, S. Pieraccini, G. P. Spada, *Chem. Eur. J.* **2004**, *10*, 2011.

[8] a) S. Ogasawara, M. Maeda, *Angew. Chem.* **2008**, *120*, 8971; *Angew. Chem. Int. Ed.* **2008**, *47*, 8839; b) S. Ogasawara, M. Maeda, *Angew. Chem.* **2009**, *121*, 6799; *Angew. Chem. Int. Ed.* **2009**, *48*, 6671.

[9] a) G. Gottarelli, S. Masiero, E. Mezzina, S. Pieraccini, J. P. Rabe, P. Samorì, G. P. Spada, *Chem. Eur. J.* **2000**, *6*, 3242; b) T. Giorgi, F. Grepioni, I. Manet, P. Mariani, S. Masiero, E. Mezzina, S. Pieraccini, L. Saturni, G. P. Spada, G. Gottarelli, *Chem. Eur. J.* **2002**, *8*, 2143.

[10] a) N. R. Klug, E. A. Whale, F. J. Davis, A. Gilbert, G. R. Mitchell, *J. Mater. Chem.* **1997**, *7*, 625; b) W. R. Brode, J. H. Gould, G. M. Wyman, *J. Am. Chem. Soc.* **1952**, *74*, 4641.

[11] G. Hohlneicher, M. Müller, M. Demmer, J. Lex, J. H. Penn, L.-X. Gan, P. D. Loesel, *J. Am. Chem. Soc.* **1988**, *110*, 4483.

5 Applications of Supermolecules – Molecular Devices and Nanotechnology

Up to now, we have discussed the formation of various molecular structures and assemblies – supermolecules – via supramolecular concepts. In this chapter, we move away from supermolecule preparation and consider practical applications of supermolecules. Approaches to functionalizing supramolecular systems are explained as various *molecular devices* are introduced. Molecular devices are functional materials that are structurally precise down to the molecular level that are constructed using the concepts of supramolecular chemistry. Supermolecules capable of electron conduction and electrical switches (molecular electronic devices), supermolecules that respond to light and manipulate photonic information (molecular photonic devices), supermolecules that can be used for information processing and calculations (molecular computer), and supermolecules that move, rotate, and catch targets (molecular machines) are introduced as examples of molecular devices. Well-defined molecular assemblies provide useful devices for direction-controlled information transfer. These examples suggest that supramolecular chemistry will be the main tool used in the development of nanotechnology – technology based on devices with nanoscale features – which is predicted to revolutionize our lives in the near future.

Contents of This Chapter

5.3 Molecular Electronic Devices – Controlling Electricity Using Supermolecules Molecular wires and molecular switches have been developed for molecular electronics. In particular, much of the progress made in the field of molecular electronics is based on the application of carbon nanotubes.

5.4 Molecular Photonic Devices – Controlling Light with Supermolecules It is expected that photonics will be used in many applications in the near future. Molecular recognition can be used to control light emission from molecules in molecular photonic devices.

5.5 Molecular Computers – Supermolecules that can Think and Calculate Molecular logic devices that can process multiple signals have been combined into a molecular calculator. A DNA-based computer with parallel information processing has also been proposed.

5.6 Molecular Machines – Supermolecules that can Catch Objects, Move and Rotate Molecules that rotate in a certain direction and actuators based on carbon nanotubes are explained. Mechanical control of molecular recognition and mechanical movement based on molecular recognition are also discussed.

5.7 Molecular Devices with Directional Functionality – Supermolecules That Transmit Signals in a Desired Direction The ability to direct the flow of information in a desired direction is crucial to molecular device development. Controlled organization of functional molecules, mainly using the LB method, was used to prepare molecular devices regulating electron or energy flow.

5.8 Supramolecular Chemistry and Nanotechnology – Looking Ahead Nanotechnology, including molecular devices, are expected to play a major role in many future technologies, such as those associated with space exploration. However, the ultimate examples of nanosized systems are seen in nature.

5.1 What is a Molecular Device?

If we could create a molecular-size object that worked like an IC tip, incredibly small computers with very high information densities could be constructed. Such a dream arouses our scientific curiosity, and could also significantly enhance our standard of living. Some of the most serious problems faced by the world today, such as environmental pollution and energy production, are at least partially due to the large sizes of various important devices, machines and apparatus. As well as resulting in poor energy efficiency, a large device/machine size limits portability. Therefore, to use such devices/machines, we have to travel to the places where they are located, which can result in traffic (and

its associated problems, such as pollution) and can encourage overpopulation in some areas. If the sizes of the devices were reduced to make them more portable, we would not need to travel to use it; we could carry the devices around with us. Therefore, the development of highly functional devices of a size comparable to cellular phones and watches would revolutionize our lifestyles and standard of living.

One of the ultimate goals of those developing new devices is the preparation of molecular devices, where molecules or molecular systems replace functional units. Molecular devices are expected to provide the key to the development of nanotechnology.

Concepts of molecular devices were first proposed in the 1970's. The example shown in Fig. 5.1 was proposed by Forrest L. Carter of the US Naval Research Laboratory. He proposed a molecular device where functional moieties were bridged by conductive links. When an electron is added from the input terminal, the positive charge at the end of conductive $(SN)_n$ chain is neutralized, which is accompanied by a change in potential. This potential change suppresses electron tunneling and affects the conduction of electrons between the V(-) terminal and the output terminal. Introducing a variety of input terminals would lead to the development of a system where the signal output was controlled by the pattern of inputs to the system.

This example is based on a covalently linked, complicated molecule which is difficult to synthesize. We can overcome this difficulty by using supramolecular concepts. Complicated functional systems can be constructed through the supramolecular assembly of relatively simple components. The supramolecular approach has the additional advantage of permitting us great freedom in terms of combining functional parts.

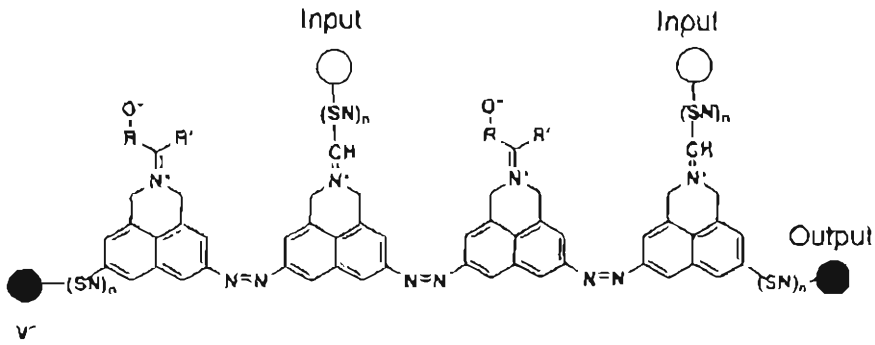

Figure 5.1. Example of a proposed molecular device

5.2
Reading Signals from Molecular Device

Before we look at the preparation and functionality of various molecular devices, we will first consider how evaluate the state of a molecular device. Evaluating the state of a molecular device is often deeply connected to an important process: reading the signal from a device. Molecular devices are usually combined with external devices that can take in signals from the device and convert them into a form that we can understand and interpret. Therefore, it is important to understand the methods used to evaluate molecular device state.

There are actually a large number of ways to evaluate the state of a supramolecular system used in a molecular device, and so only a few – the most important – are explained here (Fig. 5.2). When the targets are supermolecules dissolved in solution, spectral methods are widely used. Molecular interactions sometimes induce various changes in the nature of the supramolecular system. For example, changes in electronic state are detected by UV-Vis absorption spectroscopy and fluorescence spectroscopy. Changes in enantiomeric structure and the environment of the molecule are evaluated by circular dichroism (CD) spectroscopy. Nuclear magnetic resonance (NMR) spectroscopy and infrared (IR) spectroscopy, which are usually used to determine the chemical structure, are also useful for evaluating molecular interactions. For example, these methods provide powerful ways to determine hydrogen bond formation: hydrogen bonding causes shifts in the NMR and IR spectra, meaning that they can be used to determine the sites involved and the strength of the bonding.

Analyses of ultrathin films are also conducted via spectroscopic methods, but higher sensitivity is usually required. π-A isotherm measurement

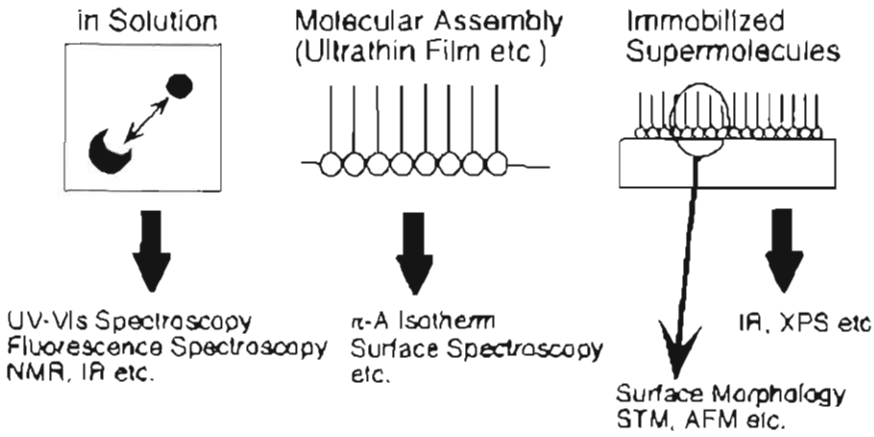

Figure 5.2 Methods of evaluating supramolecular state

is a unique way to evaluate the state of a molecular assembly. Layered LB structures or films and layered films on solid supports are typically investigated via X-ray diffraction (XRD). Elemental analyses on ultrathin films are carried out using X-ray photoelectron spectroscopy (XPS). This method is a powerful way of quantifying guests binding to the ultrathin film, as described in Chap. 2.

Methods for directly observing supermolecules have recently been developed. Scanning probe microscopy (SPM) has become a particularly useful method in the field of nanotechnology. The general concept of SPM is summarized in Fig. 5.3. A very fine tip is used in this method. As the tip approaches the sample surface, various interactions occur between the tip and the surface which result in various kinds of forces (such as atomic forces). These forces are felt by the tip and converted into electrical signals.

There are various forms of scanning probe microscopy. Among the most popular are atomic force microscopy (AFM) and scanning tunneling microscopy (STM). In AFM, the tip is scanned across the surface in such a way that the atomic force felt by the tip is kept constant (which is equivalent to saying that the tip is always the same distance from the surface). During the scan, any change in the surface topography (surface feature) produces a change in the atomic force. Therefore, to keep the atomic force constant, the tip is moved closer to or further from the surface. Therefore, the movement of the tip directly reflects the topography of the surface in AFM. STM works on a similar principle but monitors the electron tunneling current instead of the atomic force. These methods supply the surface topology to atomic-level precision. Images of supermolecules can be obtained directly. Other forces, such as those related to friction, magnetism and electrostatics, can also be monitored in other variants of SPM. High spatial resolution spectral imaging can also be performed based on near-field optical effects.

In practical molecular devices, the supramolecular system is sometimes immobilized on an external devices which reads the output from the system. An electrode is a typical example of this kind of external device. Various electrodes with ultrasmall dimensions are available, and are therefore well-suited to molecular device preparation. Electrodes can also be used as a solid support for LB films and self-assembled monolayers. In the example shown

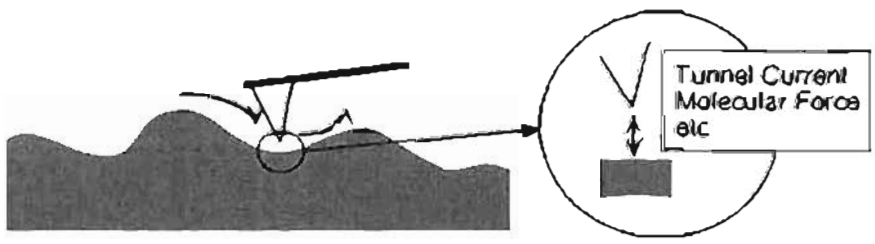

Figure 5.3. Scanning probe microscopy

in Fig. 5.4, a supramolecular component immobilized on an electrode and based on a cyclodextrin derivative is used as a sensing site for a specific guest molecule. Cyclodextrin derivatives with long alkyl chains are immobilized on the surface of an electrode using a LB or SAM method (see Fig. 4.40 for a similar example). The SAM method provides particularly stable immobilization of the monolayer component. The modified electrode was immersed in an aqueous solution of marker ions such as ferrocyanate ion. The marker ions can reach the surface of the electrode and produce redox signals when the solution does not contain the guest molecules. However, the presence of guest molecules in the solution suppresses the redox signals from the marker ion because the guest molecules bind to the cyclodextrin and block the path to the surface of the electrode. Recognition of the guest molecules by cyclodextrin was converted to a quantitative electric signal.

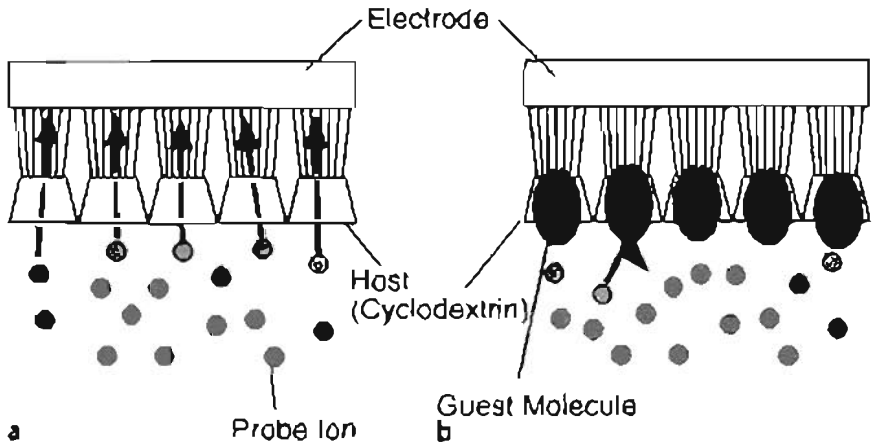

Figure 5.4. Electrical detection of guest recognition

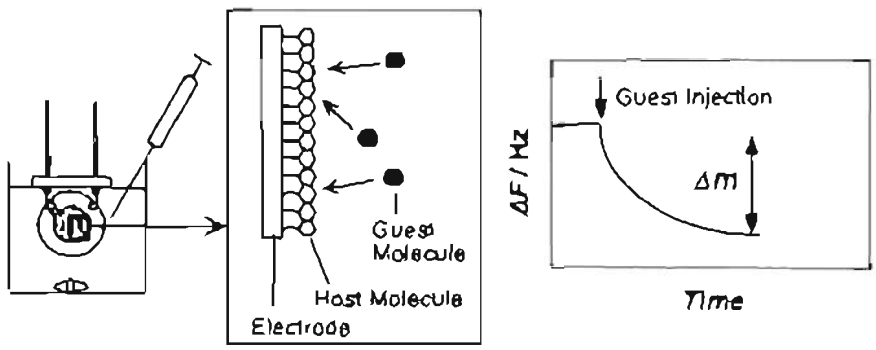

Figure 5.5. Sensitive mass detection using a quartz crystal microbalance

Other external devices are used if different output signals are required. For example, immobilizing ultrathin films of functional molecules on optical fibers allows us to detect photonic responses of functional supramolecular systems. Adsorption of specific molecules on supramolecular assemblies can be sensitively detected by surface plasmon resonance (SPR). Coupling supramolecular systems to semiconductor devices is advantageous way to prepare ultrasmall devices. Use of a field-effect transistor (FET) as an external device is a powerful method of fabricating small sensing devices. The current between the source and the drain is regulated by the gate potential. Functional supermolecules were immobilized on the gate electrode, and the surface potential changes resulting from specific guest binding to the supermolecules induced a change in the source–drain current. These sensing systems can be integrated via microfabrication techniques.

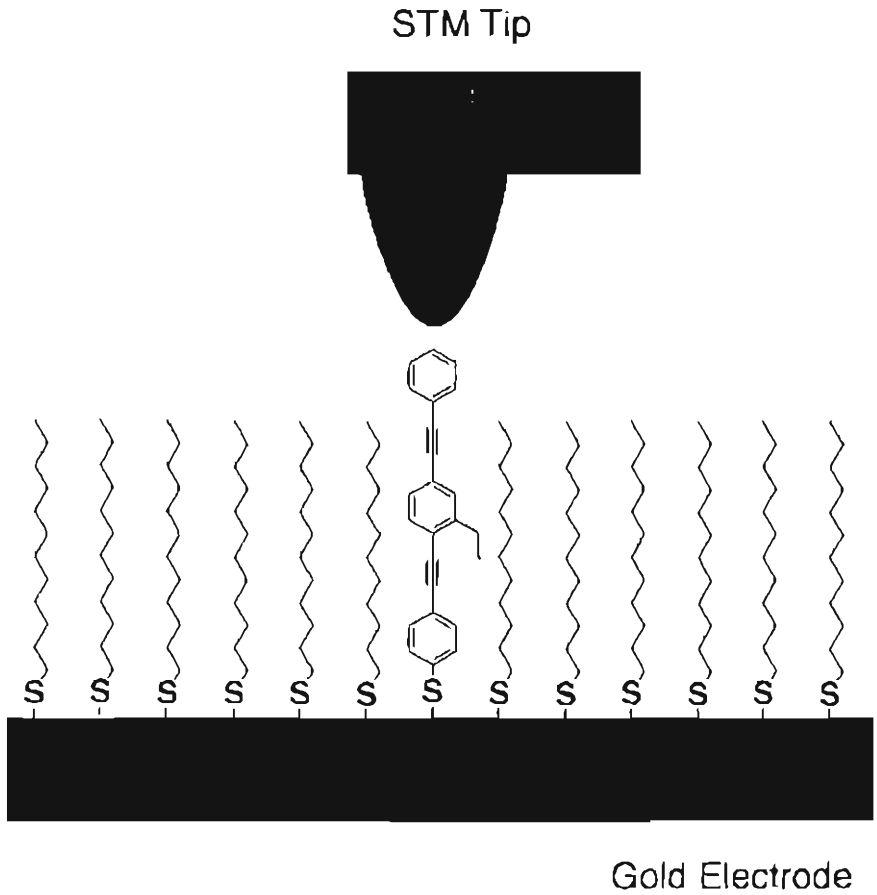

Figure 5.6. Measuring the conductivity of a single molecule

Figure 5.5 shows a unique external device, a quartz crystal microbalance (QCM). A thin plate of quartz crystal with a specific face generates piezoelectricity and exhibits a very stable resonance frequency upon the application of a voltage (this phenomenon means that quartz is widely used in timing mechanisms – in clocks for example). Metal electrodes were deposited on both sides of the quartz plate in the QCM. When some material was adsorbed onto the electrode, the resonant frequency decreased in proportion to the change in mass. In the case of a 9 MHz AT-cut QCM, a frequency change of 1 Hz was observed for a mass change of ~1 ng. Measuring frequencies to a precision of 1 Hz is not too difficult, while measuring masses to a precision of 1 ng using other methods is usually very difficult. Therefore, the QCM is very useful device for detecting tiny changes in mass. Figure 4.5 shows an example where host supermolecules were immobilized on the surface of QCM electrode. Inclusion of the guest by the host induces a decrease in frequency, and the adsorption behavior can be monitored in real time. The frequency reaches a constant value when the adsorption equilibrates.

Note that the QCM detects a very general parameter, the change in mass. Therefore, QCM sensing systems can be applied to a wide range of substances independent the properties of the guest. With appropriate immobilized supramolecular system design, QCM systems can be used to check for various guest molecules, such as nucleic acid, rectin and viruses.

Reading signals from individual molecules or supermolecules requires the use of ultrasmall external devices. Figure 5.6 shows one example of an ultrasmall external device, an STM tip. The conductive molecule is coimmobilized as a self-assembled monolayer along with an insulating thiol compound on the surface of conductive material. Scanning the surface of the SAM using the STM tip enables us to detect the current that passes through the molecule of interest. Recent progress in measuring techniques means that we can also detect signals from a single molecule using other methods.

5.3
Molecular Electronic Devices – Controlling Electricity Using Supermolecules

In the following sections, we will discuss various examples of molecular devices that have been actually developed. Most modern machines contain electrical circuits. In order to mimic but highly miniaturize such machines, it is very important to first develop molecular sized electronic parts and then find a way to combine them into molecular electronic devices.

Electron-conducting wire is the first requirement for molecular electronics. Molecules with conjugated linkages, such as conductive polymers, are strong candidates for this "molecular wire". Especially when used in supramolecular systems, A regulated conjugation length is sometimes advantageous. Figure 5.7 shows an example of a molecular wire where two pyridinium moieties are connected by a conjugated chain. The length of this molecular wire fits

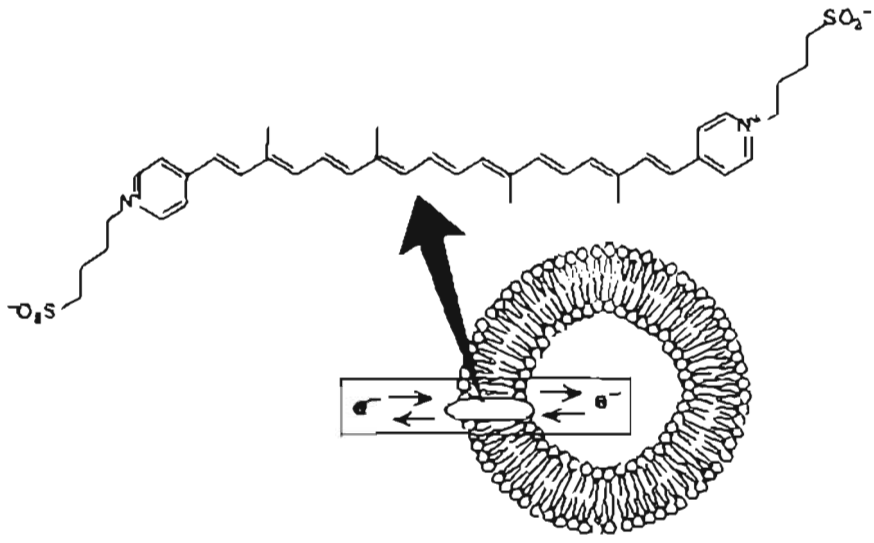

Figure 5.7. Molecular wire in a lipid bilayer

the width of a phospholipid bilayer, and the wire is accommodated effectively into the bilayer skin of a liposome. Because the surrounding bilayer was basically insulating, the molecular wire acts as an isolated conductive wire. When reduction and oxidation reactions are performed separately in the inner liposomal phase and the outer bulk phase, electrons are transmitted through this molecular wire. This system can therefore be regarded as a form of molecular wiring.

The ability to connect electronic parts is crucial to the construction of circuit-like molecular devices. However, it is quite difficult to connect components solely through covalent linkage. Therefore, it would be better to connect the electronic parts through supramolecular interactions. In fact, biological systems use a similar concept. Information is transmitted as electrical signals through nerve systems, but nerve cells are not connected to each other covalently. There is a synapse junction between the nerve cells where signals are transmitted via a chemical mediator.

Electron transfer via a noncovalent junction was achieved artificially using the example shown in Fig. 5.8. In this system, the electron donor zinc porphyrin was covalently connected to guanosine, and an electron-accepting quinone was linked to the cytosine. These two parts associate through complementary hydrogen bonding between the guanosine and cytosine. When this pair were irradiated with light of an appropriate wavelength, electron transfer occurred from the zinc porphyrin to the quinone. This example demonstrates that electrical connections can be achieved between molecular parts via noncovalent supramolecular interactions.

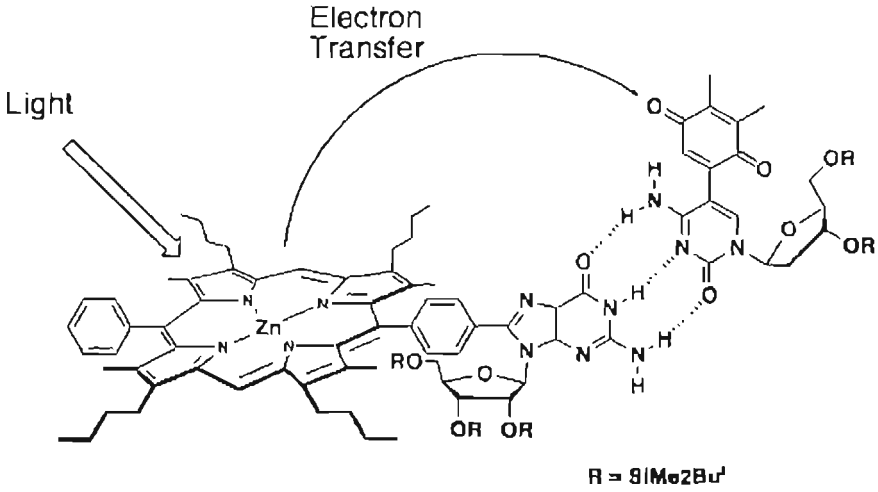

Figure 5.8. Electron transfer between a pair of supermolecules

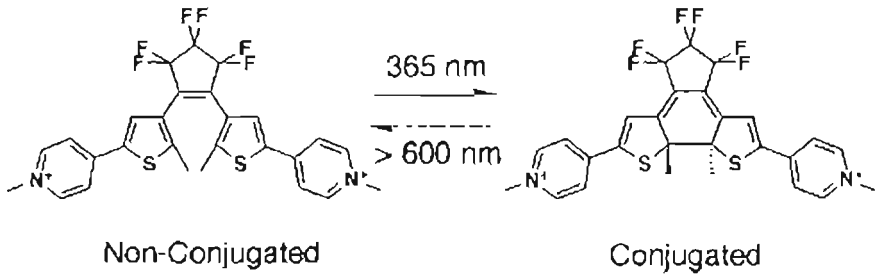

Figure 5.9. Molecular switch

An electrical switch is another important element for regulating electron flow. Direct connection and disconnection between lead wires is usually used to regulate electricity flow. The molecule shown in Fig. 5.9 mimics this kind of switch. When the center of the molecule is uncyclized, a fully conjugated path (a path of conduction) through the molecule is not available and so the molecular switch is in the OFF state. Irradiating the molecule with light at 365 nm induces cyclization of the molecule. When it is cyclized, a fully conjugated path through the molecule becomes available, and so the molecular switch is turned ON. The molecule can reverted its OFF state by irradiating it with light of > 600 nm. If this kind of molecular switch was introduced into a supramolecular system, molecular electric circuits switched by photoirradiation could be constructed.

Various molecular conductive wires and molecular switches should become available in the near future. Connecting them in a logical way would

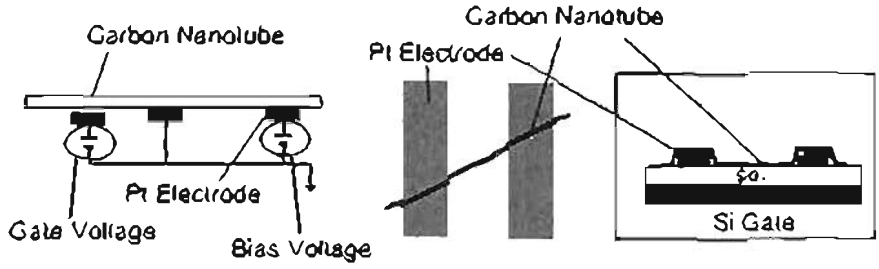

Figure 5.10. Transistor based on a carbon nanotube

result in the construction of molecular electrical circuits. However, current technologies make the construction of such circuits very difficult, and so connecting molecular devices to artificial fabricated structures could provide a more realistic approach. Such objects could be fabricated by engineering tools and connected to artificial structures such as ultrasmall electrodes. Supermolecules with sizes comparable to those of microfabricated structures would be especially useful when creating these objects. Carbon nanotubes satisfy this requirement. For example, single-walled carbon nanotubes have diameters measured in the nanometers (1 - 2 nm), but they are microns in length. In addition, the electronic state of a carbon nanotube can be estimated theoretically. These advantages mean that carbon nanotubes currently play a central role in molecular device preparation. When the nanotube structure is completely symmetric, it can be used as a one-dimensional quantum wire. In the following, a few examples of molecular electronic devices based on carbon nanotubes are introduced.

An ultrasmall transistor can be prepared from a carbon nanotube and some microelectrodes. Figure 5.10 shows the structure of the transistor, where a carbon nanotube bridges two platinum electrodes that were deposited on a plate of Si/SiO_2. The current induced upon the application of a voltage between the two electrodes was measured at very low temperatures. Maintaining the bias voltage between the two measuring electrodes, the gate voltage applied to the third electrode was altered, resulting in a current pulse. A plausible mechanism for this phenomenon is shown in Fig. 5.11. Electron transfer between different energy levels by thermal excitation was suppressed by the very low temperatures. Current flow is possible only when the Fermi potential of the electrode matches the energy level of the carbon nanotube. When the electrostatic potential of the carbon nanotube was gradually changed by scanning the gate voltage, at some point the electrode Fermi level and the nanotube energy level matched, resulting in a current pulse. Here, the quantization of the energy levels of the carbon nanotube at low temperatures is reflected in the discontinuous current response. At elevated temperatures, this quantum effect is far less noticeable, but even at room temperature the state of the nanotube

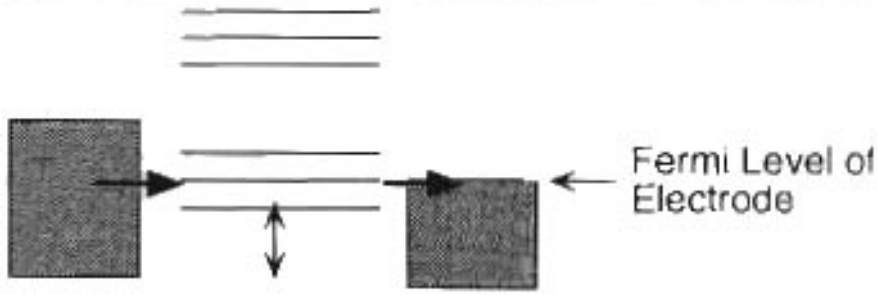

Figure 5.11. Electron conduction by matching energy levels

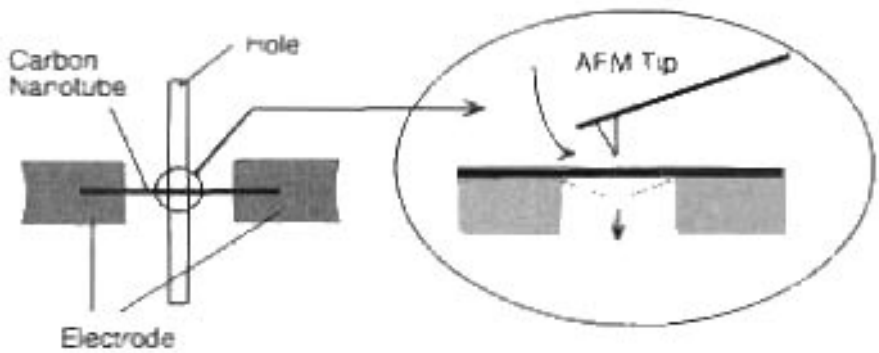

Figure 5.12. Mechanical switch based on altering the conductivity of a carbon nanotube

can still be switched (between conductive and insulating) by altering the gate voltage. This system can be regarded as a field effect transistor (FET), and the resulting molecular device is called a TUBEFET device.

Mechanically deforming the carbon nanotube alters its electric properties. In the example shown in Fig. 5.12, a carbon nanotube was bridged between two electrodes separated by a gap. When the middle of the carbon nanotube was pushed by an AFM tip, the nanotube was bent and its conductivity dropped. The electron conductivity was correlated with the degree of bending, which was measured from the position of the AFM. This process was repeatable. The bending of the carbon nanotube induced the formation of some nonconductive SP^3 orbitals within its structure, altering its conductivity. This behavior is somewhat reminiscent of a switch.

One serious issue with the construction molecular devices is how difficult it is to precisely place each supramolecular element into the correct position. It would be much easier to draw nanocircuits if we could create supermolecules at desired positions. In the example shown in Fig. 5.13, molecular wires of conductive poly(diacetylene) are drawn by an STM tip in a highly controlled

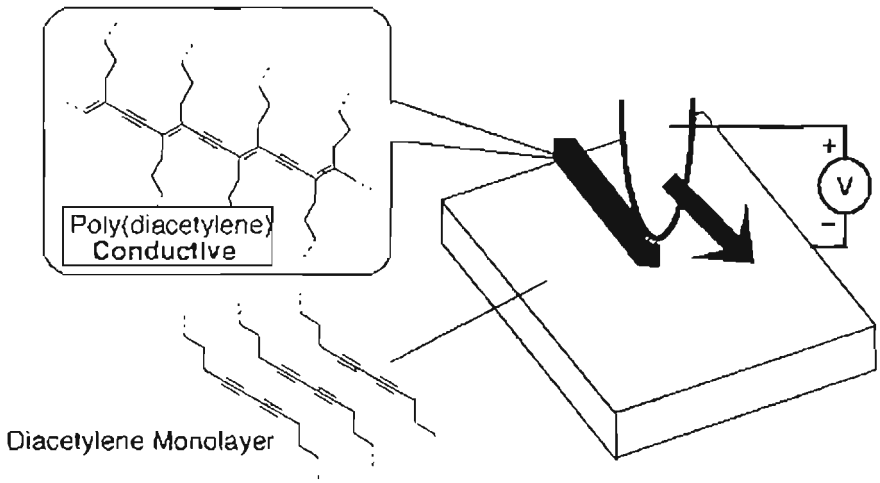

Figure 5.13. Drawing a conductive line using an STM tip

manner. The tip is used to apply an appropriate voltage to a monolayer of diacetylene derivative, forming the conductive poly(diacetylene) at the point of contact. This method would be very useful for preparing miniaturized electric circuits at desired positions on a solid support.

5.4 Molecular Photonic Devices – Controlling Light with Supermolecules

It is expected that the number of devices utilizing photonics (the optical equivalent of electronics) will increase dramatically in the near future. Light is usually a mixture of visible wavelengths that all travel at the same incredibly fast speed. Therefore, photonic systems allow us to transmit huge amounts of information within an incredibly short period of time. Photonic technology has been recently applied to various devices, such as compact discs (CDs), photocopiers and barcode readers. Rapid communication of large amounts of data between different parts of the world has been made possible through fiber optic cables, and fiber optic communication look sets to become more important than communication via electric cables in the near future. As explained in previous chapters, molecular recognition or supramolecular interactions sometimes result in spectral changes, which suggests that supermolecules would make good materials for use in photonics. Supramolecular chemistry is therefore expected to play an important role in the development of photonic devices with huge information densities.

Figure 5.14 shows an example of a molecular photonic switch in which a Ru complex and an Os complex are bridged by an azobipyridine ligand. The emission of this complex changes depending on the redox state of the

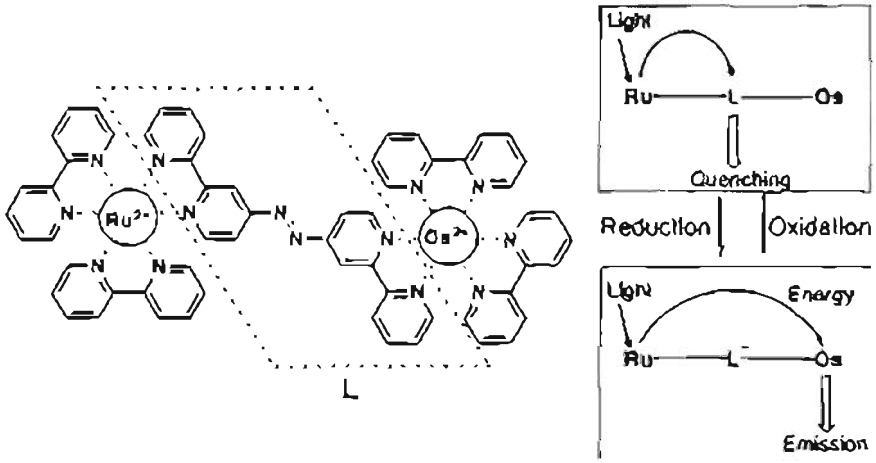

Figure 5.14. Controlling emission via redox reactions

bridging ligand. The azobipyridine is an electron acceptor in its neutral state. In this case, exciting the Ru complex with light causes the complex to pass an electron to the azobipyridine, which then relaxes thermally. In contrast, if the azobipyridine ligand is reduced, the electron-accepting nature of the ligand is suppressed. Excitation of the Ru complex then results in energy transfer to the Os complex, resulting in the emission of light. In other words, the emission behavior of the Os complex is controlled via azobipyridine redox reactions. This system can be regarded as a molecular photonic switch.

A molecular switch that responds to several kinds of stimuli has also been proposed. The molecule shown in Fig. 5.15 contains both a photoresponsive anthracene moiety and a crown ether connected via a tertiary amino group. This molecule shows switching properties based on a photoinduced electron transfer (PET) mechanism. An electron donor will quench excited anthracene, and both the tertiary amino group and the crown ether have this ability. The anthracene will therefore only emit when electron transfer is prohibited from both the amino group and the crown ether, and this can be achieved by protonating the amine and introducing sodium ions (accommodated by the crown ether). This molecular switch is therefore controlled by two inputs, and output (light emission) only occurs if both of these inputs are ON; in other words, this is an AND-type molecular logic gate.

5.5
Molecular Computers – Supermolecules That can think and Calculate

The example described at the end of the previous section is the simplest model of an information converter, because its output is controlled by the states of its

multiple inputs. Combining such molecular systems leads to the preparation of more sophisticated molecular devices.

Figure 5.16 shows two types of molecular logic devices that can be used for simple mathematics. Molecule A in Fig. 5.16 has bonding sites for a proton and a calcium ion. Light (with a wavelength of 419 nm) is only emitted from this molecule when both stimuli (protons and calcium ions) are introduced into the system. Addition of either protons or calcium ions does not induce significant emission. Therefore, again, this can be regarded as an AND-type logic gate. In contrast, the absorption behavior of molecule B shows a different dependence on these stimuli. This molecule normally absorbs at 390 nm. This behavior is also observed when both protons and calcium ions are present. However, adding either protons or calcium ions significantly suppresses the absorption (increasing transmittance). Therefore, if the transmittance at 390 nm was measured as the output signal, this system can be regarded as a XOR-type logic gate.

Combining these two logic gates yields a binary molecular calculator. Let us now denote an positive (ON) input by "01", and a negative (OFF) input by "00". We shall also use 0 and 1 to denote negative and positive gate outputs, respectively. In this case, when both inputs are OFF (00 + 00), the AND gate output is negative (0) and the XOR gate output is negative (0), giving a combined output of 00. When only one of the inputs is ON (01 + 00 or 00 + 01), the AND gate output is negative while the XOR gate output is positive, so the combined output here is 01. On the other hand, when both inputs are ON (01 + 01), the

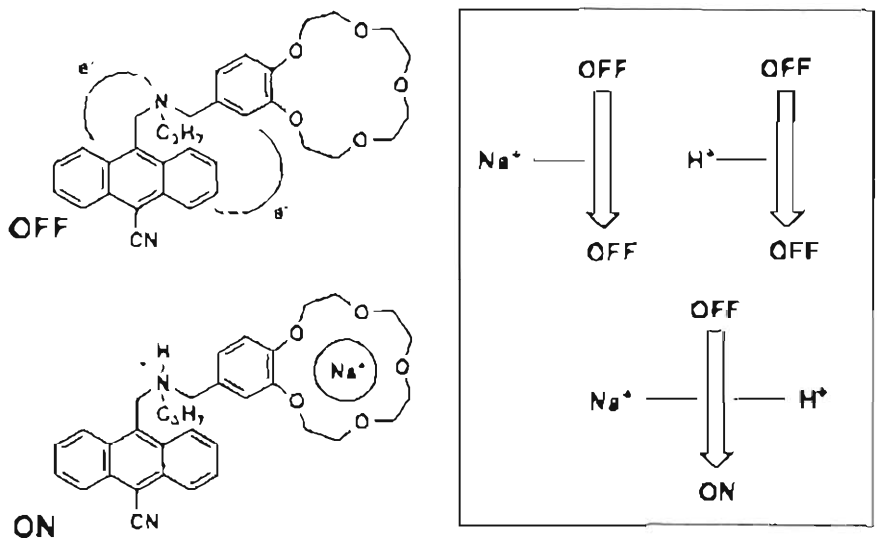

Figure 5.15. Addition of both H^+ and Na^+ induces optical emission

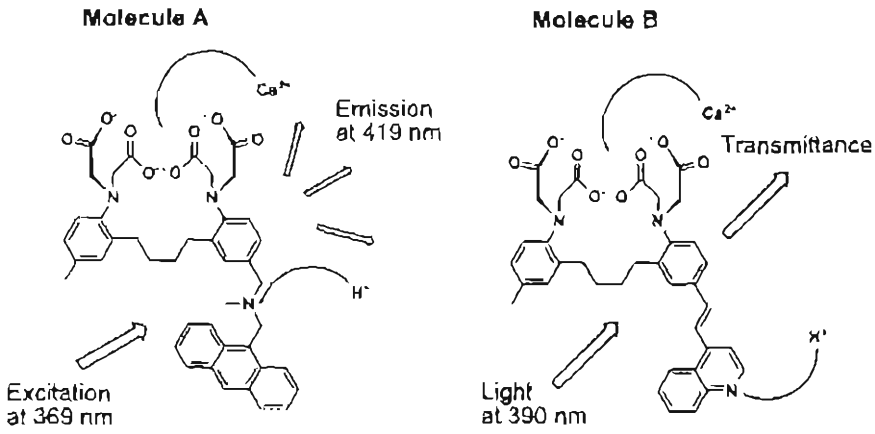

Additive		Emission
Ca^{2+}	H^+	
00	00	0
01	00	0
00	01	0
01	01	1

AND Gate

Additive		Trans-mittance
Ca^{2+}	H^+	
00	00	0
01	00	1
00	01	1
01	01	0

XOR Gate

Input (Ca^{2+} and H^+): 00 negative input; 01 positive input

Output (Emission and Transmission): 0 negative output; 1 positive output

Figure 5.16. Molecular logic gates

AND gate gives a positive output and the XOR gate a negative output, which is a combined output of 10. This binary logic is summarized below:

00 + 00 = 00 (No input)
01 + 00 = 01 (Proton input ON only)
00 + 01 = 01 (Ca^{2+} input ON only)
01 + 01 = 10 (Both inputs ON and negative XOR output)

This can be translated into the decimal system of 0 + 0 = 0, 1 + 0 = 1, 0 + 1 = 1, and 1 + 1 = 2, respectively. A supramolecular system containing molecules A and B therefore performs mathematics.

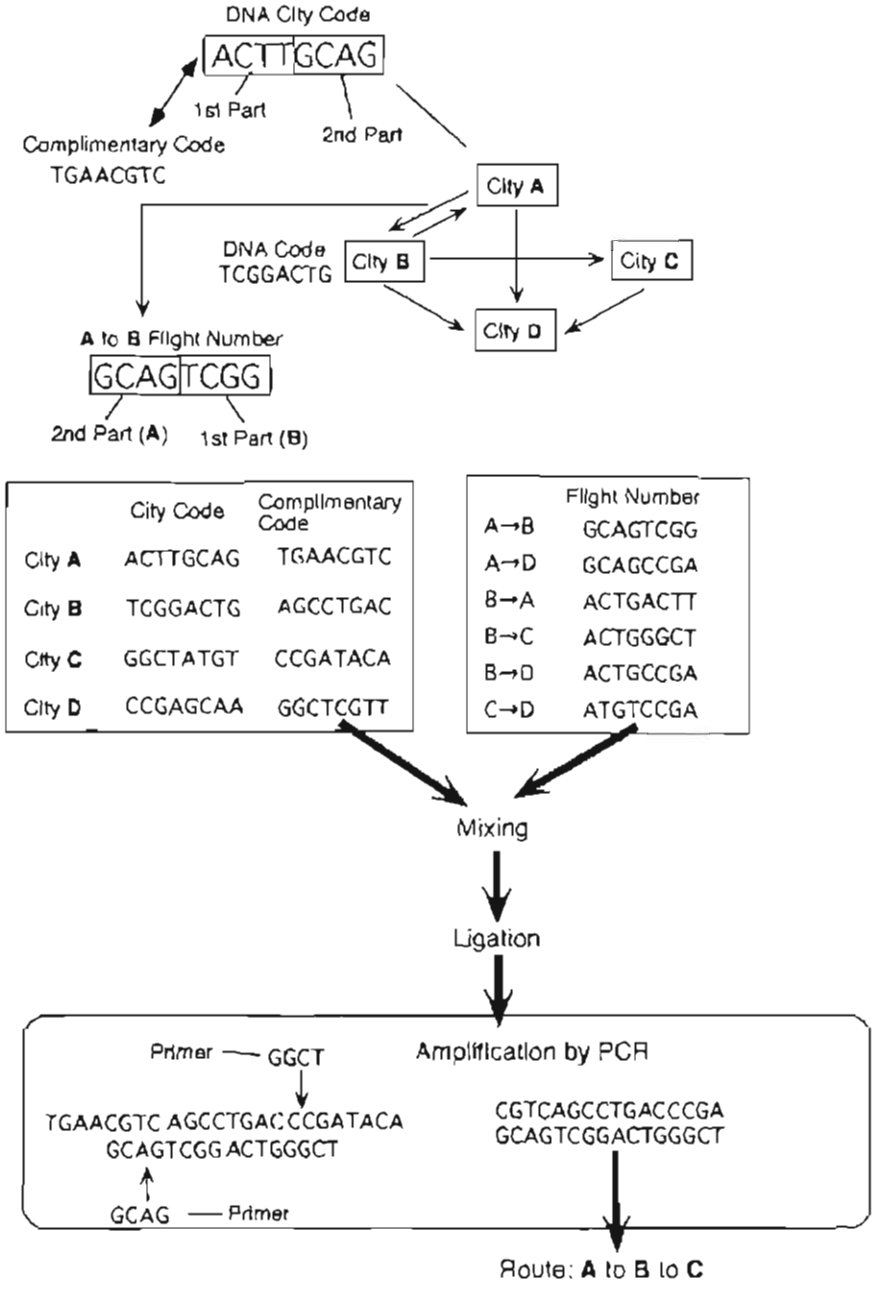

Figure 5.17. Example of DNA computing

In our body, huge amounts of information are accumulated in deoxyribonucleic acid (DNA) with incredibly high density. The blueprints of the structures of biologically important molecules – proteins – are written in DNA sequences. It is often said that the elegant and sophisticated functions seen in living creatures are programmed into the DNA strands. There have therefore been proposals to utilize the DNA molecules as a molecular computer. One example is shown in Fig. 5.17. The target of this example is to specify the correct flight route via DNA selection processes. DNA has a backbone composed of sugars, and phosphates and nucleobases are attached to every sugar unit. Adenine (A) selectively binds to thymine (T) and guanine (G) forms a specific pair with cytosine (C) between nucleobases. Two DNA strands form a complex that adopts the shape of a double helix due to these base pairings, with high precision.

DNA codes were first assigned for points. City A has a DNA city code of ACTT-GCAG. A DNA sequence of TGAA-CGTC can form a complementary pair with this code and so it is defined as a complementary code of City A. City B has a different DNA city code (TCGG-ACTG). The flight number from City A to City B is defined as GCAG-TCGG, which is derived by connecting the second part of the sequence for City A (GCAG) with the first part of the sequence of City B (TCGG). The city codes for other cities were similarly defined as GGCT-ATGT (City C) and CCGA-GCAA (City D). The corresponding complementary codes and several flight number codes are summarized in Fig. 5.17.

As an example, the selection of a flight route from City A to City C is demonstrated below. By mixing together all of the complementary codes and flight number codes, various DNA pairs were formed. The number of particular DNA pairs can be selectively amplified using the polymerase chain reaction (PCR) method. In the PCR method, short DNA segments known as primers are added and the DNA sequence between the primer sequences is selectively duplicated by the DNA polymerase. Repeating the PCR cycle allows us to selectively increase the number of desired DNA sequences. In this example, the second part of the complementary code of City A (CGTC) and the first part of the city code of City C (GGCT) were used as primers. As shown in Fig. 5.17, the PCR treatment resulted in an increase in the sequence GCAGTCGG-ACTGGGCT, which corresponds to a sequential flight from A to B and then from B to C. When we go to City C from City A, we must go via City B.

Upon describing the simplified example above, the advantages of using such a DNA system are not immediately clear. However, increasing the complexity of the problem would reveal the advantages of the DNA system. The DNA pairing occurs at once, even if the length of the DNA is increased. This is equivalent to saying that the processing time of this DNA computer does not increase as the calculations become more complicated, whereas the computers that we are used to require more processing time for more complicated calculations. This DNA computer is based on parallel processing, because the DNA pairing occurs simultaneously.

5.6
Molecular Machines – Supermolecules that can Catch Objects, Move and Rotate

Tweezers, scissors and screwdrivers are primitive tools compared to computers, but their importance and wide applicability to daily life cannot be ignored. Similarly, molecular scale mechanical devices would be very useful in nanotechnology. For example, a molecular robot that fabricates molecular wires and molecular machines that could penetrate deep inside the body would provide huge contribution in the fields of molecular electronics and medicine, respectively.

In our first example of a molecular machine, we consider a rotating molecule (a molecular bearing). The molecule shown in Fig. 5.18 has three naphthalene rings connecting to a central benzene ring; this molecule has a diameter of ~1.5 nm including the *tert*-butyl groups at the outside, and a twisted propeller-like shape because of steric hindrance. It was adsorbed onto the face of Cu(100) and it formed a monolayer structure, as observed by STM. Well-packed monolayers provided static images with clear molecular shapes. On the other hand, low coverage resulted in an ambiguous image: th motions of the molecules were too fast, resulting in unclear molecular images. Random nanometer defects were observed in the monolayer at a coverage of a little less than 100%. Interestingly, a molecule trapped in one of these asymmetric defects gave an unclear molecular image, even when the surrounding well-packed molecules were clearly observed. This suggests that the molecules in the defect were rotating due to weak interactions with the surrounding molecules. This molecular propeller has a tiny weight (1.33×10^{-24} kg) and only very small inertia. Its molecular motion can be easily controlled using an external energy supply (heat). This motional mechanism is obviously quite different to that usually used in macroscopic wheels.

A molecule that can be rotated to a particular direction by external stimuli is shown in Fig. 5.19. In this molecule, two of the same structures are connected through a double bond and the molecule has a twisted structure due to steric hindrance. Four steps involving light irradiation and thermal treatment

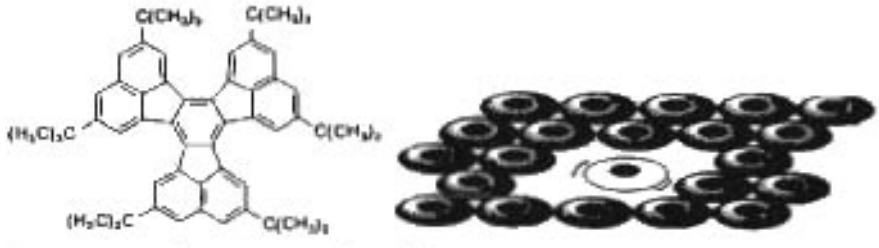

Figure 5.18. A molecule rotates within a defect

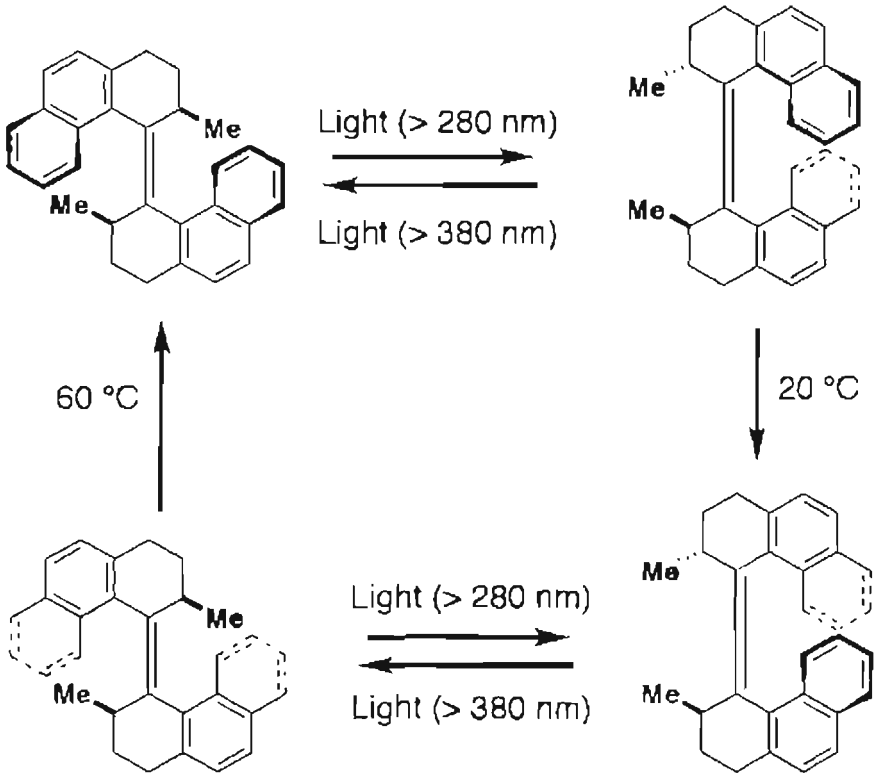

Figure 5.19. Unidirectional rotation of molecule upon irradiation with light irradiation

caused this molecule to rotate in a particular direction (counter-clockwise when viewing from the top).

The molecule in Fig. 5.20 undergoes unidirectional rotation upon certain chemical reactions. This molecule also has a twisted structure due to steric hindrance. The addition of phosgene to a system containing this molecule induced the conversion of the amino group to isocyanate. The upper half of the molecule rotated and reacted with the hydroxyl group of the lower part to form a urethane linkage. The formation of the covalent urethane linkage prohibits rotation in the reverse direction. With maintaining the urethane linkage, the upper part rotated further to achieve a more stable conformation. Finally, breaking the urethane linkage via $NaBH(OC_2H_5)_3$ caused the upper part of the molecule to undergo a half-rotation. In this example, the use of irreversible chemical reactions induces unidirectional rotation of the molecule.

Rotaxanes are unique supermolecules where cyclic molecules are threaded by linear molecules. They are powerful candidates for molecular machines,

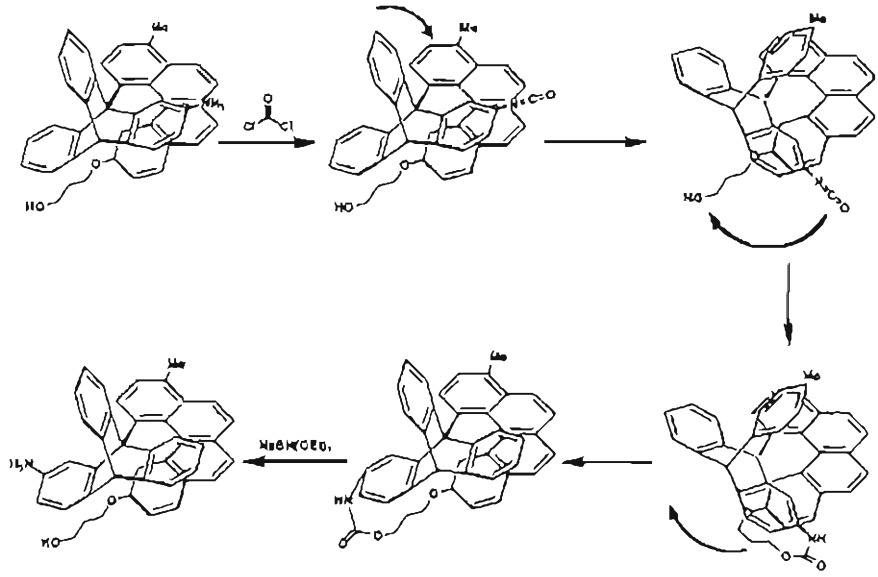

Figure 5.20. Unidirectional rotation of a molecule due to chemical reactions

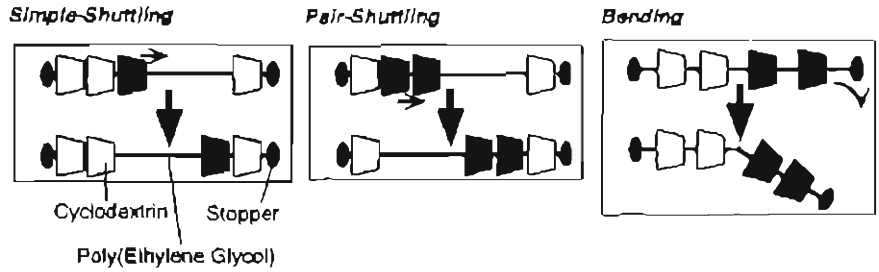

Figure 5.21. Molecular abacus based on rotaxane

and molecular shuttles based on rotaxanes have been proposed. The example described in Chap. 3 (see Fig. 3.21) shows the movement of a cyclophane along its axis molecule upon redox reaction. However, the ability to control the motions of particular cyclic molecules in a rotaxane containing many of them would be more useful in nanotechnology. Direct contact with the molecule is required for this useful task. Mechanical control of a single rotaxane molecule is shown in Fig. 5.21. A rotaxane composed of cyclodextrin rings and a polyethyleneglycol chain was nudged by an STM tip. Simple shuttling of one cyclodextrin, pair shuttling of two cyclodextrins and bending of the rotaxane molecule were all reported. This molecular shuttling is reminiscent of a Japanese abacus, so it could be called a molecular abacus.

Actuators based on the swelling and shrinking of gels are the subject of much research. They can be regarded as modeling muscle systems. However, the response times of such systems are limited, because actuator motion occurs with molecular diffusion in the gel. If each molecule could expand and shrink instead, motional response times would significantly improve. Carbon nanotubes are known to expand or shrink upon injections of electrons or

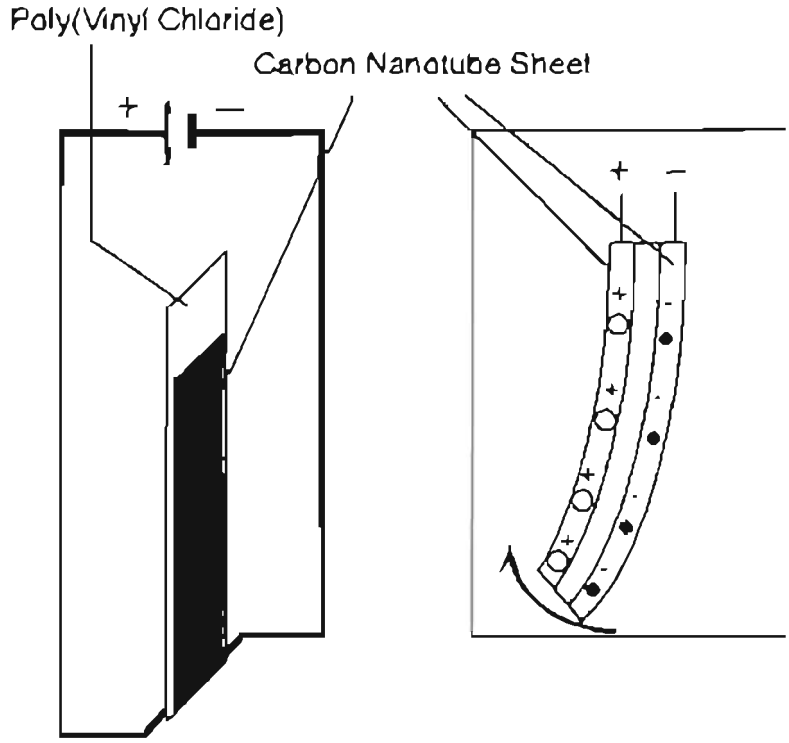

Figure 5.22. Carbon nanotube actuator

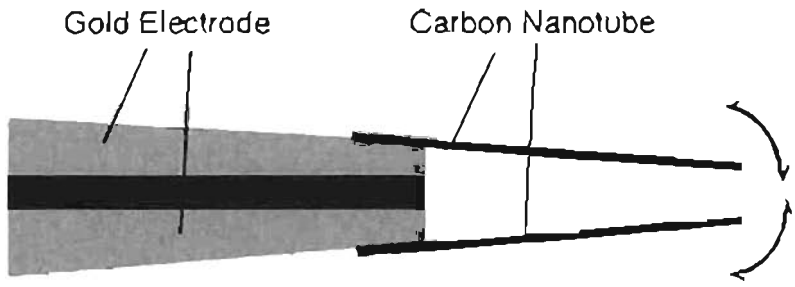

Figure 5.23. Molecular tweezers

holes. This behavior is explained by quantum effects due to changes in orbitals and band structures. This mechanical property of carbon nanotubes was utilized in the preparation of a molecular actuator (Fig. 5.22). A sheet of carbon nanotubes was first prepared by filtration, and these nanotube sheets were then attached to both sides of an insulating polymer sheet. Applying a voltage across both of the carbon nanotube sheets causes one sheet to expand and the other to shrink, which means that the total three-sheet system bends. This happens because applying a voltage across them causes a charge imbalance in the sheets, which is compensated for by the movement of counterions towards the charge. This charge compensation occurs mainly at the surfaces of the sheets, and so the counterions do not tend to diffuse deeper into the sheet. These characteristics result in a very quick mechanical response for this actuator.

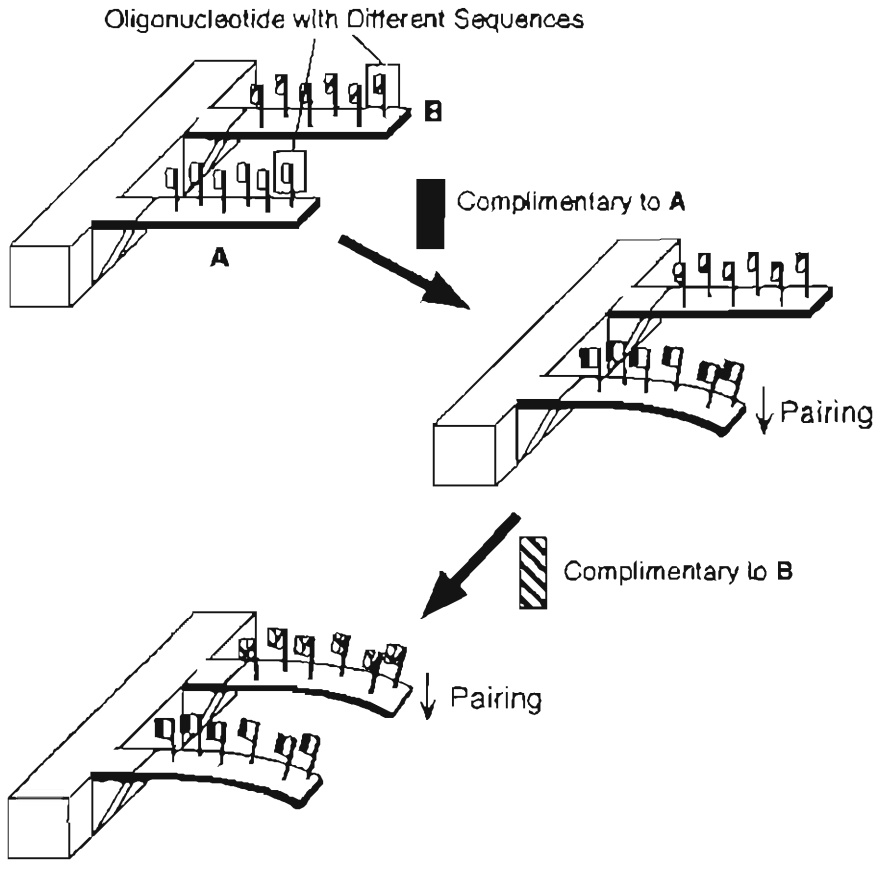

Figure 5.24. Mechanical motion upon DNA hybridization

Tools for microfabrication have also been prepared based on the unique characteristics of carbon nanotubes. In the microtool shown in Fig. 5.23, two carbon nanotubes are fixed on gold electrodes that are deposited either side

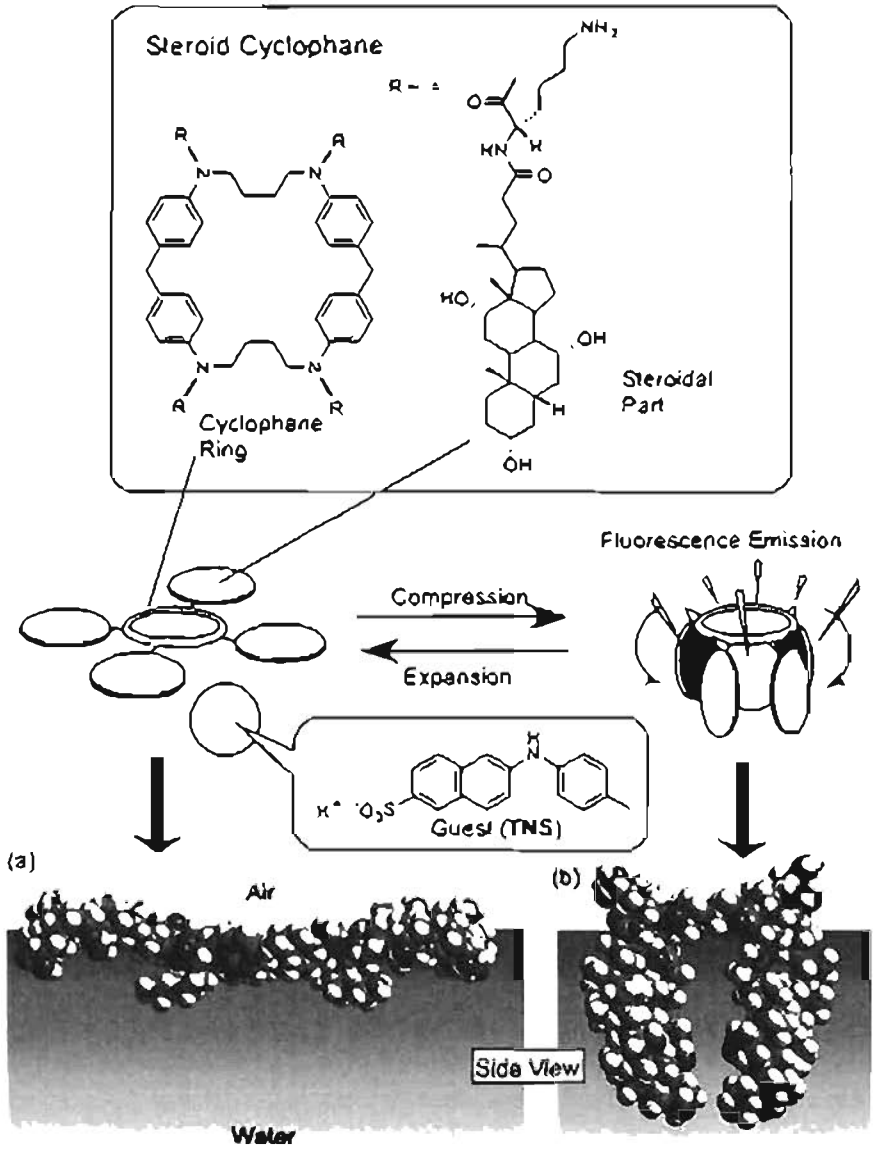

Figure 5.25. Pressure-induced emission upon molecular recognition

of a glass micropipette. Applying a voltage between these two electrodes induces opposite charges in the nanotubes (as with the sheets in the actuator described above). The oppositely charged nanotubes are attracted to each other, causing them to move towards each other and finally contact. Grounding the electrodes (and therefore the nanotubes) removes the charge and therefore causes the tweezers to move apart again. This microtool can therefore be regarded as a pair of molecular tweezers. Molecular tweezers like this have been used to catch and move clusters of tiny polystyrene spheres. This microtool has also been used as a nano-sized tester electrode; the conductivities of SiC clusters and GaAs nanowires have been directly measured in this way.

Molecular recognition is an event that occurs at the molecular level, but a large number of such recognitions can lead to macroscopic changes in substances. In the system shown in Fig. 5.24, the surface of silicon board (width 100 μm; length 500 μm; thickness 1 μm) was coated with gold, and oligonucleotides with thiol terminals were immobilized on the gold surface. If a guest oligonucleotide with a complementary sequence is introduced, it binds to the immobilized oligonucleotide to form a double helix structure. The cumulative strain induced by all of these hybridizations caused the support board to bend. In a similar way, a mechanical change was triggered in a macroscopic substance by molecular recognition between proteins.

Figure 5.25 shows the reverse of the type of conversion system described above. In this case, molecular recognition is controlled by visible mechanical changes. A host molecule with four cholic acid planes and a cyclophane ring was spread as a monolayer on the surface of water. Because the cholic moiety has a hydrophilic face and a hydrophobic face, the host molecule adopted an open conformation, contacting the hydrophilic faces to the surface of the water, at low pressure. However, compression of the host monolayer induced a change to a closed host conformation where the four cholic planes flip up from the surface of the water. The latter host conformation provides a binding medium with a high affinity to a naphthalene guest. Therefore, molecular recognition of a guest in the water phase was induced by monolayer compression. Guest binding was monitored using the associated change in surface fluorescence. In this system, the visible mechanical change (made at the 10^{-3} m level) was converted to a molecular event (at the 10^{-9} m level) – this concept bridges a huge difference in scale.

5.7 Molecular Devices with Directional Functionality – Supermolecules that Transmit Signals in a Desired Direction

An advanced molecular device would require a separate signal input and signal output. To achieve this, it is necessary to organize the functional molecules in a particular way that will lead to directional information transfer through the

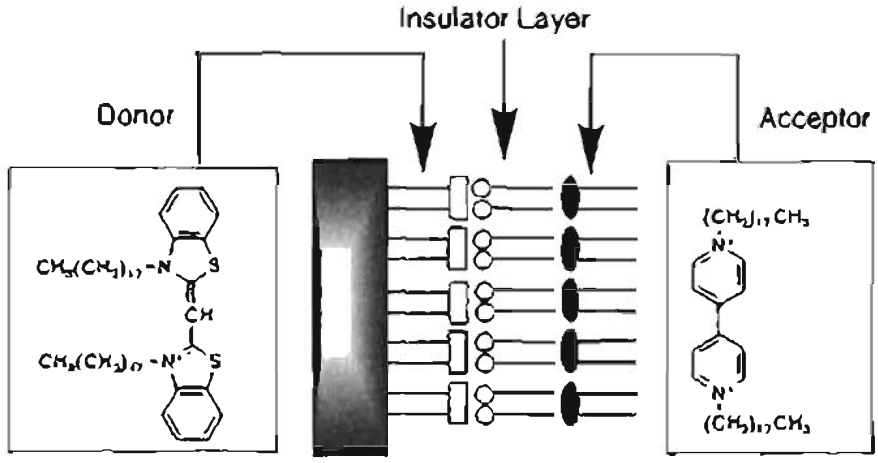

Figure 5.26. LB film for direction-specific electron transfer

supramolecular system. Techniques that can provide layered structures, such as the LB method and the alternate layer-by-layer technique, are useful for preparing molecular devices that can perform direction-specific information conversion.

Figure 5.26 shows an LB film that regulates electron transfer. Monolayers of an electron donor layer, an insulating fatty acid layer and an electron acceptor layer were transferred in a defined sequence. In this heterolayered LB film, electron transfer only occurs from the inside to the outside, and the structure of the insulator layer determines the efficiency of electron transfer. Swapping around the donor layer and the acceptor layer reverses the direction of electron transfer. Simply controlling the layering structure therefore enables us to modulate the direction and efficiency of electron flow.

Photoinduced electron transfer devices have also been constructed using the LB method (see Fig. 5.27). Excitation of the photosensitizer pyrene induces the transfer of an excited electron to viologen (an electron acceptor) and the transfer of an electron from ferrocene (an electron donor) to the ground state of the pyrene. These processes result in charge separation, a process that occurs during photosynthesis. Reversing the layering sequence causes charge separation to occur in the opposite direction. Efficient photoinduced electron transfer therefore requires the creation of organized sequences of donor, sensitizer and acceptor in order to suppress electron back-transfer, and this is easily realized using the LB technique.

A similar functional device can be constructed through the orientation-controlled assembly of molecules with donor, acceptor and sensitizer parts. Three kinds of dye - ferrocene, viologen and pyrene - were covalently con-

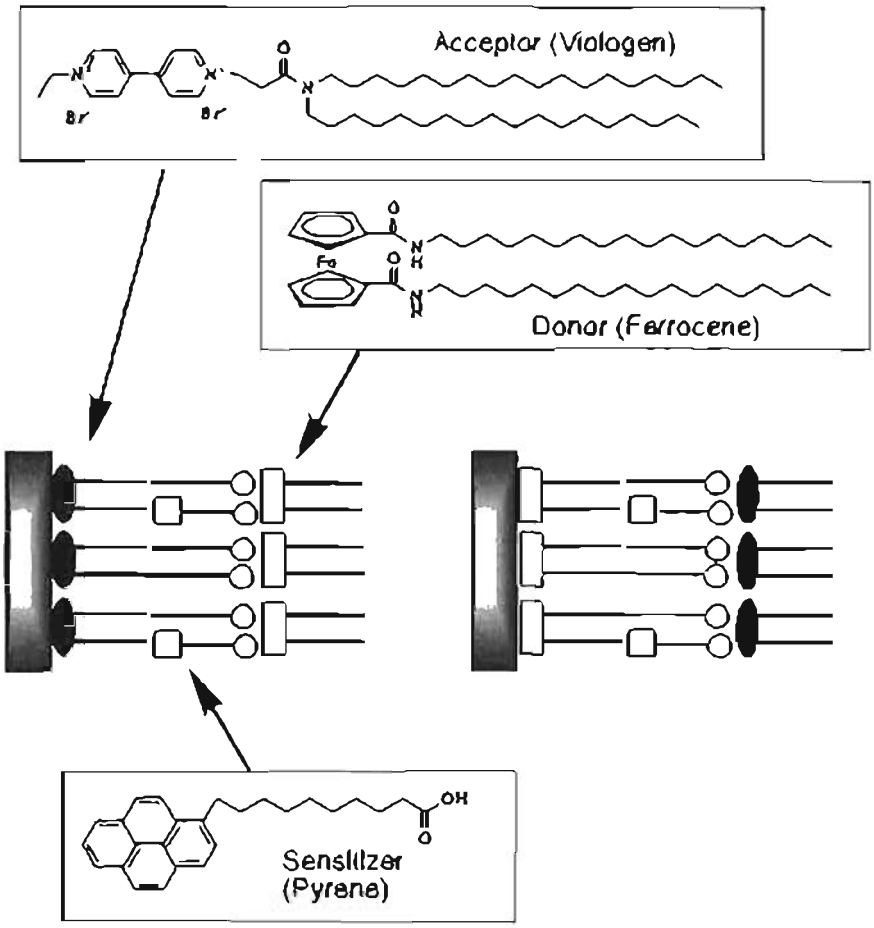

Figure 5.27. Design of LB films that exhibit photoinduced charge separation

nected in one amphiphile molecule, and a monolayer of this molecule was transferred onto an electrode. This system also shows directional photoinduced electron transfer.

Figure 5.28 shows a system used for the photocontrol of electron conductivity within a monolayer. A monolayer of an amphiphile containing azobenzene (the photocontrolled part) and tetracyanoquinone (TCNQ, which conducts electrons) was spread on water, resulting in two-dimensional photocontrolled and electrically conductive layers. Isomerizing the azobenzene part between its *trans* and *cis* isomer by alternate photoirradiation induced periodic changes in the electrical conductivity of the TCNQ part. The electrical conductivity is limited to a two-dimensional plane here, which embues a different

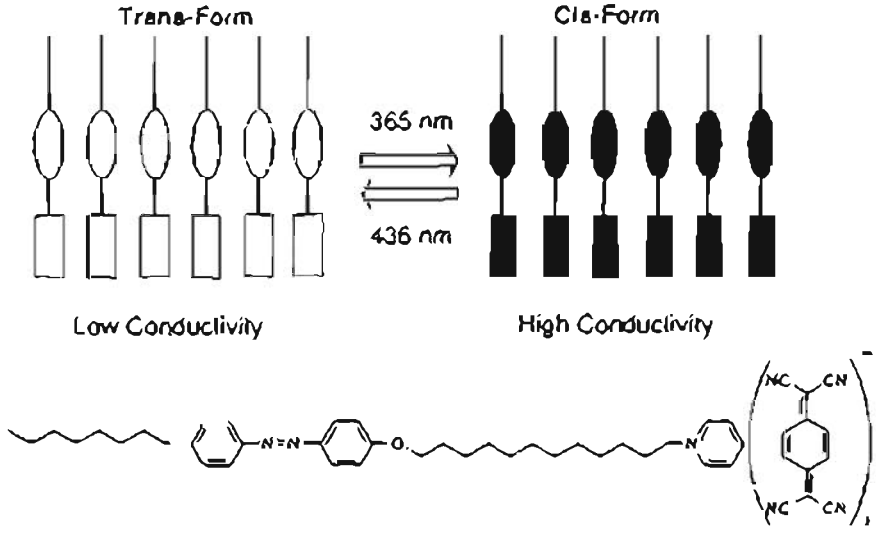

Figure 5.28. Photocontrol of conduction within a monolayer

direction-specificity to the electron flow to those described for the previous systems.

The LB film shown in Fig. 5.29 is an energy transfer device with a photoswitching layer. The switching layer is in its merocyanine form when the system is irradiated with UV light. In this case, excited thiacyanine molecules in the donor layer can transfer energy via the merocyanine to the indocarbocyanine in the acceptor layer. This results in strong indocarbocyanine fluorescence at 725 nm (λ_2). On the other hand, irradiating the system with visible light changes the switching layer into its spiropyran form, which cannot accept energy from thiocyanine. Since this cuts off the flow of energy to indocarbocyanine, it stops fluorescing and fluorescence from the thiacyanine is mainly observed at 480 nm (λ_1) instead. The energy flow from the donor layer to the acceptor layer was regulated by the photoisomerization of the switching layer. The wavelength of the input light controls the wavelength of the output signal.

In Fig. 5.30, a multilayered self-assembled film of an aminostilbazorium derivative is depicted, where the multilayer does not have a symmetric structure (the aminostilbazorium units adopt a specific orientation against the solid surface). In this aminostilbazorium derivative, the electron-donating part and the electron-accepting part are connected through conjugated linkages. Aligning this kind of molecule in a particular direction results in nonlinear optical effects. Irradiating it with light with an electric field of E and a frequency of ω induces polarization, which is expressed by polynominal equation in E. Terms greater than second-order can usually be ignored, and the main com-

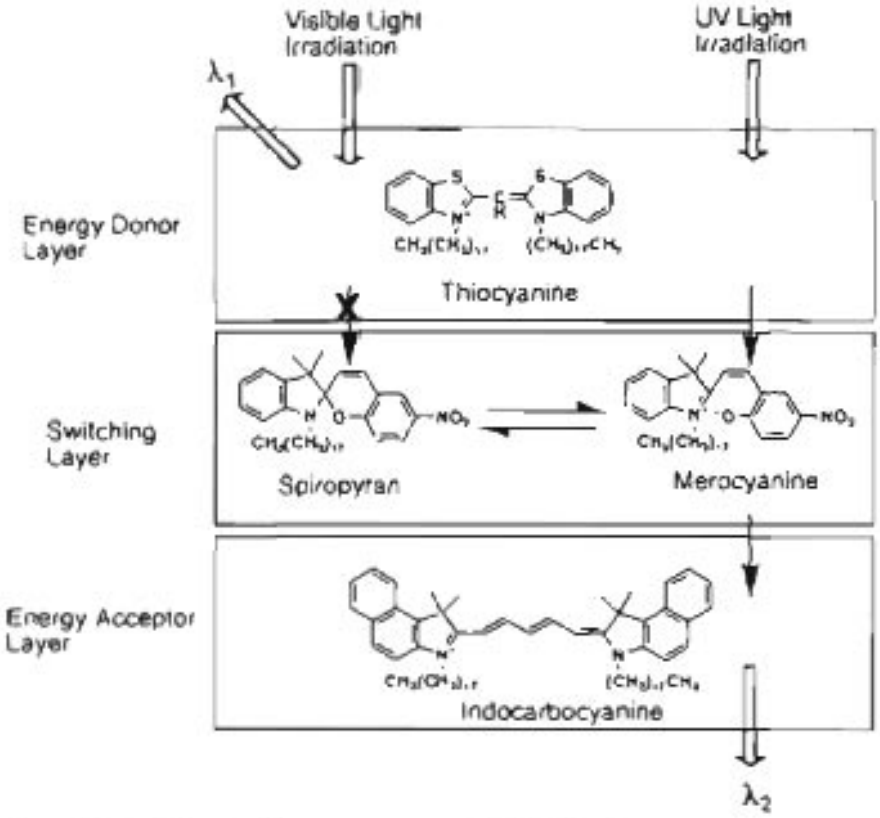

Figure 5.29. Switching device based on appropriate LB film design

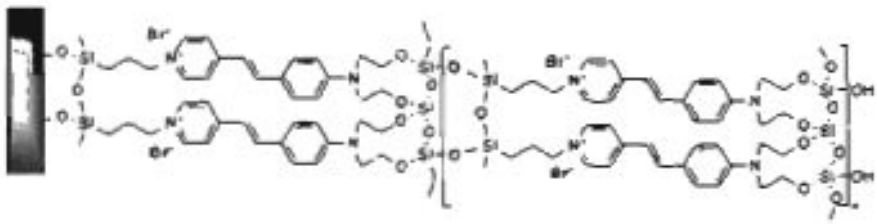

Figure 5.30. Asymmetric self-assembled monolayer used for nonlinear optics

ponent of the emitted light has a frequency of ω. At high light intensity, the contributions of higher order components with frequencies 2ω, 3ω and so on (harmonic waves) cannot be neglected. There is a significant contribution from the second-order component to the emission from the asymmetric structure. When light of frequency ω was directed onto the film shown in Fig. 5.30, the emitted light contained components of frequency 2ω. This phenomenon

is called *second harmonic generation* (SHG). This film can be regarded as molecular device that can alter the wavelength of light shone upon it.

5.8 Supramolecular Chemistry & Nanotechnology toward Future

We have discussed various molecular devices created from supermolecules in this chapter. Molecular level techniques and science will play an important roles in the development of nanotechnology in the twenty-first century. Ultrasmall devices with huge information densities will minimize pollution and energy waste, and improve our lifestyles. Tiny robots will be used in medical applications. Excursions into space – manned and unmanned – will benefit enormously from the use of nanomachines and the products of nanotechnology, which should lead to much cheaper and safer space missions.

In the issue of the regular magazine of the American Chemical Society, Chemistry & Engineering News, from February 28th, 2000, there was a special article entitled "NASA goes NANO", which described the importance of nanotechnology to space programs. For example, Mars Pathfinder, which explored Mars in 1997, was several hundreds of kilograms in weight, and the rovers Spirit and Opportunity, which were launched towards Mars in 2003, each weighed around 180 kilograms. Huge amounts of energy and money are used in Mars missions. Therefore, reducing the size and weight of the spacecraft is highly desirable from a financial point of view. For example, reducing the size of a spacecraft to that of a can of soft drink would result in massive savings. NASA has stated a goal to reduce the size of a typical space probe by 1/100, and to increase reliability by a factor of 1000 by 2020. As space probes venture further and further from Earth to perform ever more complex tasks, it becomes increasingly difficult to guide the actions of the probe by remote control, given the increasing time delay taken for signals to reach (and return from) the probe. What is needed is a "thinking spacecraft" that can fly, walk and escape based on its own judgment and that can adapt to its environment (it can "learn"). This would require onboard systems with superhigh information densities. NASA is therefore interested in the following technologies that could permit this approach: (1) nanocomputers based on organic materials and carbon nanotubes; (2) quantum computers with atomic or quark-level precision; (3) biocomputers with DNA and artificial nerves; (4) photonic computers (computers driven by photons). Some of the examples described in this chapter already provide the first steps toward some of these targets.

However, in "Nanotechnology Research Directions" (a report published by the US government in 1999), it was pointed out that current nanoscale technologies are still highly inferior to those seen in natural systems. The efficiency of the energy conversion that occurs in mitochondrial and photosynthetic systems far exceeds those obtained in artificial systems. A dog can smell and a bat can hear far more sensitively than most artificial sensors. The information pro-

cessing exhibited by brain and nerve systems is far more sophisticated than that exhibited by current computers. Nature developed superior nanotechnologies to our own several billion years ago, and most of them are based on molecular interactions – supramolecular chemistry. There are huge numbers of natural supermolecules all around us. We have a lot to learn from nature and biology. In the next chapter, some natural supramolecular systems are reviewed as well as ways to mimic them, and we suggest how biological materials may be used in new technologiesin the future.

References

5.1

1. G. Stix, "Little Big Science", Sci. Am., 285, 32 (2001)
2. K.E. Drexler, "Machine-Phase Nanotechnology", Sci. Am., 285, 74 (2001)
3. R.E. Smalley, "Of Chemistry, Love and Nanobots", Sci. Am., 285, 76 (2001)
4. N. Mathur, "Beyond the Silicon Roadmap", Nature, 419, 573 (2002)
5. M. Schulz, "The End of the Road for Silicon", Nature, 399, 729 (1999)
6. A. Aviram, M.A. Ratner, "Molecular Rectifiers", Chem. Phys. Lett., 29, 277 (1974)
7. F.L. Carter, "Molecular-Level Fabrication Techniques and Molecular Electronic Devices", J. Vac. Sci. Technol. B, 1, 959 (1983)
8. J.S. Lindsey, "Self-Assembly in Synthetic Route to Molecular Devices – Biological Principles and Chemical Perspectives – A Review", New. J. Chem., 15, 153 (1991)

5.2

9. K. Ariga, T. Kunitake, "Molecular Recognition at Air-Water and Related Interfaces: Complementary Hydrogen Bonding and Multisite Interaction", Acc. Chem. Res., 31, 371 (1988)
10. G.A. Ozin, "Nanochemistry – Synthesis in Diminishing Dimensions", Adv. Mater., 4, 612 (1992)
11. P.K. Hansma, J. Tersoff, "Scanning Tunneling Microscopy", J. Appl. Phys., 61, R1 (1987)
12. H.G. Hansma, J.H. Hoh, "Biomolecular Imaging with Atomic-Force Microscope", Ann. Rev. Biophys. Biomol. Struc., 23, 115 (1994)
13. Z.F. Shao, J. Mou, D.M. Czajkowski, J. Yang, J.Y. Yuan, "Biological Atomic Force Microscopy: What is Achieved and What is Needed", Adv. Phys., 45, 1 (1996)
14. F.-R.F. Fan, A.J. Bard, "STM on Wet Insulators: Electrochemistry or Tunneling?", Science, 270, 1849 (1995)
15. Y. Ebara, H. Ebato, K. Ariga, Y. Okahata, "Interactions of Calcium Ions with Phospholipid Membranes. Studies on π-A Isotherms and Electrochemical and Quartz-Crystal Microbalance Measurements", Langmuir, 10, 2267 (1994)
16. M.T. Rojas, R. Koniger, J.F. Stoddart, A.E. Kaifer, "Supported Monolayers Containing Preformed Binding Sites – Synthesis and Interfacial Binding Properties of a Thiolated β-Cyclodextrin Derivative", J. Am. Chem. Soc., 117, 336 (1995)
17. K. Odashima, M. Kotato, M. Sugawara, Y. Umezawa, "Voltammetric Study on a Condensed Monolayer of a Long Alkyl Cyclodextrin Derivative as a Channel Mimetic Sensing Membrane", Anal. Chem., 65, 927 (1993)
18. J. Homola, S.S. Yee, G. Gauglitz, "Surface Plasmon Resonance Sensors: Review", Sens. Actuat. B, Chem., 54, 3 (1999)

19. K. Kimura, T. Matsuba, Y. Tsujimura, M. Yokoyama, "Unsymmetrical Calix[4]arene Ionophore Silicone-Rubber Composite Membranes for High Performance Sodium Ion Sensitive Field-Effect Transistors", Anal. Chem., 64, 2508 (1992)
20. K. Ariga, K. Isoyama, O. Hayashida, Y. Aoyama, Y. Okahata, "A QCM Study on Adsorption of Macrocyclic Sugar-Cluster to Variously-Functionalized Monolayers", Chem. Lett., 1007 (1998)
21. K. Matsuura, K. Ariga, K. Endo, Y. Aoyama, Y. Okahata, "Dynamic Analyses on Induced-Fit Gaseous Guest Binding to Organic Crystals with a Quartz-Crystal Microbalance", Chem. Eur. J., 6, 1750 (2000)
22. Y. Okahata, Y. Matsunobu, K. Ijiro, M. Mukae, A. Murakami, K. Makino, "Hybridization of Nucleic Acids Immobilized on a Quartz Crystal Microbalance", J. Am. Chem. Soc., 114, 8299 (1992)
23. T. Sato, T. Serizawa, Y. Okahata, "Binding of Influenza A Virus to Monosialoganglioside (GM_3) Reconstituted in Glucosylceramide and Sphingomyelin Membranes", Biochim. Biophys. Acta, 1285, 14 (1996)
24. C. K. O'Sullivan, G.G. Guilbault, "Commercial Quartz Crystal Microbalances – Theory and Applications", Biosens. Bioelectron., 14, 663 (1999)
25. L.A. Bumm, J.J. Arnold, M.T. Cygan, T.D. Dunbar, T.P. Burgin, L. Jones, D.L. Allara, J.M. Tour, P.S. Weiss, "Are Single Molecular Wires Conducting?", Science, 271, 1705 (1996)
26. M.A. Reed, C. Zhou, C.J. Muller, T.P. Burgin, J.M. Tour, "Conductance of a Molecular Junction", Science, 278, 252 (1997)
27. C. Joachim, J.K. Gimzewski, A. Aviram, "Electronics Using Hybrid-Molecular and Mono-Molecular Devices", Nature, 408, 541 (2000)
28. S. Weiss, "Fluorescence Spectroscopy of Single Biomolecules", Science, 283, 1676 (1999)
29. W.E. Moerner, M. Orrit, "Illuminating Single Molecules in Condensed Matter", Science, 283, 1670 (1999)
30. A.D. Mehta, M. Rief, J.A. Spudich, D.A. Smith, R.M. Simmons, "Single-Molecule Biomechanics with Optical Methods", Science, 283, 1689 (1999)
31. T. Funatsu, Y. Harada, M. Tokunaga, K. Saito, T. Yanagida, "Imaging of Single Fluorescent Molecules and Individual ATP Turnovers by Single Myosin Molecules in Aqueous Solution", Nature, 374, 555 (1995)
32. H. Noji, R. Yasuda, M. Yoshida, K. Kinosita, "Direct Observation of the Rotation of F_1-ATPase", Nature, 386, 299 (1997)

5.3

33. R.F. Service, "Assembling Nanocircuits from the Bottom Up", Science, 293, 782 (2001)
34. C. Joachim, J.K. Gimzewski, A. Aviram, "Electronics Using Hybrid-Molecular and Mono-Molecular Devices", Nature, 408, 541 (2000)
35. J.M. Tour, "Molecular Electronics. Synthesis and Testing of Components", Acc. Chem. Res., 33, 791 (2000)
36. R.L. Carroll, C.B. Gorman, "The Genesis of Molecular Electronics", Angew. Chem. Int. Ed., 41, 4379 (2002)
37. G.S. McCarty, P.S. Weiss, "Scanning Probe Studies of Single Nanostructures", Chem. Rev., 99, 1983 (1999)
38. D. Feldheim, "Flipping a Molecular Switch", Nature, 408, 45 (2000)
39. M.A. Reed, C. Zhou, C.J. Muller, T.P. Burgin, J.M. Tour, "Conductance of a Molecular Junction", Science, 278, 252 (1997)
40. M.A. Reed, J.M. Tour, "Computing with Molecules", Sci. Am., 282, 86 (2000)

41. G. Ashkenasy, D. Cahen, R. Cohen, A. Shanzer, A. Vilan, "Molecular Engineering of Semiconductor Surfaces and Devices", Acc. Chem. Res., 35, 121 (2002)
42. J. Park, A.N. Pasupathy, J.I. Goldsmith, C. Chang, Y. Yaish, J.R. Petta, M. Rinkoski, J.P. Sethna, H. D. Abruña, P.L. McEuen, D.C. Ralph, "Coulomb Blockade and the Kondo Effect in Single-Atom Transistors", Nature, 417, 722 (2002)
43. Z.J. Donhauser, B.A. Mantooth, K.P. Kelly, L.A. Bumm, J.D. Monnell, J.J. Stapleton, D.W. Price Jr., A.M. Rawlett, D.L. Allara, J.M. Tour, P.S. Weiss, "Conductance Switching in Single Molecules through Conformation Changes", Science, 292, 2306 (2001)
44. A. Niemz, V.M. Rotello, "From Enzyme to Molecular Device. Exploring of Interdependence of Redox and Molecular Recognition", Acc. Chem. Res., 32, 44 (1999)
45. E. Braun, Y. Eichen, U. Sivan, G. Ben-Yoseph, "DNA-Templated Assembly and Electrode Attachment of a Conductive Silver Wire", Nature, 391, 775 (1998)
46. S. Kugimiya, T. Lazark, M. Blanchard-Desce, J.M. Lehn, "Electron Conduction across Vesicular Bilayer Membranes Induced by a Carviologen Molecular Wire", J. Chem. Soc., Chem. Commun., 1179 (1991)
47. A. Tsuda, A. Osuka, "Fully Conjugated Porphyrin Tapes with Electronic Absorption Bands That Reach into Infrared", Science, 293, 79 (2001)
48. T.M. Swager, "The Molecular Wire Approach to Sensory Signal Amplification", Acc. Chem. Res., 31, 201 (1998)
49. D.T. McQuade, A.E. Pullen, T.M. Swager, "Conjugated Polymer-Based Chemical Sensors", Chem. Rev., 100, 2537 (2000)
50. A.G. MacDiarmid, "Synthetic Metals: A Novel Role for Organic Polymers (Nobel Lecture)", Angew. Chem. Int. Ed., 40, 2581 (2001)
51. H. Shirakawa, "The Discovery of Polyacetylene Film: The Dawning of an Era of Conducting Polymers (Nobel Lecture)", Angew. Chem. Int. Ed., 40, 2575 (2001)
52. A.J. Heeger, "Semiconducting and Metallic Polymers: The Fourth Generation of Polymeric Materials (Nobel Lecture)", Angew. Chem. Int. Ed., 40, 2591 (2001)
53. H. Sirringhaus, N. Tessler, R.H. Friend, "Integrated Optoelectronic Devices Based on Conjugated Polymers", Science, 280, 1741 (1998)
54. S.L. Gilat, S.H. Kawai, J.M. Lehn, "Light-Triggered Electrical and Optical Switching Devices", J. Chem. Soc., Chem. Commun., 1439 (1993)
55. P.G. Haydon, "Glia: Listening and Talking to the Synapse", Nature Rev. Neurosci., 2, 185 (2001)
56. J.L. Sessler, B. Wang, A. Harriman, "Long-Range Photoinduced Electron Transfer in an Associated But Noncovalently Linked Photosynthetic Model System", J. Am. Chem. Soc., 115, 10418 (1993)
57. A. Harriman, Y. Kubo, J.L. Sessler, "Molecular Recognition via Base-Pairing - Photoinduced Electron-Transfer in Hydrogen-Bonded Zinc Porphyrin Benzoquinone Conjugates", J. Am. Chem. Soc., 114, 388 (1992)
58. K. Ogawa, Y. Kobuke, "Formation of a Giant Supramolecular Porphyrin Array by Self-Coordination", Angew. Chem. Int. Ed., 39, 4070 (2000)
59. S.J. Tans, M.H. Devoret, H. Dai, A. Thess, R.E. Smalley, L.J. Geerligs, C. Dekker, "Individual Single-Wall Carbon Nanotubes as Quantum Wires", Nature, 386, 474 (1997)
60. S.J. Tans, A.R.M. Verschueren, C. Dekker, "Room-Temperature Transistor Based on a Single Carbon Nanotube", Nature, 393, 49 (1998)
61. T.W. Tombler, C. Zhou, L. Alexseyev, J. Kong, H. Dai, L. Lei, C.S. Jayanthi, M. Tang, S.-Y. Wu, "Reversible Electromechanical Characteristics of Carbon Nanotubes under Local-Probe Manipulation", Nature, 405, 769 (2000)
62. P. Avouris, "Molecular Electronics with Carbon Nanotubes", Acc. Chem. Res., 35, 1026 (2002)

63. T. Rueckes, K. Kim, E. Joselevich, G.Y. Tseng, C.L. Cheung, C.M. Lieber, "Carbon Nanotube-Based Nonvolatile Random Access Memory for Molecular Computing", Science, 289, 94 (2000)
64. Y. Luo, C.P. Collier, J.O. Jeppesen, K.A. Nielsen, E. Delonno, G. Ho, J. Perkins, H.R. Tseng, T. Yamamoto, J.F. Stoddart, J.R. Heath, "Two-Dimensional Molecular Electronics Circuits", Chem. Phys. Chem., 3, 519 (2002)
65. S.J. Tans, C. Dekker, "Potential Modulations along Carbon Nanotubes", Nature, 404, 834 (2000)
66. M. Bockrath, D.H. Cobden, P.L. McEuen, N.G. Chopra, A. Zettl, A. Thess, R.E. Smalley, "Single-Electron Transport in Ropes of Carbon Nanotubes", Science, 275, 1922 (1997)
67. Y. Okawa, M. Aono, "Nanoscale Control of Chain Polymerization", Nature, 409, 683 (2001)
68. H. Sirringhaus, T. Kawase, R.H. Friend, T. Shimoda, M. Inbasekaran, W. Wu, E.P. Woo, "High-Resolution Inkjet Printing of All-Polymer Transistor Circuits", Science, 290, 2123 (2000)

5.4

69. D. Holten, D.F. Bocian, J.S. Lindsey, "Probing Electronic Communication in Covalently Linked Multiporphyrin Arrays. A Guide to the Rational Design of Molecular Photonic Devices", Acc. Chem. Res., 35, 57 (2002)
70. A.P. de Silva, H.Q.N. Gunaratne, T. Gunnlaugsson, A.J.M. Huxley, C.P. McCoy, J.T. Rademacher, T.E. Rice, "Signaling Recognition Events with Fluorescent Sensors and Switches", Chem. Rev., 97, 1515 (1997)
71. S.R. Marder, B. Kippelen, A.K.Y. Jen, N. Peyghambarian, "Design and Synthesis of Chromophores and Polymers for Electro-Optic and Photorefractive Applications", Nature, 388, 845 (1997)
72. F. Hide, M.A. DiazGarcia, B.J. Schwartz, A.J. Heeger, "New Developments in the Photonic Applications of Conjugated Polymers", Acc. Chem. Res., 30, 430 (1997)
73. K. Kalyanasundaram, M. Grätzel, "Applications of Functionalized Transition Metal Complexes in Photonic and Optoelectronic Devices", Coordinat. Chem. Rev., 177, 347 (1998)
74. U. Mitschke, P. Bauerle, "The Electroluminescence of Organic Materials", J. Mater. Chem., 10, 1471 (2000)
75. J. Otsuki, M. Tsujino, T. Iizaki, K. Araki, M. Seno, K. Takatera, T. Watanabe, "Redox-Responsive Molecular Switch for Intramolecular Energy Transfer", J. Am. Chem. Soc., 119, 7895 (1997)
76. A.P. de Silva, H.Q.N. Gunaratne, C.P. Mccoy, "A Molecular Photonic AND Gate Based on Fluorescent Signaling", Nature, 364, 42 (1993)
77. T. Gunnlaugsson, D. A. M. Dónaill, D. Parker, "Lanthanide Macrocyclic Quinolyl Conjugates as Luminescent Molecular-Level Devices", J. Am. Chem. Soc., 123, 12866 (2001)
78. E. Murguly, T.B. Norsten, N.R. Branda, "Nondestructive Data Processing Based on Chiroptical 1,2-Diethienylethene Photochromes", Angew. Chem. Int. Ed., 40, 1752 (2001)
79. P.K.H. Ho, D.S. Thomas, R.H. Friend, N. Tessler, "All-Polymer Optoelectronic Devices", Science, 285, 233 (1999)
80. P.K.H. Ho, J.-S. Kim, J.H. Burroughes, H. Becker, S.F.Y. Li, T.M. Brown, F. Cacialli, R.H. Friend, "Molecular-Scale Interface Engineering for Polymer Light-Emitting Diodes", Nature, 404, 481 (2000)

81. D.M. Kaschak, J.T. Lean, C.C. Waraksa, G.B. Saupe, H. Usami, T.E. Mallouk, "Photoinduced Energy and Electron Transfer Reactions in Lamellar Polyanion/Polycation Thin Films: Toward an Inorganic Leaf", J. Am. Chem. Soc., 121, 3435 (1999)

5.5

82. A.P. de Silva, N.D. McClenaghan, "Proof-of-Principle of Molecular-Scale Arithmetic", J. Am. Chem. Soc., 122, 3965 (2000)
83. A. Credi, V. Balzani, S.J. Langford, J.F. Stoddart, "Logic Operations at the Molecular Level. An XOR Gate Based on a Molecular Machine", J. Am. Chem. Soc., 119, 2679 (1997)
84. J.C. Ellenbogen, J.C. Love, "Architectures for Molecular Electronic Computers: 1. Logic Structures and an Adder Designed from Molecular Electronic Diodes", Proc. IEEE, 88, 386 (2000)
85. C.P. Collier, E.W. Wong, M. Belohradsky, F.M. Raymo, J.F. Stoddart, P.J. Kuekes, R.S. Williams, J.R. Heath, "Electronically Configurable, Molecular-Based Logic Gates", Science, 285, 391 (1999)
86. M. Cavallini, F. Biscarini, S. León, F. Zerbetto, G. Bottari, D.A. Leigh, "Information Storage Using Supramolecular Surface Patterns", Science, 299, 531 (2003)
87. C.P. Collier, G. Mattersteig, E.W. Wong, Y. Luo, K. Beverly, J. Sampaio, F.M. Raymo, J.F. Stoddart, J.P. Heath, "A [2]Catenane-Based Solid State Electronically Reconfigurable Switch", Science, 289, 1172 (2000)
88. L.M. Adleman, "Molecular Computing of Solutions to Combinatorial Problems", Science, 266, 1021 (1994)
89. L.M. Adleman, "Computing with DNA", Sci. Am., 279, 54 (1998)
90. G. Paun, "Computing with Membranes", J. Comput. Sys. Sci., 61, 108 (2000)
91. Q. Liu, L. Wang, A.G. Frutos, A.E. Condon, R.M. Corn, L.M. Smith, "DNA Computing on Surfaces", Nature, 403, 175 (2000)
92. R.S. Braich, N. Chelyapov, C. Johnson, P.W.K. Rothemund, L. Adleman, "Solution of a 20-Variable 3-SAT Problem on a DNA Computer", Science, 296, 499 (2002)
93. D. Faulhammer, A.R. Cukras, R.J. Lipton, L.F. Landweber, "Molecular Computation: RNA Solutions to Chess Problems", Proc. Natl. Acad. Sci. USA, 97, 1385 (2000)
94. A. Saghatelian, N.H. Völcher, K.M. Guckian, V. S.-Y. Lin, M.R. Ghadiri, "DNA-Based Photonic Logic Gates: AND, NAND, and INHIBIT", J. Am. Chem. Soc., 125, 346 (2003)
95. Y. Benenson, R. Adar, T. Paz-Elizur, Z. Livneh, E. Shapiro, "DNA Molecule Provides a Computing Machine with Both Data and Fuel", Proc. Natl. Acad. Sci. USA, 100, 2191 (2003)
96. K. Sakamoto, H. Gouzu, K. Komiya, D. Kiga, S. Yokoyama, T. Yokomori, M. Hagiya, "Molecular Computation by DNA Hairpin Formation", Science, 288, 1223 (2000)

5.6

97. R. Ballardini, V. Balzani, M.T. Gandolfi, L. Prodi, M. Venturi, D. Philp, H.G. Ricketts, J.F. Stoddart, "A Photochemically Driven Molecular Machine", Angew. Chem. Int. Ed., 32, 1301 (1993)
98. P.R. Ashton, R. Ballardini, V. Balzani, S.E. Boyd, A. Credi, M.T. Gandolfi, M. Gomez Lopez, S. Iqbal, D. Philp, J.A. Preece, L. Prodi, H.G. Ricketts, J.F. Stoddart, M.S. Tolley, M. Venturi, A.J.P. White, D.J. Williams, "Simple Mechanical Molecular and Supramolecular Machines: Photochemical and Electrochemical Control of Switching Processes", Chem. Eur. J., 3, 152 (1997)
99. V. Balzani, A. Credi, F.M. Raymo, J.F. Stoddart, "Artificial Molecular Machines", Angew. Chem. Int. Ed., 39, 3348 (2000)

100. V. Amendola, L. Fabbrizzi, C. Mangano, P. Pallavicini, "Molecular Machines Based on Metal Ion Translocation", Acc. Chem. Res., 34, 488 (2001)
101. C.A. Shalley, "Of Molecular Gyroscopes, Matroshka Dolls, and Other "Nano"-Toys", Angew. Chem. Int. Ed., 41 1513 (2002)
102. M. Barboiu, J.-M. Lehn, "Dynamic Chemical Devices: Modulation of Contraction/Extension Molecular Motion by Coupled-Ion Binding/pH Change-Induced Structural Switching", Proc. Natl. Acad. Sci. USA, 99, 5201 (2002)
103. J.K. Gimzewski, C. Joachim, R.R. Schlittler, V. Langlais, H. Tang, I. Johannsen, "Rotation of a Single Molecule Within a Supramolecular Bearing", Science, 281, 531 (1998)
104. J.K. Gimzewski, C. Joachim, "Nanoscale Science of Single Molecules Using Local Probes", Science, 283, 1684 (1999)
105. B.L. Feringa, "In Control of Motion: From Molecular Switches to Molecular Motors", Acc. Chem. Res., 34, 504 (2001)
106. N. Koumura, E.M. Geertsema, M.B. van Gelder, A. Meetsma, B.L. Feringa, "Second Generation Light-Driven Molecular Motors. Unidirectional Rotation Controlled by a Single Stereogenic Center with Near-Perfect Photocquilibria and Acceleration of the Speed of Rotation by Structural Modification", J. Am. Chem. Soc., 124, 5037 (2002)
107. R.A. van Delden, N. Koumura, N. Harada, B.L. Feringa, "Unidirectional Rotary Motion in a Liquid Crystalline Environment: Color Tuning by a Molecular Motor", Proc. Natl. Acad. Sci. USA, 99, 3945 (2002)
108. N. Koumura, R.W.J. Zijlstra, R.A. van Delden, N. Harada, B.L. Feringa, "Light-Driven Monodirectional Molecular Rotor", Nature, 401, 152 (1999)
109. T.R. Kelly, H. de Silva, R.A. Silva, "Unidirectional Rotary Motion in a Molecular System", Nature, 401, 150 (1999)
110. T.R. Kelly, "Progress toward a Rationally Designed Molecular Motor", Acc. Chem. Res., 34, 514 (2001)
111. C.A. Schalley, K. Beizai, F. Vögtle, "On the Way to Rotaxane-Based Molecular Motors: Studies in Molecular Mobility and Topological Chirality", Acc. Chem. Res., 34, 465 (2001)
112. V. Balzani, M. Gómez-López, J.F. Stoddart, "Molecular Machines", Acc. Chem. Res., 31, 405 (1998)
113. A. Harada, "Cyclodextrin-Based Molecular Machines", Acc. Chem. Res., 34, 456 (2001)
114. K. Kinbara, T. Aida, "Toward Intelligent Molecular Machines: Directed Motions of Biological and Artificial Molecules and Assemblies", Chem. Rev., 105, 1377 (2005)
115. H. Shigekawa, K. Miyake, J. Sumaoka, A. Harada, M. Komiyama, "The Molecular Abacus: STM Manipulation of Cyclodextrin Necklace", J. Am. Chem. Soc., 122, 5411 (2000)
116. R.H. Baughman, C. Cui, A.A. Zakhidov, Z. Iqbal, J.N. Barisci, G.M. Spinks, G.G. Wallace, A. Mazzoldi, D. De Rossi, A.G. Rinzler, O. Jaschinski, S. Roth, M. Kertesz, "Carbon Nanotube Actuators", Science, 284, 1340 (1999)
117. P. Kim, C.M. Lieber, "Nanotube Nanotweezers", Science, 286, 2148 (1999)
118. O. Inganäs, I. Lundström, "Carbon Nanotube Muscles", Science, 284, 1281 (1999)
119. J. Fritz, M.K. Baller, H.P. Lang, H. Rothuizen, P. Vettiger, E. Meyer, H.-J. Güntherodt, C. Gerber, J.K. Gimzewski, "Translating Biomolecular Recognition into Nanomechanics", Science, 288, 316 (2000)
120. C.M. Niemeyer, M. Adler, "Nanomechanical Devices Based on DNA", Angew. Chem. Int. Ed., 41, 3779 (2002)
121. C. Mao, W. Sun, Z. Shen, N.C. Seeman, "A Nanomechanical Device Based on the B-Z Transition of DNA", Nature, 397, 144 (1999)

122. K. Ariga, Y. Terasaka, D. Sakai, H. Tsuji, J. Kikuchi, "Piezoluminescence Based on Molecular Recognition by Dynamic Cavity Array of Steroid Cyclophanes at the Air-Water Interface", J. Am. Chem. Soc., 122, 7835 (2000)
123. K. Ariga, T. Nakanishi, H. Tsuji, D. Sakai, J. Kikuchi, "Piezoluminescence as the Air-Water Interface through Dynamic Molecular Recognition Driven by Lateral Pressure Application", Langmuir, 21, 976 (2005)

5.7

124. H. Kuhn, "Electron-Transfer in Monolayer Assemblies", Pure Appl. Chem., 51, 341 (1979)
125. P.S. Vincett, G.G. Roberts, "Electrical and Photo-Electrical Transport Properties of Langmuir-Blodgett Films and a Discussion of Possible Device Application", Thin Solid Films, 68, 135 (1980)
126. T. Ito, I. Yamazaki, N. Ohta, "External Electric Field Effect on Interlayer Vectorial Electron Transfer from Photoexcited Oxacarbocyanine to Viologen in Langmuir-Blodgett Films", Chem. Phys. Lett., 277, 125 (1997)
127. K. Naito, A. Miura, "Photogenerated Charge Storage in Hetero-Langmuir-Blodgett Films", J. Am. Chem. Soc., 115, 5185 (1993)
128. T. Cassagneau, T.E. Mallouk, J.H. Fendler, "Layer-by-Layer Assembly of Thin Film Zener Diodes from Conducting Polymers and CdSe Nanoparticles", J. Am. Chem. Soc., 120, 7848 (1998)
129. A. Wu, D. Yoo, J.K. Lee, M.F. Rubner, "Solid-State Light-Emitting Devices Based on the Tris-Chelated Ruthenium(II) Complex: 3. High Efficiency Devices via a Layer-by-Layer Molecular-Level Blending Approach", J. Am. Chem. Soc., 121, 4883 (1999)
130. M. Fujihira, K. Nishiyama, H. Yamada, "Photoelectrochemical Responses of Optically Transparent Electrodes Modified with Langmuir-Blodgett Films Consisting of Surfactant Derivatives of Electron-Donor, Acceptor and Sensitizer Molecules", Thin Solid Films, 132, 77 (1985)
131. M. Fujihira, M. Sakomura, "Photoinduced Intramolecular Electron-Transfer Across Monolayers Consisting of Linear A-S-D Triad Amphiphilic Molecules", Thin Solid Films, 179, 471 (1989)
132. M. Fujihira, H. Yamada, "Molecular Photodiodes Consisting of Unidirectionally Oriented Amphipathic Acceptor Sensitized Donor Triads", Thin Solid Films, 160, 125 (1988)
133. H. Tachibana, T. Nakamura, M. Matsumoto, H, Komizu, E. Manda, H. Mino, A. Yase, Y. Kawabata, "Photochemical Switching in Conductive Langmuir-Blodgett Films", J. Am. Chem. Soc., 111, 3080 (1989)
134. I. Yamazaki, N. Ohta, "Photochemistry in LB Films and Its Application to Molecular Switching Devices", Pure Appl. Chem., 67, 209 (1995)
135. I. Yamazaki, S. Okazaki, T. Minami, N. Ohta, "Optically Switching Parallel Processors by Means of Langmuir-Blodgett Multilayer Films", Appl. Opt., 33, 7561 (1994)
136. W.B. Lin, S. Yitzchaik, W.P. Lin, A. Malik, M.K. Durbin, A.G. Richter, G.K. Wong, P. Dutta, T.J. Marks, "New Nonlinear-Optical Materials - Expedient Topotactic Self-Assembly of Acentric Chromophoric Superlattices", Angew. Chem. Int. Ed., 34, 1497 (1995)
137. L.R. Dalton, A.W. Harper, R. Ghosn, W.H. Steier, M. Ziari, H. Fetterman, Y. Shi, R.V. Mustacich, A.K.Y. Jen, K.J. Shea, "Synthesis and Processing of Improved Organic Second-Order Nonlinear Optical Materials for Application in Photonics", Chem. Mater., 7, 1060 (1995)

5.8

138. R. Dagani, "NASA Goes NANO", Chem. Eng. News, Feb 28th, 36 (2000)
139. R. Dagani, "NanoSpace 2000: Melding Two Worlds", Chem. Eng. News, Feb 28th, 39 (2000)
140. G. Musser, "The Spirit of Exploration", Sci. Am., 290, 52 (2004)

The Chemical Society of Japan Award for 2004

Photochromism and Molecular Mechanical Devices

Masahiro Irie

Department of Chemistry, Rikkyo University, 3-34-1 Nishi-Ikebukuro, Toshima-ku, Tokyo 171-8501

Received March 21, 2008; E-mail: iriem@rikkyo.ac.jp

It is a dream for chemists to synthesize molecular systems, which can transform changes of molecular shape induced by external stimuli, such as chemicals, photons, and electrons (or holes), to macro-scale motion of the materials and perform mechanical work. To realize this dream we first prepared photoresponsive polyamides having azobenzene chromophores in the main chain. Although the polyamides changed conformation in solution upon photoinduced trans–cis isomerization, we failed to link the conformational change to macro-scale motion of polymer films and gels. During the course of study on photochromism of diarylethene single crystals we found that the surface morphology as well as the bulk shape of the single crystals reversibly changes upon photoisomerization of the component diarylethene molecules in the crystals. The photoinduced shape changes of the molecules in the densely packed crystals give rise to mechanical motion of the crystals and launch a tiny silica-particle. This is the first molecular system, which directly transforms changes of molecular shape to macro-scale motion of the materials and performs mechanical work. This account describes the progress of the research.

1. Introduction

It is of particular interest from both scientific as well as technological points of view to have synthetic molecules make mechanical motion by external stimuli and link the motion to large macro-scale mechanical work of bulk materials. Mechanical work means controlled, large amplitude, or directional motion of the materials, which results in a net task being performed. Most chemical reactions induced by external stimuli, such as chemicals, photons, and electrons (or holes), are accompanied by a change of molecular shape. The shape change results in machine-like motion at the molecular level. In biological systems, the bending motion of myosin upon release of adenosine diphosphate at the molecular level is used to drive muscles and perform large macro-scale mechanical work.[1] On the other hand, there is no man-made molecular machine, which is based on the shape changes of molecules and can perform macro-scale mechanical work in the real world.[2–6] The shape changes of synthetic molecules at the molecular level fail to be linked to the large macro-scale mechanical motion of materials. So far there is no guiding principle which leads to man-made molecular machines.

In this account, our effort to achieve macro-scale mechanical work of molecular materials based on photoinduced molecular shape changes will be described. We first tried to develop photoresponsive polymers having photochromic molecules and induce photomechanical work of polymer films and gels. Although we could connect the shape changes of the photochromic molecules to conformational change of the polymer chains in solution, we failed to link the changes to macro-scale mechanical motion of the solid polymer films or gels. We finally succeeded to transform the shape changes of molecules to the macro-scale mechanical work using photochromic molecular crystals.

2. Photoresponsive Polymers[7]

The first attempt to link photoinduced shape changes of molecules to macro-scale mechanical work of polymer fibers was carried out by Merian[8] in 1966. He assumed that the trans–cis photoisomerization of azobenzene dyes causes shrinkage of the fiber when the dyes are molecularly dispersed in the fiber, because the azobenzene unit is known to change geometrical structure. The length of the dye used changes from 21 to 16.5 Å upon photoisomerization from the trans to the cis form, as shown in Figure 1. Upon photoirradiation the fiber length was found to shrink as much as 0.1%. Although he attributed the fiber shrinkage to the change of the molecular shape, local photo-heating due to non-radiative transition of the photo-excited azobenzene dyes should be taken into account as the main origin of the photoinduced shrinkage, as evidenced later by Matějka et al.[9]

Another approach to use photoisomerization of azobenzene dyes for mechanical work of polymer gels was carried out by Prins et al.[10,11] They reexamined the experiment by Lovrien,[12] who demonstrated that the conformation of poly(methacrylic acid) chains changes upon photoirradiation in the presence of the azobenzene dye chrysophenine G in water, and applied the molecular-scale conformational change to the shape change of the polymer gel. The trans–cis photoisomerization of the azobenzene derivative changes its hydrophobic nature

Published on the web August 11, 2008; doi:10.1246/bcsj.81.917

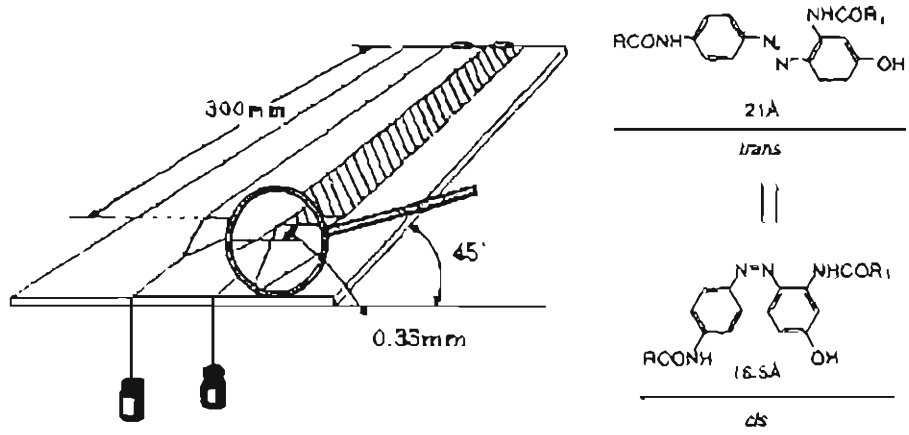

Figure 1. Photoinduced contraction of fabric dyed with trans–cis photoisomerizable dye, shown in the right side.

to hydrophilic and the amphiphilic property change affects the binding of the azobenzene dyes to the polymer chain. The binding force change affects the conformation of the polymer chains as well as the shape of polymer gels. This is the first successful example of photostimulated macro-scale mechanical work.

The attractive reports by Prins et al.[10,11] activated research on the photomechanical effect of polymer films and gels, and various polymers having photochromic chromophores, such as azobenzene or spirobenzopyran derivatives, were prepared.[12–18] Although many polymer films and gels were reported to exhibit macroscopic shape changes upon photoirradiation, there remains the question as to the relative contribution of the local photo-heating and the real photochemical reaction to the observed photoinduced shrinkage. Mateějka et al.[9,19] carefully examined the contribution of the local photo-heating effect to the photoinduced shrinkage of a maleic anhydride–styrene copolymer with covalently bound pendant azobenzene groups swollen in diethyl phthalate. They measured the temperature increase of the polymer gel by inserting a thermocouple into the gel along with the photogenerated force. It was found that the force change well correlates with the change in temperature of the gel. The decisive role played in the contraction of the gel is local heating due to light absorption, not ascribed to molecular shape changes of the azobenzene chromophores. The large heat effect observed even in the contraction of the solvent-swollen gel strongly indicates that many works should be carefully reexamined to check and evaluate the real photochemical effect.

Under these circumstances we decided to carry out a fundamental study on the conformational changes of polymer chains in solution upon photoirradiation.[1] If the conformational changes of polymer chains are reversibly induced by photochemical reactions, the changes will probably be linked to macro-scale shape changes of polymer films and gels.

First, we prepared polyamides having azobenzene chromophores in the main chain, as shown in Scheme 1.[20] The most convenient way to know the conformational changes of polymer chains is to measure the viscosity of the polymer solution. The intrinsic viscosity $[\eta]$ of polyamide I in polar *N,N*-dimethylacetamide was found to decrease from 1.22 to 0.5 dL g^{-1} upon ultraviolet light ($410\,\text{nm} > \lambda > 350\,\text{nm}$) irradiation and

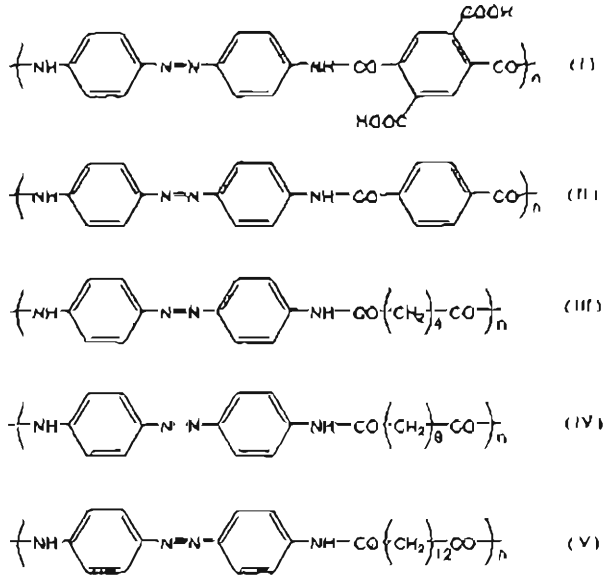

Scheme 1. Photoresponsive polyamides.

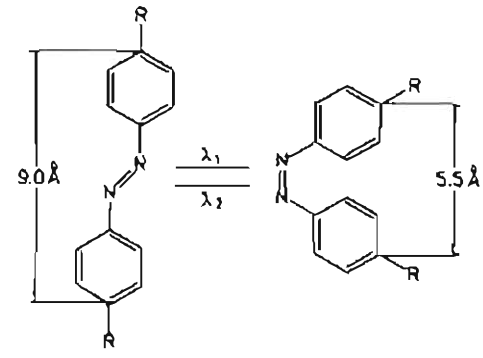

Figure 2. The geometrical structure change of an azobenzene residue along with trans–cis photoisomerization.

to return to the initial value in 30 h in the dark at 20 °C. The decrease is ascribed to the geometrical structure change of the azobenzene unit, as shown in Figure 2.

The decrease is not due to the intramolecular dipole–dipole

Table 1. Effect of Backbone Structure of the Polymers on the Photodecrease of the Solution Viscosity

Polymer	η_{sp} (UV)/η_{sp}(dark)[a]	$(1 - \varepsilon_c/\varepsilon_t)y$[b]
Polyamide II	0.37	0.47
Polyamide III	0.59	0.79
Polyamide IV	0.80	0.69
Polyamide V	0.96	0.52

a) η_{sp} (UV) and η_{sp} (dark) are specific viscosities under irradiation with ultraviolet light ($410 > \lambda > 350$ nm) and in dark before irradiation in *N*-methyl-2-pyrrolidone in the presence of LiCl (1.3 M), respectively. Concentration of the polymer was 0.3 g dL^{-1}. b) Relative content of the *cis* form of the azobenzene residues in the photostationary state under ultraviolet irradiation ($410 > \lambda > 350$ nm). ε_c, ε_t, and y are extinction coefficients of the *cis* and *trans* forms at 390 nm and the content of the *cis* form in the photostationary state.

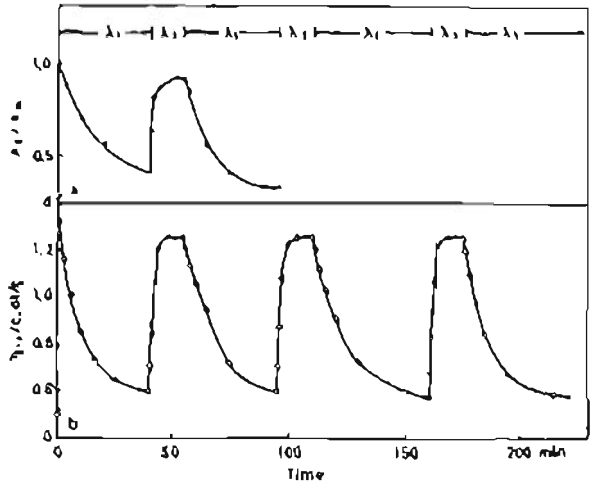

Figure 3. Changes in (●) content of the *trans*-azobenzene residues in polyamide I backbone and (○) viscosity of the polyamide in *N,N*-dimethylacetamide on alternate irradiation with ultraviolet ($410 > \lambda > 350$ nm) and visible ($\lambda > 470$ nm) light at 20 °C. Polymer concentration was 0.9 g dL^{-1}.

interactions, because the polarity of the solvent used is high enough and the photo-effect was not observed for polymers with flexible methylene chains, as shown in Table 1. Although the specific viscosity of stiff polyamide II decreased as much as 63% upon ultraviolet irradiation, the photo-effect decreased with increasing number of methylene units in the main chain. The photodecrease of the specific viscosity was scarcely observed for polyamide V having 12 methylene units. When alternatively irradiated with ultraviolet ($410 \text{ nm} > \lambda > 350$ nm) and visible ($\lambda > 470$ nm) light, the viscosity of *N,N*-dimethylacetamide solution of polyamide I reversibly changed as much as 60%, as shown in Figure 3.

It is of particular interest to know how fast long polymer chains change their conformation in response to a light pulse. The photoisomerization of azobenzene chromophores can be induced in less than 10^{-9} s with a short laser pulse. The conformational change subsequent to the photoisomerization can

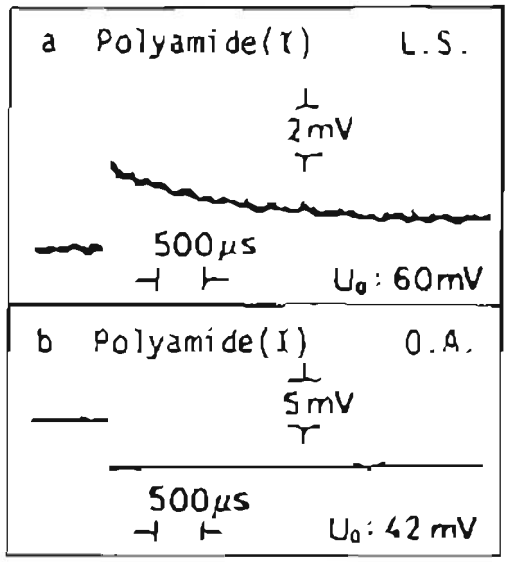

Figure 4. Chain unfolding and *cis* to *trans* photoisomerization of polyamide I in *N,N*-dimethylacetamide solution (0.31 g dL^{-1}). The oscillograms illustrate changes of light-scattering intensity at 514 nm (a) and optical absorption at 514 nm (b) during and after 20 ns flash of 530 nm light.

be followed with a time-resolved light-scattering system combined with the laser pulse source.[21] The Debye eq 1 relates light-scattering intensity R_θ to the mean square radius of gyration $\langle s^2 \rangle$.

$$\frac{K_c}{R_\theta} \approx \frac{1}{\overline{M}_w} + \frac{16\pi^2\langle s^2\rangle}{3\lambda_0^2\overline{M}_w}\sin^2(\theta/2) + 2A_2 \qquad (1)$$

Polyamide I was irradiated with a 20-ns laser pulse (530 nm) in *N,N*-dimethylacetamide. The *cis* to *trans* photoisomerization of the backbone azobenzene units was followed by time-resolved optical absorption and subsequent conformational change of the polymer chain by time-resolved light scattering. Before each laser experiment the polymer was pre-irradiated with ultraviolet light and brought to a compact conformation, and then the unfolding process was traced by laser photolysis. The optical absorption change indicated that the *cis* to *trans* isomerization is completed in 100 ns. Figure 4a shows a typical oscilloscope trace illustrating the change in light-scattering intensity during and after the laser pulse. The change of the light-scattering intensity R_θ reflects the conformational change involving the change in $\langle s^2 \rangle$, as shown in eq 1. The initial rapid increase is due to a concurrent decrease in the optical absorption, as depicted in Figure 4b. The slow decrease of the scattering intensity indicates that the conformational change from the compact to the extended conformations takes place in about 1 ms.

The large difference in the response times for the optical absorption and the light scattering suggests a two-step mechanism for the photostimulated unfolding process. During the isomerization of the backbone azobenzene residues, the total chain conformation remains in the initial compact conformation. After the isomerization is completed, the conformation relaxes to a more stable extended conformation in 1 ms